Spring 2021

Prototypical Arm Motions from Human Demonstration for Upper-Limb Prosthetic Device Control

Yuri Gloumakov
Yale University Graduate School of Arts and Sciences, yuri.gloumakov@yale.edu

Abstract

Prototypical Arm Motions from Human Demonstration for Upper-Limb Prosthetic Device Control

Yuri Gloumakov

2021

Controlling a complex upper limb prosthesis, akin to a healthy arm, is still an open challenge due to the inadequate number of inputs available to amputees. Designs have therefore largely focused on a limited number of controllable degrees of freedom, developing a complex hand and grasp functionality rather than the wrist. This thesis investigates joint coordination based on human demonstrations that aims to vastly simplify the controls of wrist, elbow-wrist, and shoulder-elbow wrist devices.

The wide range of motions performed by the human arm during daily tasks makes it desirable to find representative subsets to reduce the dimensionality of these movements for a variety of applications, including the design and control of robotic and prosthetic devices. Here I present the results of an extensive human subjects study and two methods that were used to obtain representative categories of arm use that span naturalistic motions during activities of daily living. First, I sought to identify sets of prototypical upper-limb motions that are functions of a single variable, allowing, for instance, an entire prosthetic or robotic arm to be controlled with a single input from a user, along with a means to select between motions for different tasks. Second, I decouple the orientation from the location of the hand and analyze the hand location in three ways and orientation in three reference frames. Both of these analyses are an application of data driven approaches that reduce the wide range of hand and arm use to a smaller representative set. Together these provide insight into our arm usage in daily life and inform an implementation in prosthetic or robotic devices without the need for additional hardware.

To demonstrate the control efficacy of prototypical arm motions in upper-limb prosthetic devices, I developed an immersive virtual reality environment where able-bodied participants tested out different devices and controls. I coined prototypical arm motion control as *trajectory* control, and I found that as device complexity increased from 3 DOF wrist to 4 DOF elbow-wrist and 7 DOF shoulder-elbow-wrist, it enables users to complete tasks faster with a more intuitive interface without additional body compensation, while featuring better movement cosmesis when compared to standard controls.

Prototypical Arm Motions from Human Demonstration for Upper-Limb Prosthetic Device Control

A Dissertation

Presented to the Faculty of the Graduate School

of

Yale University

in Candidacy for the Degree of

Doctor of Philosophy

by

Yuri Gloumakov

Dissertation Director: Aaron Michael Dollar

June 2021

ACKNOWLEDGEMENTS

First and foremost, I would like to thank Professor Aaron Dollar for giving me the opportunity to learn and do research across fascinating topics and helping me become an independent researcher. I would also like to thank Professor Brian Scassellati, Professor Madhuudan Venkadesan, and Professor Francisco Valero-Cuevas for providing helpful feedback in preparing this dissertation.

This work would not have been possible without the contribution of all the GrabLab members throughout my tenure at Yale. In particular, I would like to thank Professor Adam Spiers for guiding me in the early stages and Dr. Joao Bimbo in the final stretches. Of course, I have to thank Neil for always being available to discuss research with me, his knowledge of all things continues to amaze me. And to all the other members of the lab, thank you for having made this journey as scholarly as it was fun.

TABLE OF CONTENTS

LIST OF FIGURES

LIST OF TABLES

1 INTRODUCTION

1.1 Motivation

In our evolution, the human arm has long shifted away from its primary role of gaiting to becoming a remarkable tool that enables us to complete a wide range of manipulation tasks. Unlike gait, the tasks that our arms now accomplish are often much more complex, and range from reaching, grasping, and transferring objects and tools [1], [2]. In combination, these movements enable us to complete tasks that are often referred to as activities of daily living (ADL); these include feeding, dressing, supporting movement, and communicating. Many efforts have therefore been placed on preserving functional abilities and healthy arm motions in the elderly, rehabilitating stroke victims, and augmenting amputee patients with prosthetic devices. This work, in particular, focuses on the later.

Enabling upper-limb prosthesis users to effectively position and orient an end-effector is an ongoing challenge, often overshadowed by grasping [3]. For transradial amputees, it is arguably as important to be able to have wrist rotation as it is to have multiple grasp types when attempting to complete ADL tasks. A lack of proper joint control can lead to unnatural movements [4], with many users developing overuse syndromes [5]. The absence of an intuitive control interface is part of the reason why 3 degree of freedom (DOF) wrist devices are not mainstream on the market, which does nothing to abate the high prosthesis abandonment rates [6]. For more extreme levels of upper-limb amputation, namely transhumeral amputation and shoulder disarticulation, 4 DOF (elbow-wrist) and 7 DOF (shoulder-elbow-wrist) prosthetic devices add an additional level of control complexity that makes the control problem even more challenging. This thesis therefore aims to create an intuitive prosthesis control, and to further encourage the development and consumer acceptance of a physical device.

Advancements in prosthetic devices alone are inadequate without an intuitive or practical way for amputees to control them [7], and various groups have attempted to bridge the gap. One approach is to determine synergies between the residual limb and the device, such as between shoulder or elbow and the wrist in transradial amputees [8]–[11]. These methods make use of surface electromyography (sEMG) signals or kinematic data obtained from inertial measurement units (IMUs) from the residual limb, and are trained, using artificial neural networks (ANNs), to interpret

user intention and activate the proper control response. Although these are robust under certain conditions, aside from requiring additional sensing equipment, they are impractical for mass use due to the very involved training and retraining phase that is unlikely to reach the majority of potential prosthesis users.

Synergistic controls have also been proposed without the use of ANNs, such as on-line optimization techniques in transhumeral amputees [12]. Wrist or elbow rotation could also be directly coupled to shoulder abduction [13], [14]. Bimanual manipulations have also inspired a wrist device control that mirrors the opposing healthy wrist by taking advantage of symmetric or anti-symmetric motions [15]. In shoulder disarticulate amputees, directly controlling the 3 DOF of the device's shoulder becomes less tractable, and solutions have included controlling the whole arm in the end-effector space using a foot interface [16] or, in the case of a wheelchair mounted robotic arm, a joystick [17]. These proposed approaches offer users an additional control input beyond the two-site sEMG [18], and while they enable users to perform complex arm motions, they also impose a cognitive burden that limits their efficacy. One way for a control interface to be successful is to enable the same capabilities afforded by multiple simultaneous inputs that are able to complete complex movements while making use of the simplicity of an existing sEMG prosthetic interface.

Prosthetic cosmesis is the art of making prosthetics appear human-like, and is a priority among amputees [19]. Despite many efforts placed on generating human-like motions in robots and robotic arms [20]–[22], prosthetic control research has not yet taken this into consideration. I coin the term "movement cosmesis" to refer to how human-like a prosthetic control appears, and include it in evaluating different methods.

1.2 Objective

The primary aim of this thesis is to generate smart control modes for various prosthetic devices. The approach is to reduce the dimensionality of the activities that a prosthetic arm would need to perform and find intuitive ways to extract a generalizable subset of motions. The main goal is therefore to identify a data driven analysis pipeline that can be verified both heuristically and quantitatively. A robust analysis approach would generalize between different arm models, whether analyzing just the wrist or the whole arm. This is particularly important since there is no one correct way to analyze the data, and heuristics cannot be relied upon when the motion is unintuitive. Literature suggests that whole arm motions are planned around the desired location of the hand rather than the angle positions of the joints [16]. Therefore, if a categorization approach is able to generate intuitive and useful arm motion groupings based on joint-angles alone, then it will likely generate useful elbow-wrist and wrist groupings as well.

Subset of motions for each device should be tested against state of the art approaches. The objective would then be verify the choice of analysis methods that generated the motions, and demonstrate the efficacy of the proposed prosthesis control approach. The efficacy of virtual reality testing would be evaluated as well.

1.3 Outline

This thesis covers a series of extensive human subject studies, investigating both healthy arm and prosthesis use. Chapter 2 introduces a study where able-bodied participants completed tasks related to ADL in a controlled laboratory environment. The 6 DOF of information of each arm segment was recorded, and included the hand, elbow, shoulder, and torso. Shoulder, elbow, and wrist joint angles are then extracted. The dimensionality of arm motion is further reduced through a series of data driven approaches that looked to identify natural categorization of arm kinematics, while offering insight into categories of ADL. Prototypical arm motions are then calculated from each cluster, and are presented as a template for use in a prosthetic device, coined as *trajectory* control. Since the primary goal was to address inadequacies in prosthesis use, categorization of arm motion included just the wrist data at first as it applies to controlling 3 DOF prosthetic wrist device. Analysis was then extended to the 4 DOF elbow-wrist and 7 DOF shoulder-elbow-wrist prosthetic devices by considering both the elbow and wrist simultaneously, and the entire shoulder, elbow, and wrist complex, respectively. Potential shortcomings of this control approach are also discussed and one solution is proposed through the characterization of motion variation within each motion cluster.

Chapter 3 makes use of the same data, but provides a different analytical perspective. Observations from Chapter 2 motivated a look at hand use alone, rather than the whole arm. Instead of reducing the dimensionality to joint angle trajectories, motion is instead analyzed by decoupling location and orientation information of the hand. Categories of hand use are found by analyzing both the Cartesian trajectories of the hand through space, as well as the desired end-point locations that subjects normally place their hands with respect to their torso. Orientation groups are then found within each location category. This provides a verification of the results found in Chapter 2, while also presenting an additional control method for prosthetic devices.

Chapter 4 describes a virtual reality testing platform and a series of pilot tests aimed at evaluating the *trajectory* control method. Virtual reality has been gaining popularity as a low-cost approach to evaluate prosthetic devices [23], and the absence of complex prosthetic devices on the market necessitated its use. It also provided a platform to address the challenges that prosthesis users will likely face, and therefore motivate the development of physical devices. A

virtual 3 DOF prosthetic wrist device is designed and programed to be controlled by able-bodied participants whom are offered different types of prosthesis controllers. Preliminary evaluations point to the benefits of *trajectory* control while reaffirming the motivation to pursue more complex prosthetic devices.

Finally, Chapter 5 presents a comprehensive human subject study that builds upon findings from Chapter 4. Improvements are made to the virtual reality testing platform by adding more realistic testing conditions. 4 DOF elbow-wrist and 7 DOF shoulder-elbow-wrist devices are included in the experiment as well. Beyond just evaluating the efficacy of *trajectory* control in different prosthetic devices, insight is also made into prosthesis use in general. Practical limitations of *trajectory* control are discussed.

2 PROTOTYPICAL ARM MOTIONS

In this Chapter I present a data driven categorization and identification of prototypical upper-limb motions related to ADL. The goal is to identify motions relevant to different degrees of upper-limb disability or amputation, and therefore shoulder, elbow, and wrist motions are investigated. In addition, motion variation is established using fPCA and results encourage further investigation for use in real-world applications.

2.1 Background

Despite the complexity of arm motions that enable us to accomplish many different tasks, there is a degree of regularity between individuals that does not impose much cognitive burden [24], [25]. In fact, upper-limb motions have been successfully described using dynamic movement primitives [26].This may be surprising since there are infinite solutions to position and orient the end-effector with an over-constrained 7 degree of freedom (DOF) arm. Mathematical models have even been found to successfully predict certain arm motions, such as a jerk minimization model [27]. I therefore predict that the spectrum of arm motions can be distilled to a small, yet representative, subset of motion models. This can be done heuristically, for example, by separating tasks based on ADL categories, such as feeding and dressing, or by subdividing whole tasks into reaching and transferring motions. This might lead to intuitive, and potentially useful, motion categories for a full 7 DOF arm (shoulder-elbow-wrist), but is an impractical approach when looking to obtain categories of motion for a 3 DOF (wrist) and 4 DOF (elbow-wrist) models; hereafter "arm motions" refer to any of any of the three arm models.

Instead, I implement unsupervised learning techniques that use data driven approaches to extract categories of motion that minimize the variation within while maximize the variation between them; this is also known as clustering. Clustering is a knowledge discovery approach that quantitatively builds a categorization model, as opposed to training a classifier with pre-labelled data, and would therefore be most appropriate at identifying motion categories that could be quantitatively validated. Obtaining subsets of upper-limb movements can be useful in a variety of domains, including operating a semi-autonomous prosthetic device by combining series of sub-motions to accomplish a larger set of tasks. Since the goal is to eventually have prostheses users interface with these motion categories, the intuition

behind the results must play a role. Therefore, I first confirm that the clustering results for the 7 DOF arm align with heuristics, and then proceed with examining 4 and 3 DOF motions with more confidence.

Research groups investigating control of active prosthetic wrists and elbows have previously used joint synergies while primarily focusing on a single sub-motion, namely reaching [10], [28]. Our methodology aims not to only validate reaching as a unique motion category, but also stratify all sub-motions to a hierarchical structure and formalize the sub-motion categories, which include motions related to reaching, transferring, and manipulation. In addition to the present focus of developing prosthesis controls, this work enables future efforts to take advantage of and focus on demonstrable categories of motion.

Previous research efforts on upper limb motion have spanned various disciplines and techniques aimed at gaining insight into how humans make use of and control their upper limbs. Research methods have included neural networks, non-linear control, and musculoskeletal modelling [29]. Some investigations have attempted to control upper-limb prosthetic devices by identifying and making use of underlying healthy motion patterns [30], [31]. These include performing pattern recognition of simultaneous motion primitives [11] or using artificial neural networks to discriminate or predict upper-limb functions [10], [32] in healthy participants. Other groups extracted subsets of arm motion primitives from healthy participants using functional principal component analysis (fPCA) [33]–[35]. Instead of using a linear combination of movement primitives to perform a complete task, a more straightforward approach to controlling an upper-limb device could instead be made up of a sequence of individual sub-motions, as is proposed in this paper. Hierarchical description and on-line motion recognition of non-ADL motion segments have been performed in [36]. However, efforts were on creating non-deterministic automatic motion recognition technology of whole body motions rather than on sequential motion segments. Other relevant fields, including rehabilitation, have analyzed the ranges of joint angles as a measure of healthy motion patterns [2], [37], [38]. Although efforts have been made to extract underlying motion patterns [10], [33], [36], none have deterministically stratified arm motions related to ADL.

2.2 Experiment Design

The aim of this experiment was to collect data related to healthy arm motions, specifically time-series information of each body segment location in space and joint angles. This required an in-lab set up, where conditions could be

highly controlled and where motion could be studied in detail. The protocol was designed to include tasks that maximize the range of actions that people normally perform while minimizing fatigue.

2.2.1 Task Protocol

Due to the large variety of motions that the human arm can achieve, it was important to focus our clustering efforts on motions that are relevant to daily life, i.e. common tasks related to ADLs (Figure 2.1). The selected tasks that were included in the present work were largely inspired by standardized 'outcome measure' assessment tools of arm function, such as AM-ULA [39], and reports that surveyed motion-impaired participants regarding which tasks they prioritize [6], [40], [41]. The identified tasks were crucial for independent living, and included food preparation, hygiene, dressing, grooming, and eating are listed in Table 2.1 accompanied by task specifications in Figure 2.2; none of which are considered physically challenging. Only a subset of AM-ULA tasks were included that had identifiable start and end points, such that complex motions that occurred during a task could be segmented into distinct motion segments. For example, the drinking task involves distinct sub-motions such as reaching, drinking, and returning the cup to the table. Tasks that lacked distinct motion segments were omitted and include folding a towel or donning a shirt. Omitted tasks also include small amplitude cyclical tasks, such as stirring with a spoon or cutting with a knife. The 24 tasks were segmented to 2 to 6 motion segments, yielding 85 distinct motion segments that were collected from each participant.

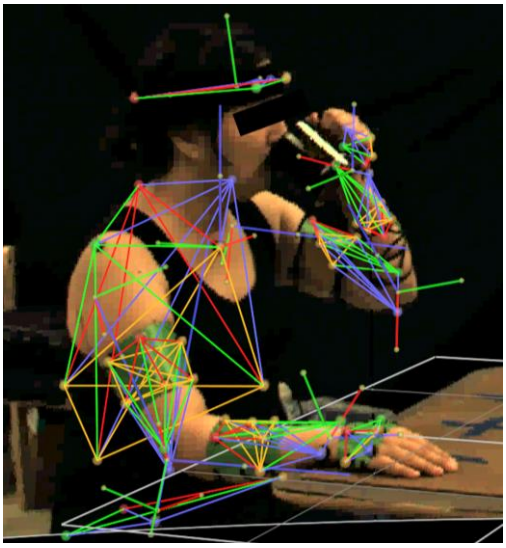

Fig 2.1 – Subject performing an ADL task, drinking from a mug. The subject's motion capture 'skeleton' is superimposed in this image. Redundant markers are included to enable the prediction of occluded marker locations and maintain the ability to identify joint centers.

Table 2.1 – Tasks and corresponding motion segments

Task Code	Standing Tasks[a]
t2b	(1) reach box on top shelf (2) move box to bottom (3) return hands
b2t	(1) reach box on bottom shelf (2) move box to top (3) return hands
t2m	(1) reach box on top shelf (2) move box to mid (3) return hands
m2t	(1) reach box on mid shelf (2) move box to top (3) return hands
m2b	(1) reach box on mid shelf (2) move box to bottom (3) return hands
b2m	(1) reach box on bottom shelf (2) move box to mid (3) return hands
ke	(1) bring key to keyhole (2) turn key (3) turn back (4) remove key from keyhole and return hand
kn	(1) reach for door knob (2) turn knob (3) turn back (4) return hand
dh	(1) reach for door handle (2) open door (3) return hand
oh	(1) reach for can on top shelf (2) bring can down in front of the body
mp	(1) reach for mug in C1 (2) take a sip (3) return mug (4) return hand
md	(1) reach for mug in C2 (2) take a sip (3) return mug (4) return hand
mc	(1) reach for mug in C3 (2) take a sip (3) return mug (4) return hand
cp	(1) reach for cup in C1 (2) take a sip (3) return mug (4) return hand
cd	(1) reach for cup in C2 (2) take a sip (3) return mug (4) return hand
cc	(1) reach for cup in C3 (2) take a sip (3) return mug (4) return hand
st	(1) reach for suitcase (2) transfer suitcase to table (3) return hands
ax	(1) bring hand to contralateral axilla (2) return hand
pt	(1) bring hand to back pocket (2) return hand
	Sitting tasks[a]
sp	(1) reach for spoon (2) bring spoon to bowl (3) scoop (4) bring to mouth (5) return spoon (6) return hand
fr	(1) reach for fork (2) stab the middle of the plate (3) bring to mouth (4) return fork (5) return hand
ms	(1) reach for mug (2) take a sip (3) return mug (4) return hand
cs	(1) reach for cup (2) take a sip (3) return cup (4) return hand
pr	(1) reach for cup (2) pour (3) return cup (4) return hand

[a]Unless otherwise specified, standing tasks started and ended with the subjects' hands by their side while for sitting tasks the hands were to start and end on the table palm side down.

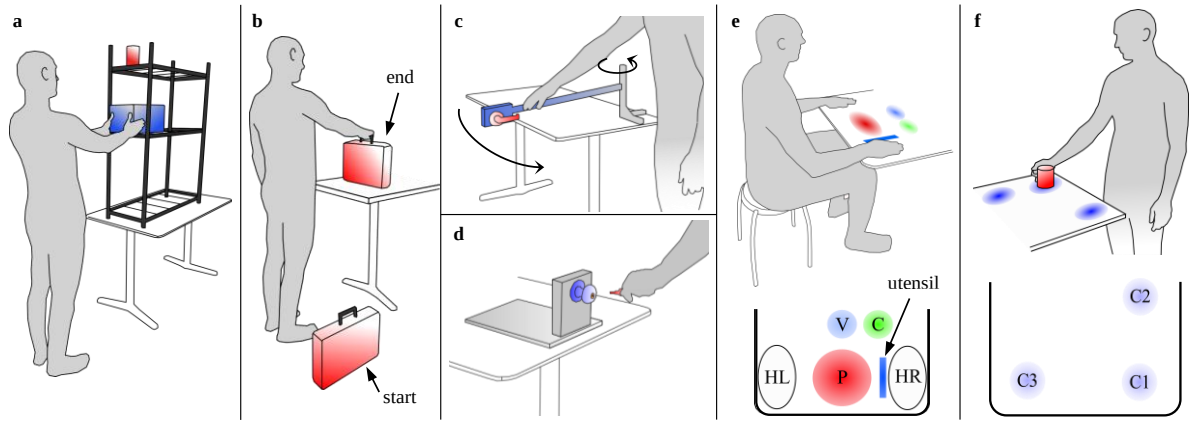

Fig 2.2 – Depictions of several selected protocol tasks: (a) a box object was to be moved from one specified shelf to another. The object on the top shelf is the location of the can during overhead reaching tasks. (b) The initial and final locations of the suitcase tasks, (c) simulated door opening task, and (d) simulated door knob and key tasks. (e) The set up for the sitting tasks: the left and right hand start and end in HL and HR, a utensil is placed next to HR, a bowl or plate are placed in P, a cup or mug is placed in C, and a container to collect the water during the pouring task is placed in V. (f) The three target locations of the standing cup and mug tasks, during which the table is elevated to simulate a countertop, where C2 is 25 cm from C1 and C3 is 45 cm from C1. The task conditions for left handed participants are mirrored. Table height is 74 cm, and is elevated to 92 cm to simulate a counter top for the standing cup and mug tasks. The mug (9.5 cm height, 8 cm diameter), can (7.5 cm height, cm diameter), box (21x37x19 cm), and suitcase (43x9x30 cm) weigh 0.36, 0.09, 0.23, and 1.36 kg respectively. The shelves are 80, 140, and 180 cm above the floor. Door knob and handle are 90 cm above the floor, and the simulated door swivels with an 84 cm radius.

Alternative tasks and protocols were considered but ultimately excluded. This includes the Southampton Hand Assessment Procedure (SHAP) and the Box and Blocks, assessment tools that have been used to evaluate rehabilitation progress post stroke and prosthetic devices. Since both are timed tests with predefined hand positions, arm motions are unlikely to be "natural". While I steered away from timing the tasks or requiring the completion of tasks to be performed in any specific way, the protocol included tasks that were in part inspired by SHAP, such as *pouring from a cup* and *using a key*.

Each task was repeated 3 times, providing a way to average and smooth the motions as well as account for outliers during analysis. Though participants were instructed to begin and end each task in predefined 'rest poses', hands by

the side of the body for standing tasks and with the palms on the table for sitting tasks, minimal instruction was given on how the tasks should be completed. Participants were free to complete the tasks in any way that felt "natural". Although many breaks were included throughout the experiment to further avoid physical and mental fatigue, such as between tasks, participants were given as many additional breaks as they requested; most opted out, but some took one or two additional 5 minute breaks. The tasks was inverted for left-handed participants.

The protocol was completed by 12 (6 male, 6 female) healthy participants, chosen to uniformly span the age groups of 20-70 so as to make the motion analysis results as generalizable as possible (also for prosthesis application); this resulted in a final age range of 24 to 71, mean of 43, and standard deviation of 15. Participants performed 24 individual tasks over the course of a single 5 hour visit.

2.2.2 Data Acquisition

Arm motions were recorded with Vicon Motion Capture System (Oxford Metrics Limited, Oxford) using 12 infrared 'Bonita' model cameras (100 frames/second), 1 video reference camera, and 55 reflective markers placed on the body. The video camera was synchronized with the motion capture cameras and was used to help with marker identification within the Nexus software.

2.3 Data Analysis

The purpose of this analysis is to identify how upper-limb motions related to ADL cluster and obtain a subset of representative motions using data driven approaches. The data processing and analysis pipeline is illustrated in Figure 2.3. The motion data is first converted to joint angle trajectories and manually segmented into sequential reaching and manipulation movements. Each sub-movement is then averaged across repetitions. A distance matrix is created and used for clustering. Clusters are evaluated twice: first to decide on the number of clusters, then against alternative algorithms. Finally, representative motions are obtained from each cluster and their respective variances are computed. Since the 4 DOF shoulder-elbow model was included solely to compare against the 7 DOF system, this portion of the analysis is limited to only obtaining the clusters.

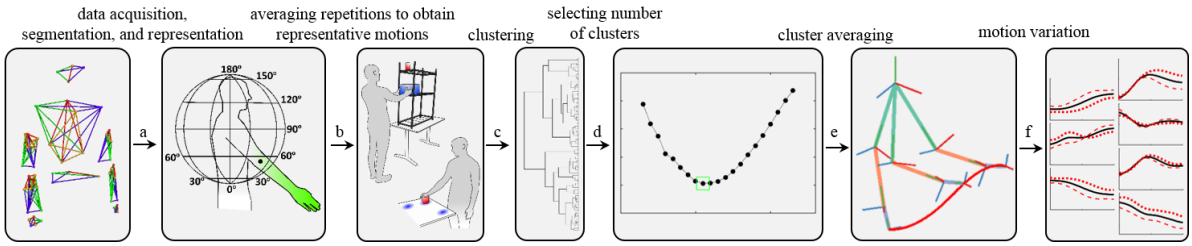

Fig 2.3 – General framework of the data processing and analysis. (a) Cartesian coordinates of markers tracking human motion are converted to arm joint angles, creating a set of feature variables generalizable across subjects. (b) Repetitions of different motions and subjects are segmented and averaged. (c) The motions are compared using DTW and clustered using agglomerative hierarchical clustering with Ward's linkage distance. (d) The L method is used to select the number of clusters from the dendrogram. (e) Each cluster is averaged and (f) within cluster variations are calculated using fPCA. Steps (b-f) are repeated for each of the three DOF arm models. Steps (b-d) are repeated once more for the 4 DOF shoulder-elbow model.

2.3.1 Motion Representation

Recorded human arm motion data can be represented in several different ways, such as joint angles of the shoulder, elbow, and wrist, or Cartesian coordinates of each arm segments. Although the joint angle method suffers from the unequal impact that different joints have on the end effector trajectory, fewer variables are required to reconstruct the upper-limb than Cartesian coordinates. A lower dimensional representation of arm motion is an important factor for calculating similarities while joint angle trajectories are easily interpretable and implementable prosthetic devices. The simplicity of the joint-angle system was therefore used through the rest the paper. The simplicity of the joint-angle system was therefore explored in this chapter, and the Cartesian location of the hand is explored in the next.

The upper-limb joint angle systems are based on 3 DOF wrist, 4 DOF elbow-wrist, and 7 DOF shoulder-elbow-wrist models, defined according to [42], hereby referred to simply as 3 DOF, 4 DOF, and 7 DOF models, respectively. Additional analysis is performed on the 4 DOF shoulder-elbow to verify some of the observations made for the 7 DOF model. The shoulder angles consist of plane of elevation, angle of elevation [43], and internal axial rotation, using the second option for the humerus coordinate system in [42] and is detailed in Figure 2.4. The elbow angle is formed using the forearm and humerus, while wrist angles include supination, wrist flexion, and ulnar deviation. For left-

handed participants, the joint angles were inverted so that they are congruous to right-handed participants for the purpose of analysis.

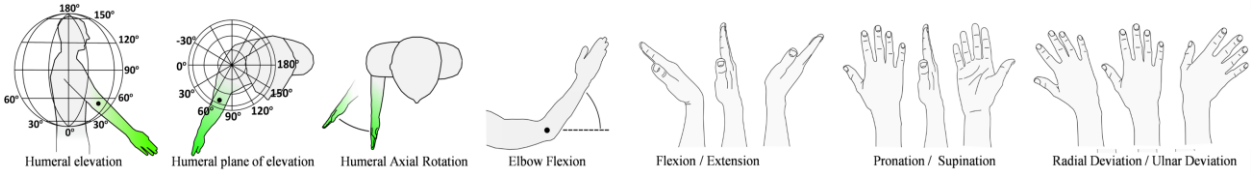

Fig 2.4 – Humeral elevation and plane of elevation are depicted using the globe system described in [45]. The elbow is positioned below the shoulder in the image to depict humeral axial rotation.

2.3.2 Motion Segmentation

Hand motions during ADLs, whether reaching or manipulating an object, can be seen as a composite of a series of individual sub-motions through which generalized tasks, such as drinking from a cup, are accomplished. Many quantitative approaches exist to human motion segmentation and are often based on analyzing various features of motion or use statistical and machine learning tools, such as principal component analysis (PCA) or Hidden Markov Models (HMM) [44]–[47]. Ultimately, verification of segmentation is performed heuristically by comparing results to predefined ground truths. Therefore, instead of implementing an automatic segmentation technique, the start and end points of each motion segment were manually defined by identifying when the end effector reached zero velocity, when a food item was acquired (analogous to [48]), completed a transfer or task, or returned the object to the table or the hand to its 'rest pose' (Table 2.1).

2.3.3 Divergence Measure

One challenge with comparing time-series data is the difference in duration. Linear resampling of the data fails at properly aligning the epochs, and divergences between motions would appear larger than they should. Modeling the data on the other hand, for example with polynomials, leads to a loss of information. Dynamic time warping (DTW) [49] works by resampling the time-series to equal in length while simultaneously minimizing the sum of square Euclidean distances, and given that the interest is in the kinematics of the arm and not the time component, this was an appropriate option. It works according to the following equation,

$$D(i,j) = min\begin{Bmatrix} D(i-1,j) + d(i,j) \\ D(i-1,j-1) + d(i,j) \\ D(i,j-1) + d(i,j) \end{Bmatrix}, D(1,1) = d(1,1) \quad (1)$$

where d(i,j) corresponds to the Euclidean distance between the DOF of frame i of one motion segment and the DOF of frame j of the second motion segment. The optimal path is then calculated through matrix D(i,j) by starting at the last frames of each of the motions and moving backwards through the smallest distance values.

Because similar motions may be moving in opposite directions, such as bringing the cup to the mouth and returning it to the table, it was necessary to calculate DTW twice, once with the original data and once with one of the motions moving in reverse; saving the smaller of the two calculations. Divergence values are normalized by dividing by the new time duration obtained during DTW. This is done so that the DTW comparison made between longer and shorter motions segments are comparable, and I refer to it as normalized-DTW. While this approach may bias longer segment comparisons, provided that the arm motion segments are on the same time scale this error is minimized. Although more robust DTW normalization methods exist, such as normalizing by the square root of the length [50], they did not significantly alter the results, and are therefore excluded from the analysis.

2.3.4 Averaging Motions

Averaging of motions was performed during two separate phases throughout the analysis. The first time it was to average repetitions to obtain a single representative motion across participants; each final motion segment was an average of 36 motions (three from each participant). The second use of averaging was to identify a representative prototypical motion for each cluster. There are a variety of ways to computing a time-series average, the simplest one entails a linear resampling followed by a frame by frame averaging. DTW barycenter averaging (DBA) algorithm [51] is used instead, as it better handles phase shifts in the motions and epoch alignment. This method is based on the idea that an average is simply the point that minimizes the summed distances between the data and itself. Same is done in DBA, where a consensus segment is identified by minimizing the DTW distance with all other data time-series data.

One precaution that had to be made during DBA is that it is prone to local minimums, where the consensus segment will accentuate the amplitude of certain frames to minimize the DTW distance [51]. Although more complex algorithms exist that attempt to deal with such issues, such as [52], I simply limited the amount of frames that can be warped to the minimum amount possible when performing DTW between the shortest and the longest motion segment pair in each group.

2.3.5 Agglomerative Hierarchical Clustering

In the present study I sought a clustering algorithm that effectively minimizes variation within clusters, maximizing the difference between clusters, while depicting the underlying structure of the data. In order to further distinguish arm motions, the algorithm would ideally result in clusters that are "spherical" rather than interconnected. Agglomerative hierarchical clustering [53], [54] with Ward's linkage criterion, or simply distance, accomplishes this while presenting the data in an easily interpretable dendrogram illustrating the distance relationship between the motion segments. The algorithm works by successively merging clusters based on a distance criterion until all but one cluster containing all of the data remains. Ward's linkage criterion, unlike complete linkage (furthest-neighbor) or single linkage (nearest-neighbor), creates distinct "spherical" clusters by accounting for both the within and cumulative cluster variances according to

$$W = SS_{12} - (SS_1 + SS_2) \tag{2}$$

where W is the calculated Ward's distance value, SS_{12} is the sum of squares of the combined cluster, and SS_1 and SS_2 are the sum of squares of each of the members of the cluster to its respective centroid. Although this method does not make adjustments to the clustering once a merge decision has been made, proper outlier and noise handling will mitigate this issue; I do so by averaging repetitions, outlined in Section 1.2.4.

A set number of clusters can be extracted from the dendrograms in a variety of ways. While heuristics can be used to select a seemingly reasonable number of clusters for the 7 DOF model, the 4 DOF and 3 DOF models do not lend themselves to an easy interpretation. Therefore a data driven approach called the L method [55] wa used to identify an "optimal" number of clusters. The method was used with a greedy evaluation approach, as recommended in [55], and only considers the Ward's distance (2) value between the two clusters being merged. Unlike other approaches that only evaluate the data locally or are sensitive to noise, the L method makes use of the entire set of distance values between each merging pair to determine the point of transition, the "knee", between the internally homogenous and non-homogenous cluster merging phases (Figure 2.5). It works by linearly fitting each phase while varying the sequence of points that belong to each and calculating the total error, $RMSE_{tot}$, according to

$$RMSE_{tot} = \frac{c-1}{b-1} \times RMSE(L_c) + \frac{b-c}{b-1} \times RMSE(R_c) \tag{2}$$

where c and b correspond to the partitions of the distance data belonging to the left and right side, respectively, and L_c and R_c are the lines of best-fit, respectively. L_c and R_c must have at least two points, and c and b always add up to

the total number of points. A value of c which minimizes $RMSE_{tot}$ corresponds to the "optimal" number of clusters. Certain improvements to the L method were additionally recommended by the authors [55], and are implemented in the results. These include adjusting the number of mergings that are being evaluated and removing the set of data left of the point corresponding to the largest distance.

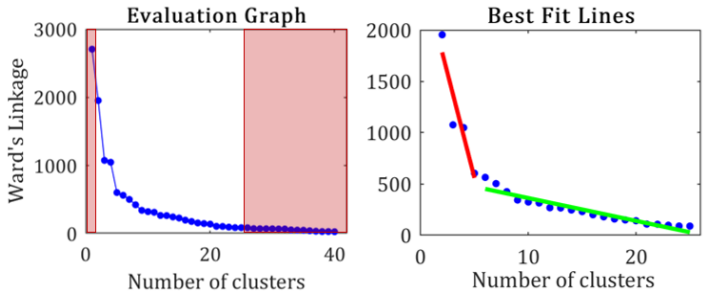

Fig 2.5 – Left plot depicts the suggested windowing of the merge distance data, as suggested in [57]. The right plot depicts an application of the L method; identifying the "knee" of the graph.

2.3.6 Cluster Quality

By re-computing the hierarchical clustering dendrogram using individual motions, rather than the average of each motion type, an evaluation score that captures how consistently repetitions cluster can be computed,

Table 2.2 - Compute clustering quality pseudocode

Input: vector of cluster membership ID of each motion segment

Output: evaluation score as a %

```
1:  Let max_score equal to 3060 // 12 subj.*85 motion segments *3 repetitions
2:  Initialize score to 0
3:  foreach cluster do
4:      foreach pair of cluster members do
5:          if cluster members are repetitions then add 1 to score
6:      end
7:  end
8:  return score / max_score * 100
```

The quality score is at its maximum for a single cluster containing all of the motion segments and decreases monotonically as the number of clusters increase. The evaluation score could theoretically remain at 100% up to 1020

clusters; 85 unique motions from 12 participants. Common clustering methods are additionally evaluated to validate the selection of the primary methodology: K-medoids clustering and Euclidean distance between motions represented using coefficients belonging to cubic Bézier fits.

The algorithm provides an opportunity to compare the selected cluster methodology to alternative motion representation and cluster methods. K-medoids clustering is tested using DTW divergences, similar to [38]. Unlike K-means, K-medoids identifies a median motion segment instead of calculating a centroid. At each iteration, distances between representative cluster medians and the motion segments are calculated, cluster membership is reassigned, and new medians are computed. Ten repetitions of this algorithm were performed to account for local minimums.

An alternative divergence measure was tested; cubic Bézier curves were fit to each joint angle trajectory using least squares, yielding a set of Bézier control points that represented each motion segment. Cubic Béziers have been shown to accurately represent human motion during data compression [56] and hand trajectories [57]. One benefit to using Bézier curves over traditional polynomials is that the first and last control points correspond to the start and end locations of a trajectory. Cubic Bézier curves yielded feature vectors of 12, 16, and 28 elements long for the 3 DOF, 4 DOF, and 7 DOF models, respectively, corresponding to 4 control points. Euclidean distances between the feature vectors were calculated and Hierarchical clustering with Ward's linkage criterion was then used for clustering.

2.3.7 Within Cluster Average and Variation

In order to obtain variation within each cluster, an average was first found, motions were resampled to be equal in duration, and fPCA [58] was used to extract the principal components (Figure 2.6). Each set of the first *n* principal components then explain some amount of variation. Greater motion variability in a cluster will require more principal components to describe the same amount of variation than clusters with homogenous segments.

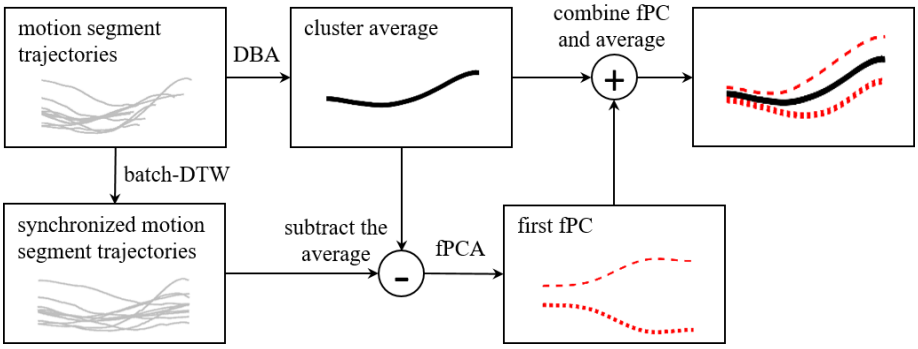

Fig 2.6 – Flowchart depicting the within cluster variation analysis pipeline. Top left panel represents the recorded motion segments belonging to a single cluster for one of the DOF, represented using joint angle trajectories.

As described in section 2.2.1., each motion within a cluster is an average of 36 individual repeated motion segments, therefore a cluster with 2 motions can also be analyzed as a set of 72 individual motion segments. All of the individual motions that occur while replacing the object or returning the hand are first reversed. Then, as in section 2.3.4, DBA is used to identify the average of each cluster, initializing it to have the same number of frames as the longest motion. The individual motions are then resampled to equal in length using batch-DTW [59]. Unlike linear resampling, batch-DTW is better suited for this application by aligning epochs independently for each motion, thus better capturing motion variability. Batch-DTW is an asymmetric DTW algorithm which simultaneously aligns multiple time-series data and retains a non-increasing time-duration, something that is impossible to achieve using standard DTW. It works by first selecting a reference time-series segment, in our case it is the average motion of a cluster, and performing DTW with each of the other time-series data. Each set of frames that are repeated for a single frame of the reference segment were averaged. An example would be if the optimal warping path included *(i-1,j)*, *(i,j)*, *(i+1,j)*, where the $(i-1)^{th}$, i^{th}, and $(i+1)^{th}$ frames of motion M_i are aligned with the j^{th} frame of the reference motion M_j. Batch-DTW would take the following average of the three frames

$$\frac{\left(M_i(i-1,:)+M_i(i,:)+M_i(i+1,:)\right)}{3}$$

Three 3rd order B-Spline [60] elements were fit to each of the newly aligned motion segments (using least squares). The coefficients of the curves are used as feature variables when calculating the principal components [58]. Since the motion alignment considers only the positions of the joint angles, velocity and acceleration information is lost, therefore instead of a 5th order fit as recommended in [27], 3rd order was chosen instead. Three equally spaced B-spline elements were primarily used to better capture the start, middle, and end phases of the joint angle trajectories.

2.4 Results

Figure 2.7 displays dendrograms obtained for the joint angle 7 DOF full-arm model, 4 DOF elbow-wrist model, 3 DOF wrist-only model, and the 4 DOF shoulder-elbow model. A horizontal cut is used to segment each of the dendrograms to obtain a subset of clusters according to the L method described in [55] using the greedy approach, whose results accompany the dendrograms in Figure 2.8. The L method identified the following set of clusters: 5 clusters for the 3 DOF model, and 11 clusters for the 4 DOF elbow-wrist and 7 DOF models. The 4 DOF shoulder-elbow trajectory dendrogram is nearly identical to the 7-DOF model barring two motions being placed in difference clusters, st-2 (transfer suitcase to table) and fr-2 (use fork).

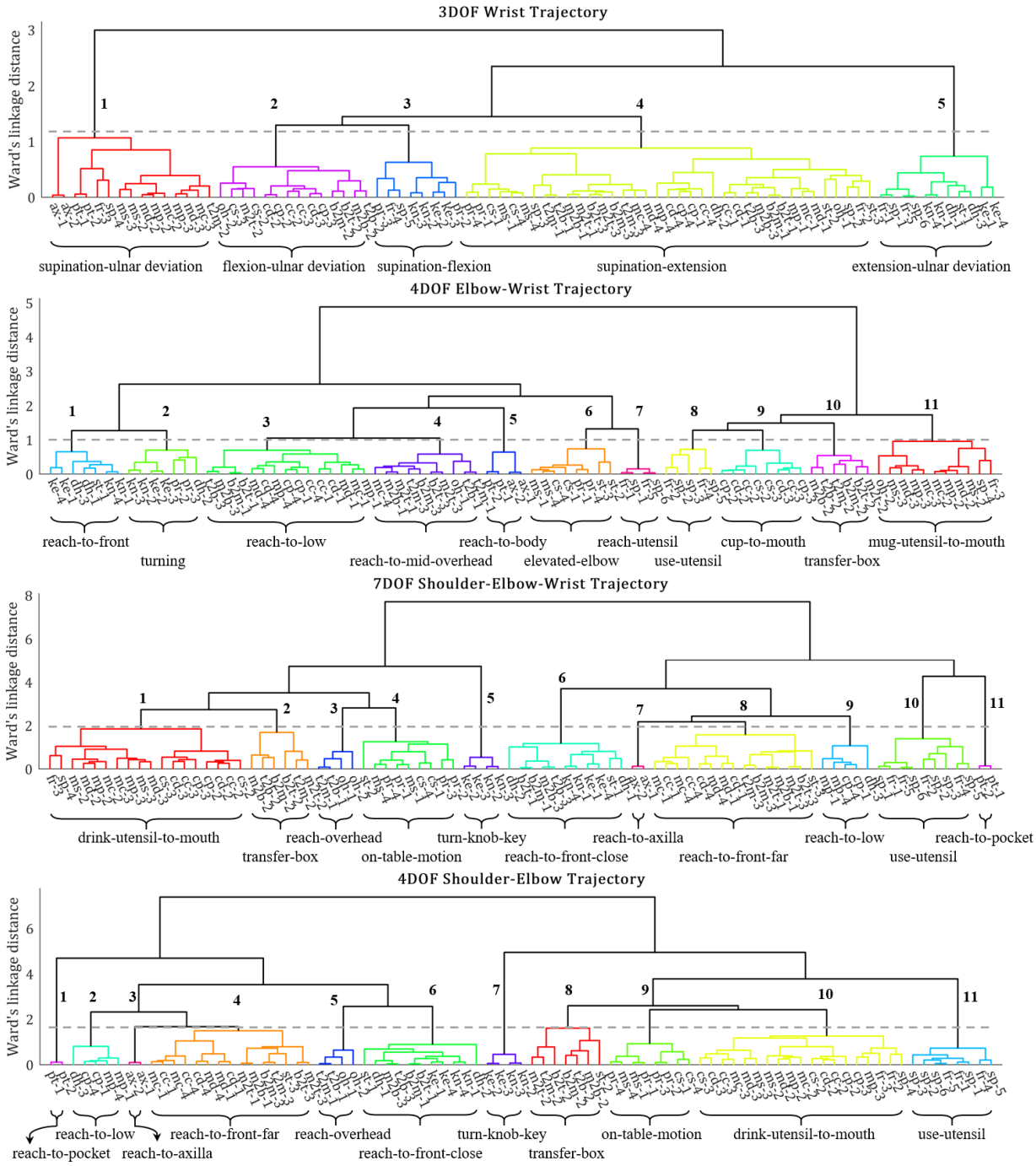

Fig 2.7 – Dendrograms for the 3, 4, and 7 DOF models. Location of the horizontal cut (dashed line) was chosen using results of the L method. An appropriate cluster name accompanies each of the clusters: major axes of wrist rotation for the 3 DOF model and generalized description of the motions for the 4 and 7 DOF models. Cluster colors are auto-generated and are unrelated between dendrograms.

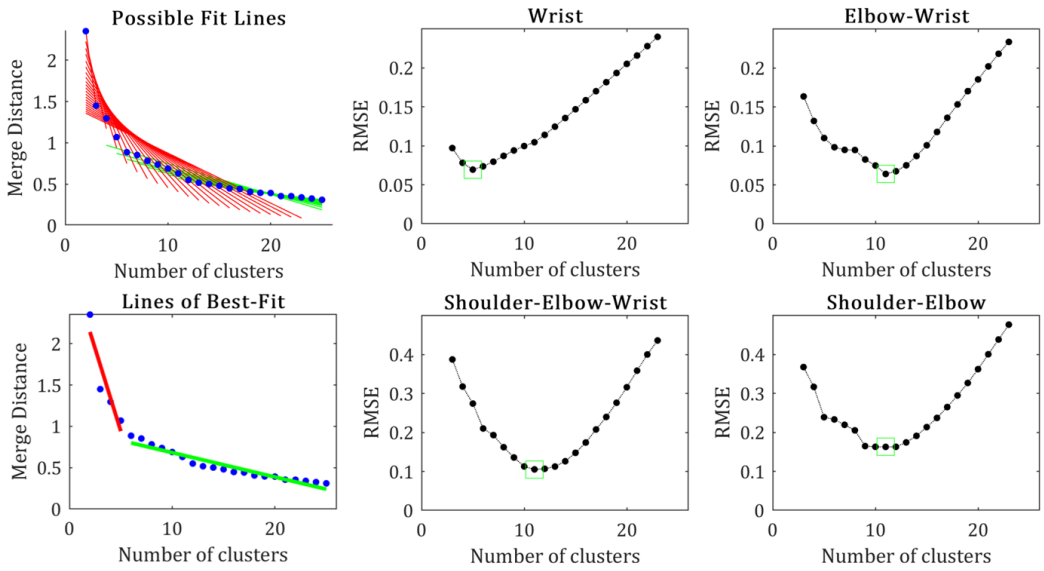

Fig 2.8 – L method results for each of the models. An example of the identified "knee" for the Wrist model is included in two plots in the left column.

One of the L method adjustments recommended by the authors [55] was to dynamically adjust the number of mergings being evaluated down to a minimum of 20 points. In our case, the identified "knee" for 25 merging points was equivalent and I therefore left the additional 5 points in. The largest merging distance for each DOF model was the first merging and therefore the data being evaluated started with the merging distance between 2 and 3 clusters.

Evaluation of the chosen methodology is shown against an alternative divergence measure and clustering algorithm while varying the number of clusters from 1 to 25 (Figure 2.9). This was done for each DOF model. The chosen clustering methodology consistently outperforms the other methods for almost every number of clusters.

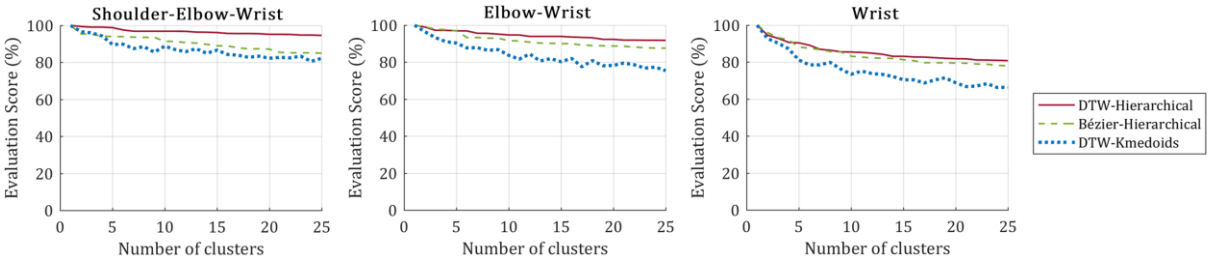

Fig 2.9 – Quality of clustering for different divergence measures and clustering algorithms across a range of number of clusters. Scoring metric assessed how frequently repetitions from the same individuals clustered together.

Due to practical limitations in representing multi-DOF motion with images or complex equations, all the resulting prototypical averaged motions are displayed with only the first principle component in Figures 2.10-2.14. In Figures 2.10 and 2.12, the start, middle, and end poses of the arm are displayed, while in Figure 2.14 only the start and end poses are displayed. The location of the end effector is also traced out throughout the motion. The stick model is created using forward kinematics of the average motion's DOF in MATLAB (MathWorks, US) according to [42], and the accompanying skeleton model was created using an online skeletal animation tool, KineMan (http://www.kineman.com). The motions for the wrist and elbow-wrist models were depicted using a simulated prosthetic hand in Unity.

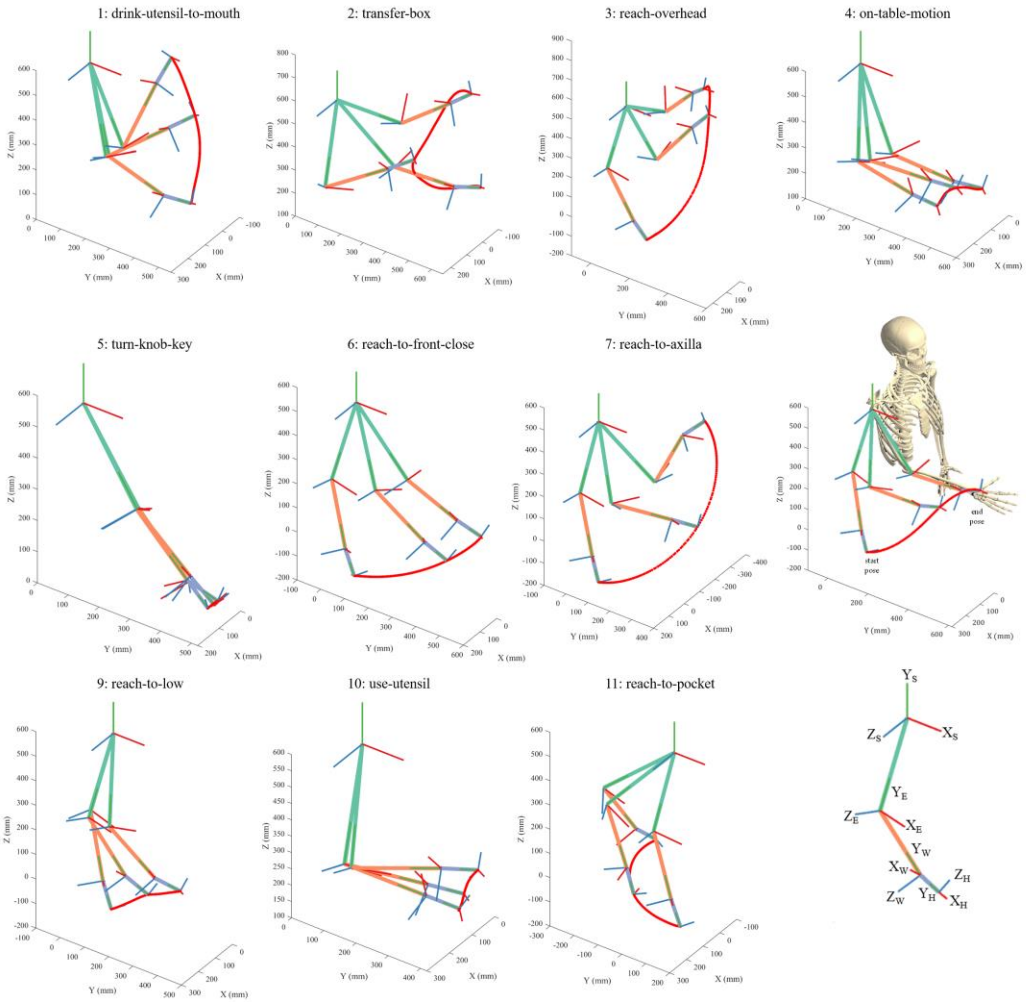

Fig 2.10 – Forward kinematics are used to display the average motion of each of the 11 clusters for the 7 DOF model. A skeleton model in the final pose is included for the 8th cluster: *reach-to-front-far*. Three reference frames are displayed with X, Y, and Z axis using subscripts S, E, W, and H for shoulder, elbow, wrist, and hand, respectively. The shoulder coordinate frame is fixed throughout the motion. Humerus, forearm, and hand lengths correspond to an average adult.

Fig 2.11 – Individual joint angle trajectories for the average of each cluster for the 7 DOF model are displayed along with the first principal component. α was set to equal the proportion of total variation explained by that component. Shoulder1-3 correspond to humeral elevation, plane of elevation, and internal rotation, respectively, while Wrist1-3 correspond to supination, flexion, and deviation, respectively.

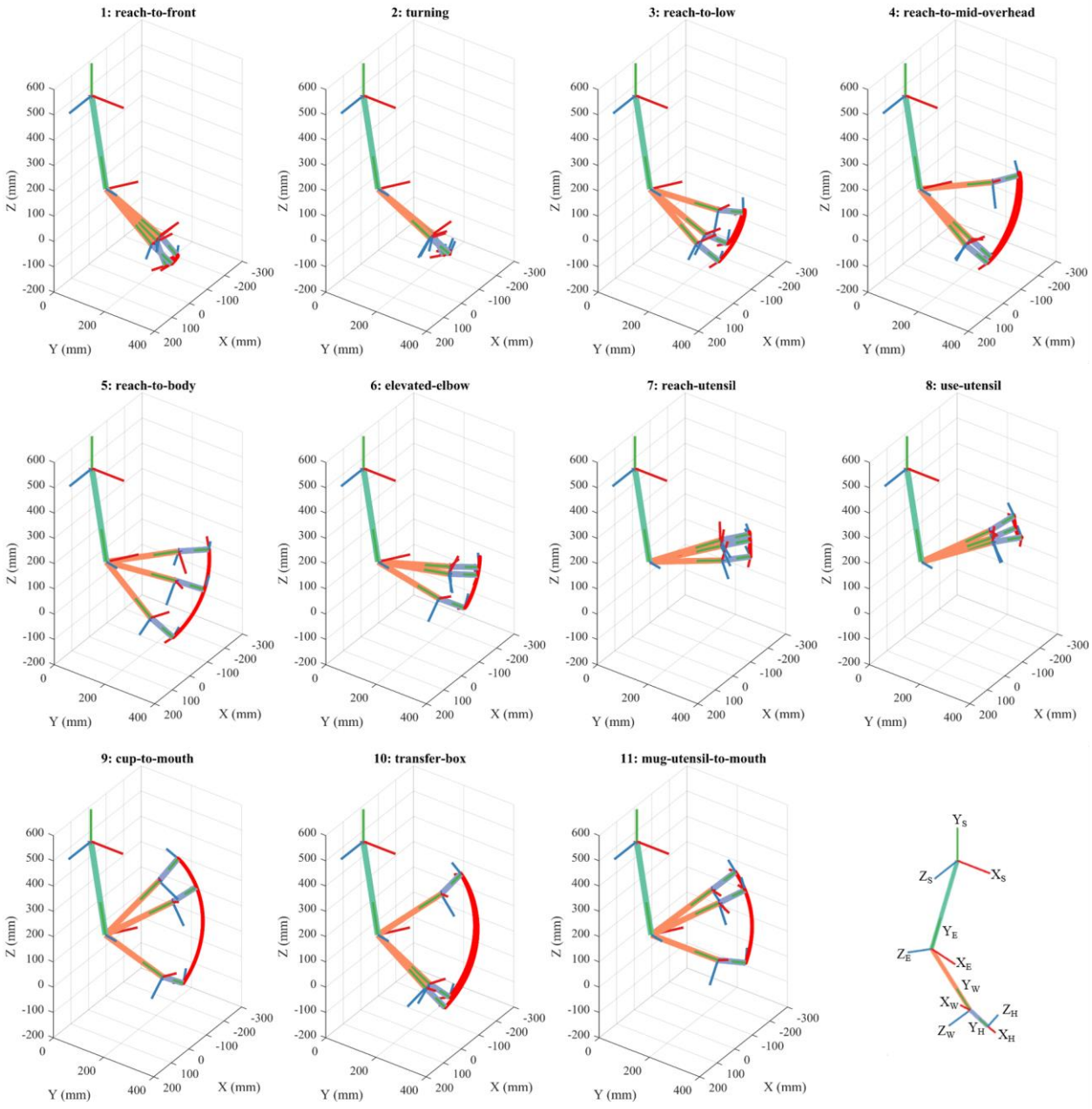

Fig 2.12 – Forward kinematics are used to display the average motion of each of the 11 clusters for the 4 DOF model. Three reference frames are displayed with X, Y, and Z axis using subscripts S, E, W, and H for shoulder, elbow, wrist, and hand, respectively. The shoulder and elbow coordinate frames are fixed throughout the motion, and are only included to provide a reference. Humerus, forearm, and hand lengths correspond to an average adult.

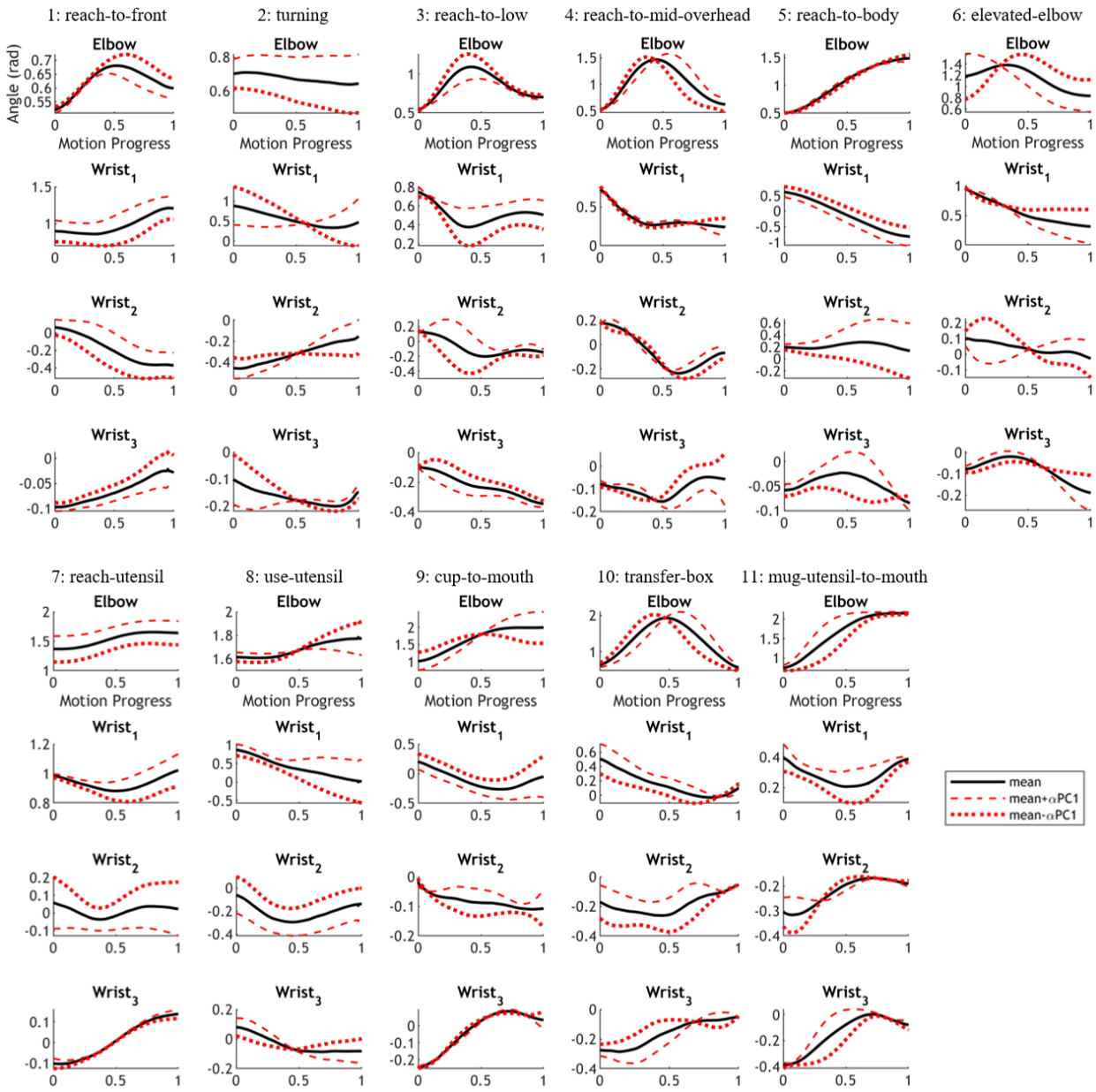

Fig 2.13 – Individual joint angle trajectories for the average of each cluster for the 4 DOF model are displayed along with the first principal component. α was set to equal the proportion of total variation explained by that component. In order, joint angles correspond to elbow flexion, wrist supination, wrist flexion, and wrist deviation.

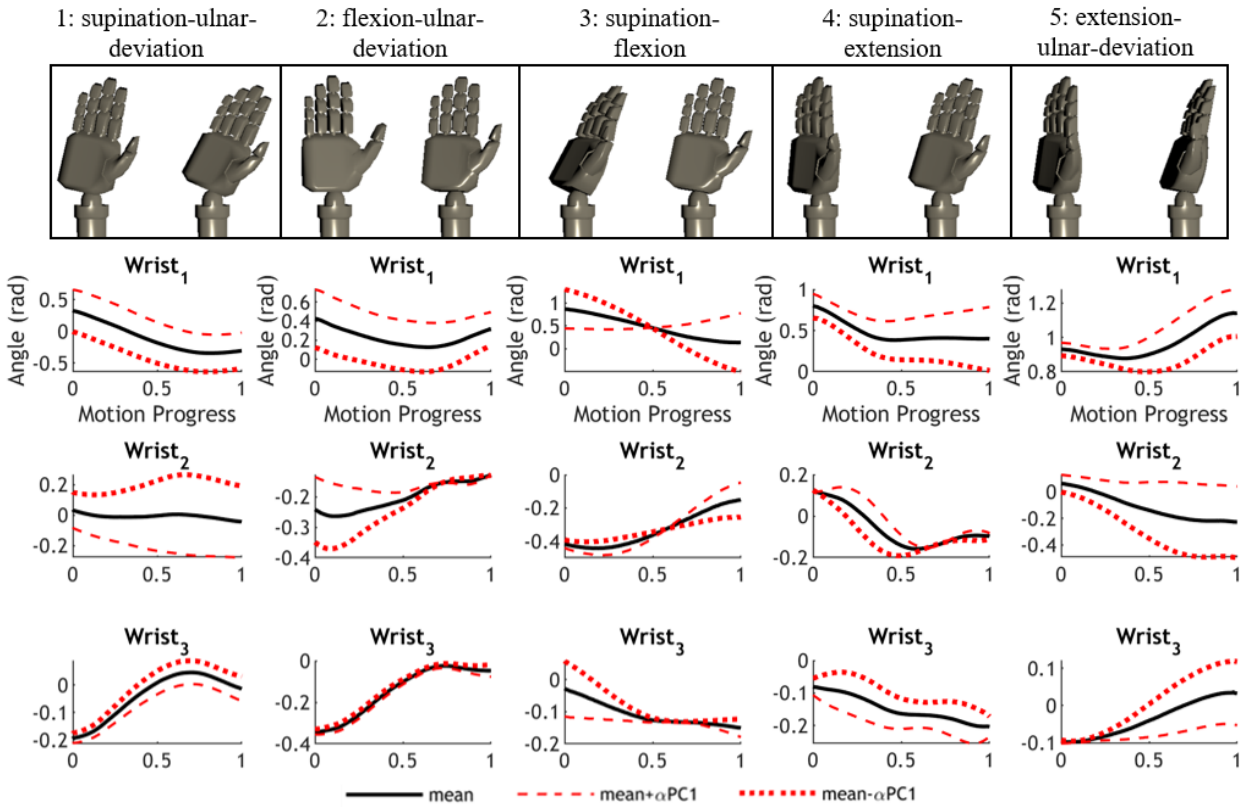

Fig 2.14 – Start and end poses of each cluster for the 3 DOF model are shown at the top along with the average joint angle trajectories and the first principal component right below. The three joint angles in order correspond to supination, flexion, and deviation. α was set to equal the proportion of total variation explained by the principal component. Red arrows indicate the general direction of motion for each of the DOF.

Variation of the motions within each cluster is captured using fPCA. The percent of the variability explained by each set of principal components, i.e. the first n number of principal components, is summarized in Figure 2.15. For each cluster the average pair-wise divergence between cluster members is additionally included, calculated using normalized-DTW. The analysis indicated that while some clusters needed only 3 principal components to describe 80% of the variation, others needed as many as 8.

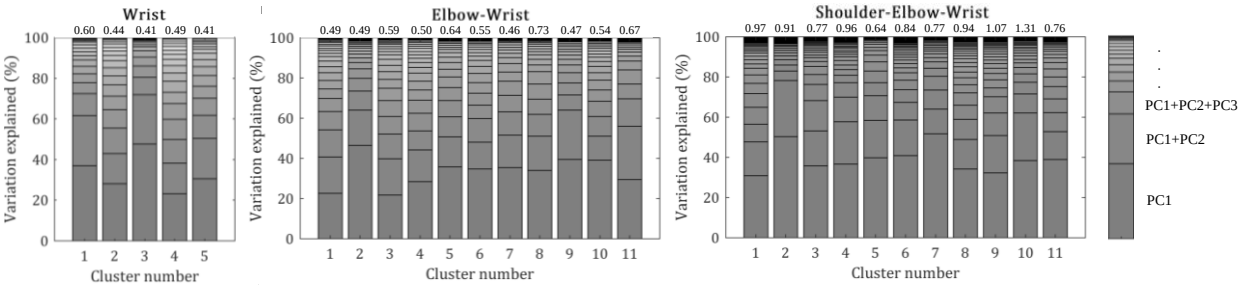

Fig 2.15 – The variation explained by each set of principal components for each joint angle system's averages are displayed. Note that clusters requiring more principal components to explain the same amount of variation is generally consistent with a greater amount of motions they represent. Average pair-wise divergence is included at the top of each bar.

2.5 Discussion

Although the hierarchical tree does not output a specific number of clusters, clustered groups can be obtained by transecting the dendrogram at a desired value. The most straightforward method is using a straight line cut as is seen in Figure 2.7. The location of this cut was chosen using a data driven approach called the L method with greedy evaluation, chosen over global primarily due to greater reliability when selecting the number of clusters [55]. Global evaluations have shown only minor deviations and were not considered in the analysis.

According to the L method, unlike for the 4 DOF elbow-wrist model, 7 DOF and 3 DOF models have a clear RMSE minimum suggesting 11 and 5 clusters, respectively. Clusters obtained for the 7 DOF model, consistent with the spatial control hypothesis where control of the joints is in the subspace of the hand location [61], can be estimated using hand start and end locations while smaller groupings within each cluster are based on other movement characteristics. This suggests that either the wrist motion is synergistic with the shoulder and elbow joints along the motion path [10], [62], or that its range of motion was not significant enough to influence clustering. Depending on the set of motions being studied, it is likely that both are factors. To test this the 4 DOF shoulder-elbow trajectories were analyzed, which identified nearly identical clusters to the 7 DOF model, further suggesting that arm motions primarily clustered according to task location. Therefore when designing a 7 DOF prosthetic device control scheme, priority should be given to the location of the end effector, something that other prosthetists have identified as well [16]. The 3 DOF model too created clusters primarily based on starts and ends of the wrist joint angle trajectories.

Although the global minimum is located at 11 clusters, the 4 DOF elbow-wrist model has an additional RMSE minimum at 6 clusters, indicating the possibility of a second plausible interpretation: clustering result for the 4 DOF model is not a gradual transition between the 7 DOF and 3 DOF models, but rather it exhibits both of their minimums simultaneously. I therefore suspect that 11 and 6 cluster minimums correspond to hand location and wrist orientation, respectively. Although the dendrogram structure for the 4 DOF model is more difficult to interpret, given that 11 clusters were ultimately identified despite the absence of shoulder angles, it would appear that task location information is largely maintained in the elbow trajectory, consistent with the efforts in [10].

3 DOF clusters are summarized as motion types, such as supination or deviation, referring to the most significant degree(s) of freedom. The dart-throwing motion (DTM), a hybrid of flexion and ulnar deviation, which has been described as a more stable and controllable axis of rotation [63], is re-discovered in our analysis as the prototypical motion of the 2nd cluster. Since dendrogram interpretation is limited without animation, and while cluster descriptions for all three models are generalized in Figure 2.7, accompanying figures are included that provide more detail. (Figures 2.10-2.14).

When it came to clustering quality, the chosen divergence measure and clustering algorithm outperformed Bézier and K-medoids methods at almost every number of clusters, reassuring its selection. The performance of K-medoids did not monotonically decrease with added clusters due to the algorithm reaching local minimums despite multiple iterations. Using Bézier coefficients to measure similarities between motions performed worse than DTW likely due to Bézier coefficients merely approximating the data whereas DTW takes the full joint angle trajectories into account and thus calculates a more representative divergence value.

Average pair-wise divergence and fPCA analysis captured the spread of each cluster and the directions of that spread, respectively. Although some clusters require as many as 8 fPC's to describe 80% of the variation, if the average pair-wise divergence is small, this does not necessarily mean that all of those fPC's are required to accurately reconstruct the motions for practical use in a prosthetic device. The torso could potentially compensate for the variation during reconstruction as well.

The demonstrated cluster prototypical motions in Figures 2.10, 2.12, and 2.14 are accompanied Figures 2.11, 2.13, and 2.14 that indicate how these motions vary that could also be used to inform how to dynamically tune the trajectories to compensate for the motion variation within the cluster. This may be an indispensable aspect of control

when, for example, reaching locations occur in continuous space. Future work should take advantage of fPCA findings in implementation of motion control and online adjustments.

If a common set of feature variables is identified, comparison may potentially be made with cyclical motions as well. One challenge is that cyclical motions do not have well defined start and end points, and therefore rely on alternative representation methods such as wavelet or discrete Fourier transform [64]. However, these methods would not be appropriate for the non-cyclical type of data considered thus far in this study.

The decision to use joint angle data as the feature vector largely relies on the ability of recorded motions to be easily interpreted across individuals and its low dimensional representation when compared to other approaches, an important factor when calculating a similarity matrix to be used for clustering. However, this gives each joint angle an equal weight when calculating the differences between motions, which deserves consideration since each joint has a very different effect on the location of the end effector; while it may have be less of an issue for Cartesian coordinates of the upper-limb segments. Additionally, proximity to the discontinuities in two of the shoulder joint angles may cause them to have an even larger impact when measuring motion similarity since the angle range is likely to be greater than for the other joint angles. Finally, although the decision to analyze the 3, 4, and 7 DOF arm models is relevant in a variety of applications, the methodology can be extended to alternative systems, such as to a full body kinematic chain.

2.6 Conclusions

This chapter described a method that categorizes human arm motion during the performance of ADL tasks. Using data driven techniques to measure similarity between motions, average, and cluster, 11 motion categories were identified for the 4 DOF elbow-wrist and 7 DOF shoulder-elbow-wrist models and 5 motion categories for the 3 DOF wrist model. These clusters can be distinguished primarily based on start and end configurations of motions, further differentiated by specific types of manipulation.

The results align with intuition as well, making the proposed method a good candidate to describe other DOF time-series systems. The application of this work is not task specific and is not exhaustive of the full set and complexity of motions within each task category, but instead provides a general framework that may be either applied in its current form for general use, improved on using fPCA, or could further be adapted to task specific scenarios to increase motion specificity. An example includes obtaining a partial hierarchy of motions exclusively for feeding [30]. The proposed

approach could also be applied to a subset of the presented data, such as decoupling the reaching location from the wrist orientation, as is demonstrated in Chapter 3.

3 DECOUPLING LOCATION AND ORIENTATION

In Chapter 2, 7 degree of freedom (DOF) joint angle trajectories of the arm were clustered; 3 DOF for the shoulder, 1 for the elbow, and 3 for the wrist. One major observation was that clusters seemingly depended strongly on hand location, agreeing with the spatial control hypothesis [61]. Thus, in this chapter, I aim to recreate and expand on the analysis by decoupling the 7 DOF arm motion into Cartesian coordinates of hand trajectories and orientations, and explore alternative prosthesis or robotic arm controls. Extensions include a comparison of the hand trajectory with straight-line trajectories and end-point locations, using a data driven approach to identify the number of clusters, and a per-cluster analysis of the distribution of hand orientations. The goal of decoupling location from orientation is threefold: gain further insight into reaching motions, reduce the ADL hand motion space to representative groups, and identify subsets of hand orientations within clusters using data driven approaches.

3.1 Background

Upper-limb reaching has been the forefront subject of many research endeavors including balance confidence in seniors [65], influence of object presence on motion dynamics [66], developing novel prosthesis control using joint synergies [10], evaluating rehabilitation efforts [67], and ergonomics [68]. Whether the research goal is to evaluate rehabilitation outcomes across all tasks or analyze arm movement dynamics for specific tasks, a hierarchical description of the hand workspace can be leveraged to justify these efforts at every subcategory of ADLs.

Although in the past the hand has been considered to take a straight-line path with a bell-shaped velocity profile that minimizes jerk [27], [61], it was later shown that this is only the case under certain conditions [25], [57]. I suspect that by analyzing the deviation of the actual hand trajectories from the straight-line approximations, hereafter simply called original paths and straight-line paths, respectively, we will gain insight into why certain motions cluster together. For the path analyses, a strictly non-dynamic kinematic model is used, considering only the three-dimensional coordinate locations of the hand.

Given the significance of hand orientation relative to the forearm (commonly also referred to as wrist angles) in completing ADLs [3] and avoiding compensatory movements [4], unconstrained hand usage are analyzed, particularly orientation, during ADLs within a particular task space as defined by clusters of task location. Previous research on wrist orientations include investigating wrist synergies with elbow and shoulder postures [62], [69] and reaching direction [70], as well as obtaining a trajectory of wrist poses used in ADLs [71].

Desired hand positions and trajectories could alternatively be viewed as inputs to a control system, rather than joint positions, as has been neurologically demonstrated [72], and I leverage this to develop a biomechanical analysis of human arm motion to inspire a range of technologies, such rehabilitation programs for stroke patients [73], [74]. One major application of discretization is in a semi-autonomous sequential control of upper-limbs prosthetic devices or wheelchair-mounted robotic arms [17], [75]. In these cases, end-effector locations, trajectories, and orientations can be individually selected from a list and executed using conventional velocity control inputs, such as sEMG placed on the residual limb of the amputee [18]. While end-point locations of tasks can be used to reliably discretize the 3-dimensional ADL workspace, path trajectories can be used to recreate motions that appear natural and predictable in prosthetic devices and robotic applications. Trajectories could be implemented either instead of or in addition to using task locations in controlling arm devices whereby unique lists of trajectories are available to a user depending on the current position of the end effector. Hand orientations can subsequently be chosen from one of the available options for the location. Iuse the term "hand orientation" instead of "wrist angle" in this chapter given that the wrist is analyzed in various reference frames.

3.2 Data Analysis

The flowchart of the analysis is summarized in Figure 3.1. Subject data that was collected and prepared in Chapter 2 was used in for this analysis as well. After task segmentation, which yielded a total of 85 distinct motion segments per subject, representative end-point locations and trajectories were obtained by averaging across subjects and repetitions. Using the start and end points of each segment, a straight line was generated using the same number of time steps as the original path and likewise averaged. For generalizability, locations and trajectories are all described using the subject's torso as the reference frame.

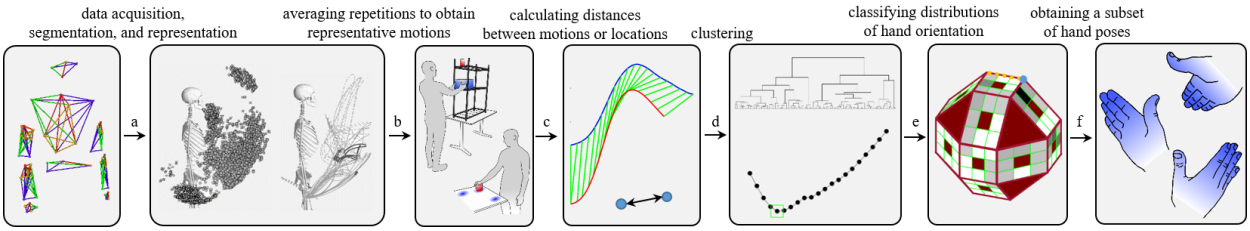

Fig 3.1 – Flowchart outlines the steps in the analysis. (a) Cartesian marker data is recorded and analyzed using either the trajectory or the end-point location of the hand. Additional markers are presented for reference. (b) The recorded tasks are then segmented into sub-movements and averaged across repetitions and individuals to obtain individual representations of each motion. (c) A distance matrix is obtained for each data representation, using either DTW for the trajectory data (top) or a Euclidean distance (bottom) for the end-point locations, followed by (d) a clustering step using agglomerative hierarchical clustering, in which the number of clusters is selected using the L method. (e) Hand orientations are classified to discrete orientations using the categorization obtained from end-point location clustering. (f) Subsets of hand poses are extracted from the orientation distributions. Steps (a)-(d) are repeated for each of the three motion representations, while (e)-(f) are repeated 3 times for each coordinate frame for one of the motion representations, namely end-point location.

Using methods described in Chapter 2, for straight-line path and original-path data, divergences are computed using DTW between each pair of average segments followed by a clustering step with hierarchical clustering. For end-point locations, divergences were calculated using a standard Euclidean distance calculation. For path data, averages were found using DBA. Cluster results obtained from the three representations are then evaluated and compared. I proceed with analyzing the coordination between task location and hand orientations. All analysis methods used on the trajectory path data have been demonstrated to work well with similar data, namely, trajectory data described in Chapter 2, and are therefore only briefly summarized.

3.2.1 Orientation Classification

An intuitive way to represent the large distribution of hand orientations is via a grid of square faces on a rhombicuboctahedron (with eight triangular and eighteen square faces, Figure 3.2a and 3.2b): a spherical like geometric object whose facets represent a classification of hand orientations. Each of the 18 main square faces can be

thought of as a palm plane (i.e. the palm of the hand is placed coplanar with the surface), and within each of those main squares, the 8 smaller squares represent an orientation of the hand in that plane (with the thumb aligning with that square, with the central square of the 3x3 grid empty). This yields 18x8 (144) hand orientation "bins" all in 45° increments from the three major hand orientation axes. The number of bins is chosen by balancing coarseness and usefulness in control; too few (such as the facets of a cube) and the bins might not be useful, too many and the bins lose their visual intuition.

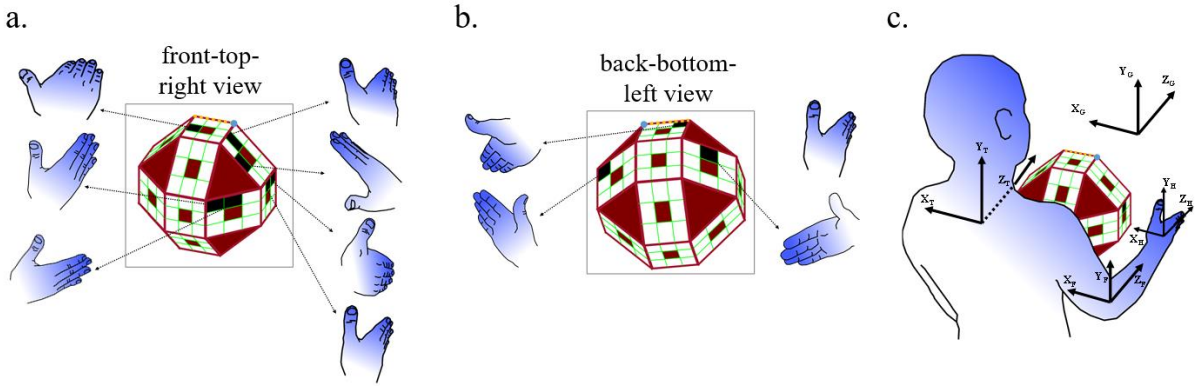

Fig 3.2 – X_H is normal to the palm and always faces the center of the rhombicuboctahedron while the thumb, Y_H indicates the orientation around the palm axis; Z_H is aligned with the direction of the fingers. Example hand orientations are shown for some of the bins (highlighted). The hedron is displayed in two orientations (a) and (b), such that all sides can be visible. A dotted line and a circle are added to aid in visualizing the rotation. (c) Reference coordinate axes, global, torso, forearm, and hand, with respective subscripts, are all aligned such that the displayed hand is classified to the same bin.

In human-robot collaboration, object manipulation and sensing requires a careful consideration of a reference frame, which may simplify computation and improve accuracy [76]. Therefore, hand orientations are analyzed and compared in three reference frames: global, torso, and forearm, with each being useful in different applications. While the global reference frame is fixed to the room, the torso and forearm reference frames are defined according to [42]. In order for the classified distributions to be comparable across reference frames, the axes are aligned such that the hand orientation is classified to the same bin as seen in Fig. 4c. Although orientations can be transformed between reference frames, each reference frame representation encodes the data differently such that each will yield a different number of hand orientation clusters, thus orientations in each reference frame are evaluated independently.

3.2.2 Obtaining a Subset of Hand Orientations

In order to identify a representative set of hand orientations in each set of task locations I evaluate the dispersion of hand orientations, divide the distribution into smaller sets until a target dispersion is reached, and calculate an average orientation for each set. Dispersion is calculated by averaging the distances between pairs of orientations,

$$d_{ij} = 2 * \cos^{-1}\left(\left|\langle q_i, q_j \rangle\right|\right) \tag{3}$$

$$Dispersion = \frac{\sum_{i,j=1}^{n} d_{ij}}{n} \tag{4}$$

where d_{ij} is the distance between a pair of orientations, q_i is the quaternion representing a hand pose in an end-point location, and n is the number of hand orientations in a location cluster. The dispersion value is reduced by re-clustering the set of orientations into smaller groups until a threshold of 22.5° is achieved; such that the cluster average represents a dispersion equivalent to a bin on the rhombicuboctahedron, i.e. orientations that exceeded a distance of 22.5° would be classified to a different bin. Because calculating the pairwise distance for every splitting permutation is computationally infeasible, divisive hierarchical clustering is performed using k-means; k-means was rerun 1000 times to avoid local minimums. Cluster averages are computed using a quaternion averaging algorithm developed in [77]. The algorithm works by identifying an orientation that minimizes the total rotation from all other orientations. Additionally, clustering ensures that the obtained average hand orientations are as distinct as possible. For brevity, analysis is performed on end-point location clusters only. Orientation distribution of trajectory clusters and orientation trajectories will be explored in future work.

3.2.2 Orientation Distribution Comparison

In order to identify similarity between different distributions of hand orientations, histogram distance calculation is used [78]. A distance matrix is created by calculating the summed absolute difference between classifications normalized by the size of the distribution,

$$S_i = \sum_{a=1}^{n} A_{ia} \tag{5}$$

$$D_{ij} = \sum_{a=1}^{n} \left| \frac{A_{ia}}{S_i} - \frac{A_{ja}}{S_j} \right| \tag{6}$$

where A is a vector representing the results of the classification, i and j are the distributions being compared, and n is the number of bins. Although a statistical significance is not associated with this distance, from the magnitude a sense of relative similarity between distributions can nonetheless be obtained.

3.3 Results

3.3.1 Cartesian Location

Cluster results and accompanying descriptions for each representation method are shown in Figure 3.3 and Figure 3.4 corresponding to end-point locations and trajectory data, respectively. Scatter plot of the un-averaged end-points, grouped according to the clustering performed on the averages, are shown in the Figure 3.3 as well. An additional third-person view for the averaged locations is shown in Figure 3.5. Un-averaged trajectories were not visually informative and were thus excluded. Skeleton models were created using an online animation tool, KineMan (http://www.kineman.com), and inserted into the figures for reference.

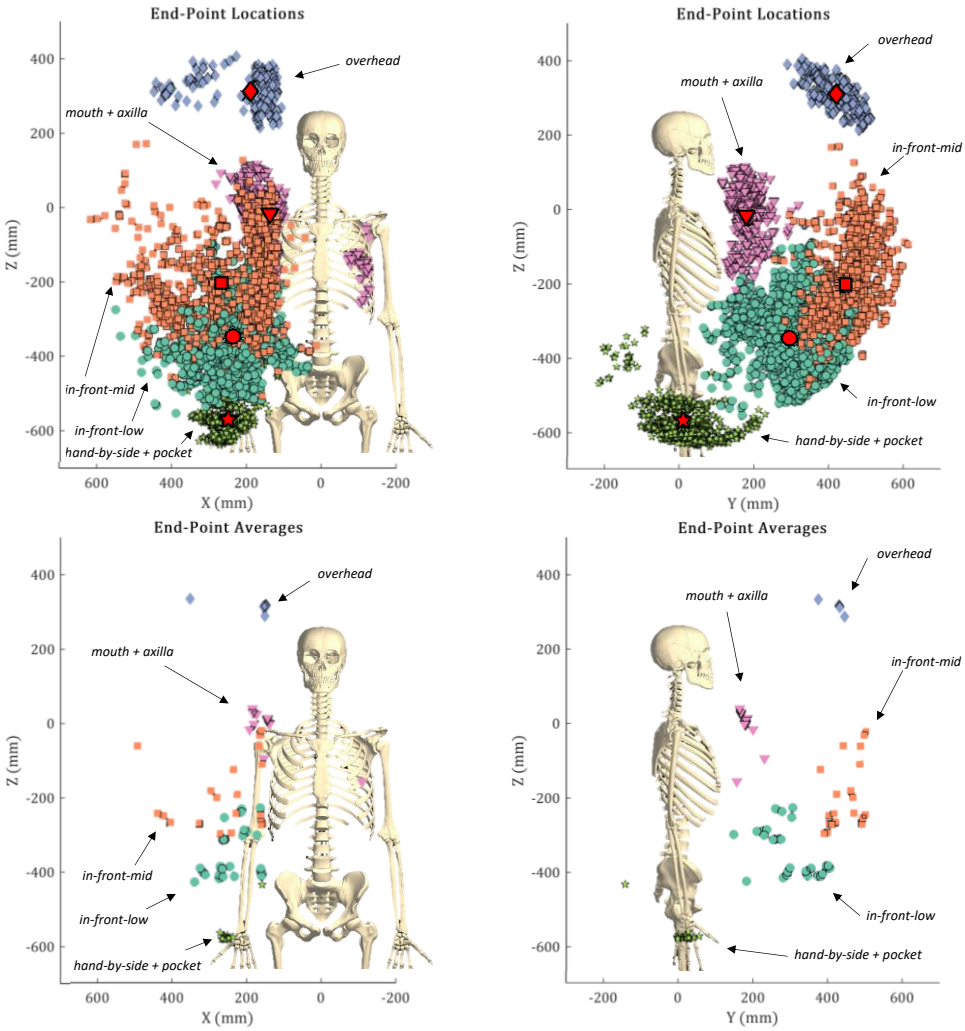

Fig 3.3 – Visual representations of the end-point locations (top) and the averages (bottom). The end-point locations of the un-averaged repetitions are classified according to average results. Centroids (red) are included in the top results. The origin is located halfway between markers placed on the C8 spinal segment and at the top of the sternum.

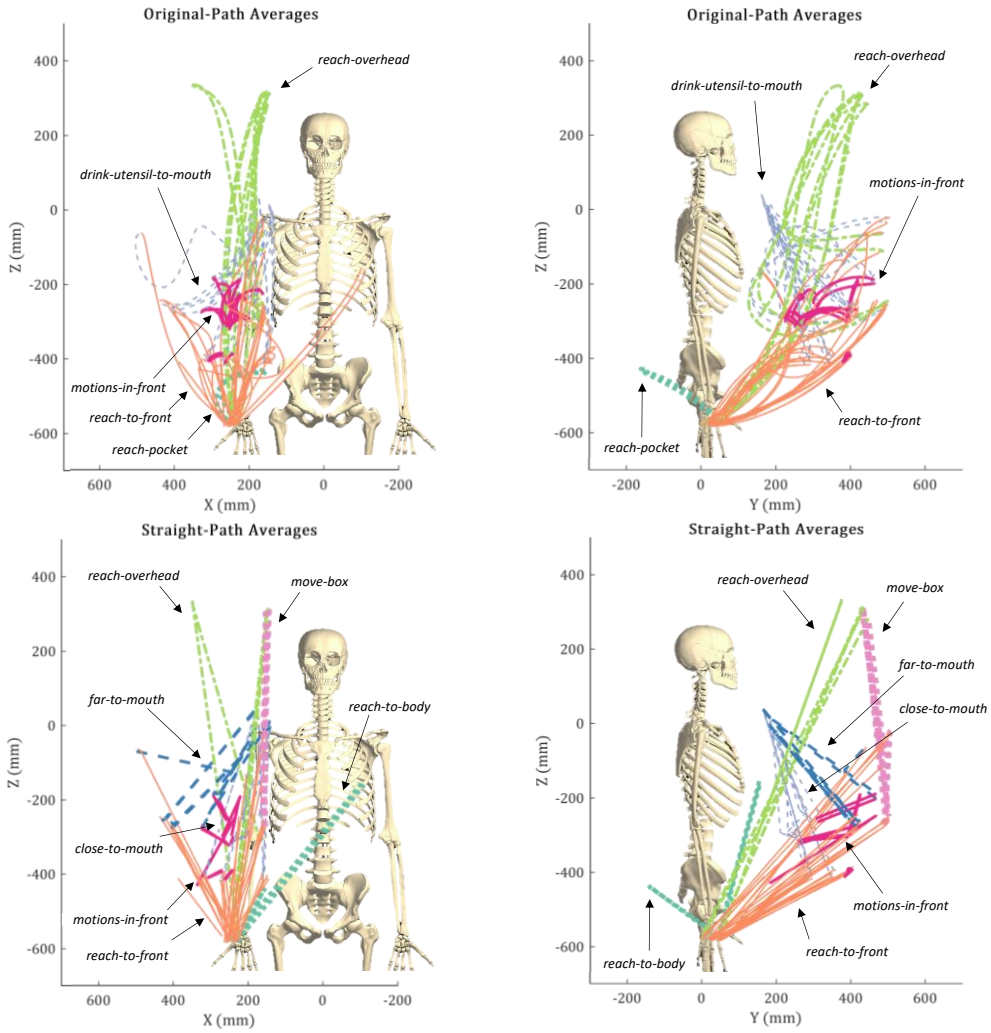

Fig 3.4 – Visual representations of the original-path trajectories (top) and straight-path trajectories (bottom). Clusters are identified with unique line patterns and colors. Cluster labels are additionally included. The origin is located halfway between markers placed on the C8 spinal segment and at the top of the sternum.

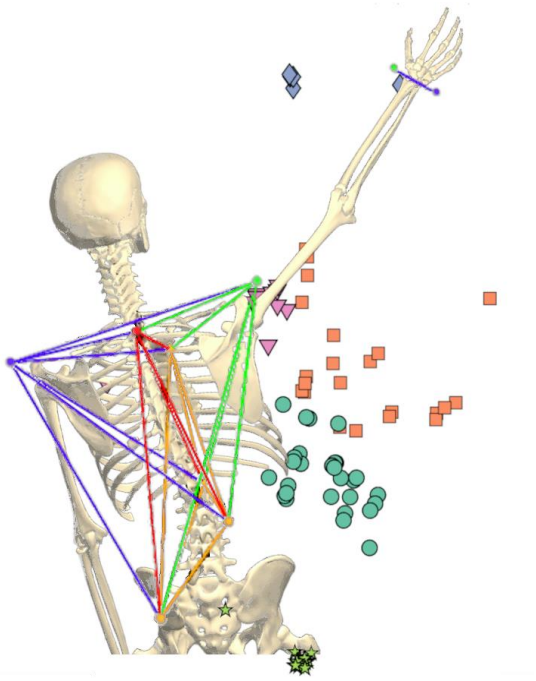

Fig 3.5 – A participant's motion-captured hand and torso locations are superimposed on a skeleton model performing an ADL task, *reaching overhead*. Redundant markers enabled the prediction of occluded marker locations. Other reaching targets are displayed as well; discretized according to clustering results. Note the hand appears to reach to the side in the torso reference frame.

The L method, described in Chapter 2, identified 5 clusters for the end-points of motion segments, 5 clusters for the original-path trajectories, and 7 clusters for the straight-line path trajectories (Figure 3.6). Detailed results depicting the results of hierarchical clustering are shown in Figure 3.7. Number of clusters for each method was selected using the L methods and demonstrated in the plots using a horizontal cut. Tasks segments and end-point locations are listed according to Table 2.1.

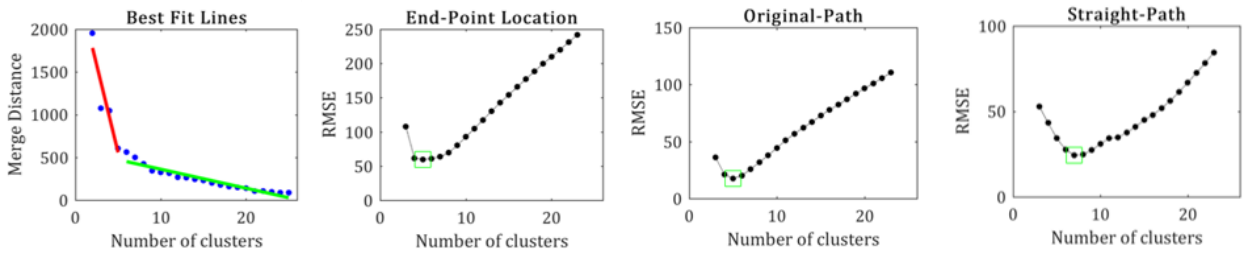

Fig 3.6 – L method results for each data representation. An example of the identified "knee" for end-point locations is included in the top right.

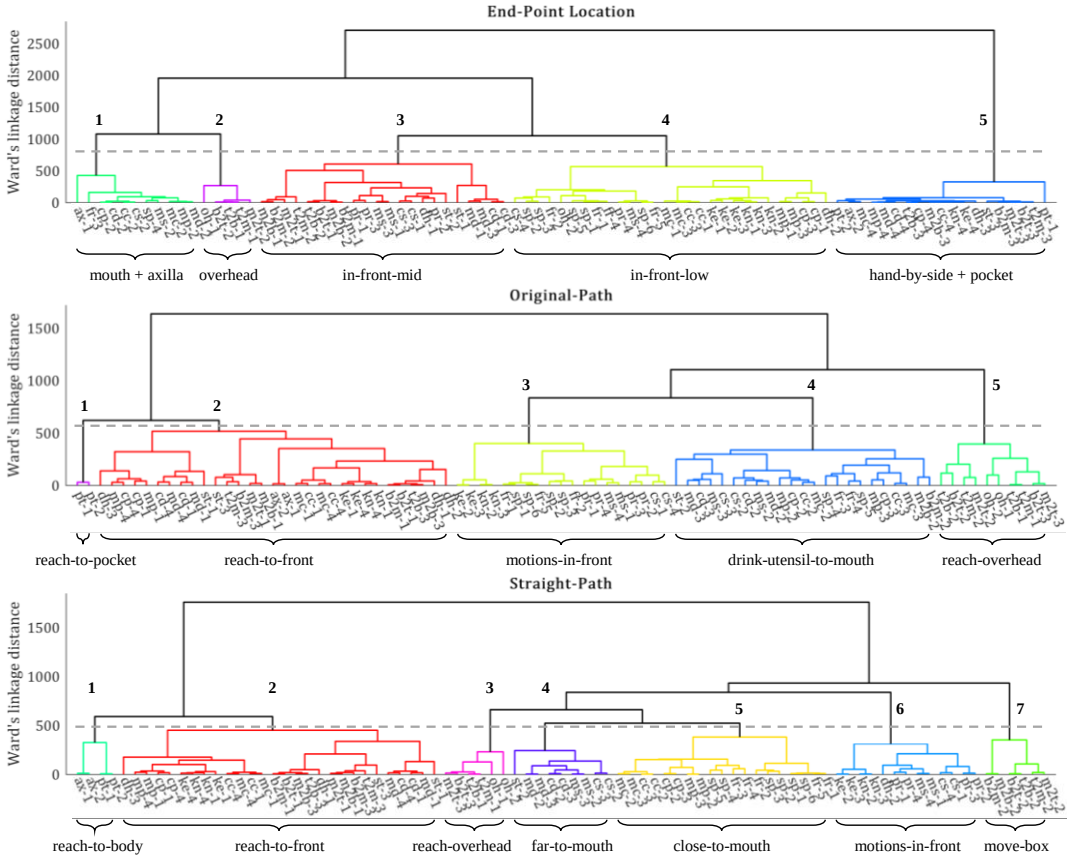

Fig 3.7 – Hierarchical clustering results are displayed for end-point locations and paths. Clusters are numbered and colored and are extracted using horizontal cuts according to the L method. Cluster colors were automatically generated and are unrelated between dendrograms. Task segments and end-point locations are listed according to Table 2.1.

Evaluation of the clustering quality of each representation method is shown in Figure 3.8, calculated according to the pseudocode in Table 2.2 in Chapter 2. The number of clusters is varied from 1, containing all data, to 25 clusters. Evaluation could theoretically go on up until all data points belong to their own cluster, but results are less informative at that range. Original-path trajectory clustering outperformed the other methods while end-point locations performed the worst at almost every number of clusters.

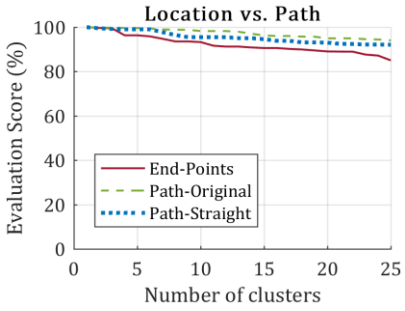

Fig 3.8 – Evaluation of clustering for each of the representation methods across a range of number of clusters. Scoring assessed how frequently repetitions clustered together.

3.3.2 Orientation Distribution

Distribution of hand orientations are presented in Figure 3.9 using the rhombicuboctahedron representation shown in the global, torso, and forearm coordinate frames for each of the 5 end-point location clusters for a total of 15 distributions. The initial dispersion, based on the average pairwise distance between orientations, is displayed at the top right of each distribution. Sets of hand orientations are additionally shown below each distribution that represent the average hand poses for the sub-clusters that reduced dispersion below 22.5º. Note that for three of the of forearm locations, the subsets are identical, suggesting that distribution differences were not significantly different.

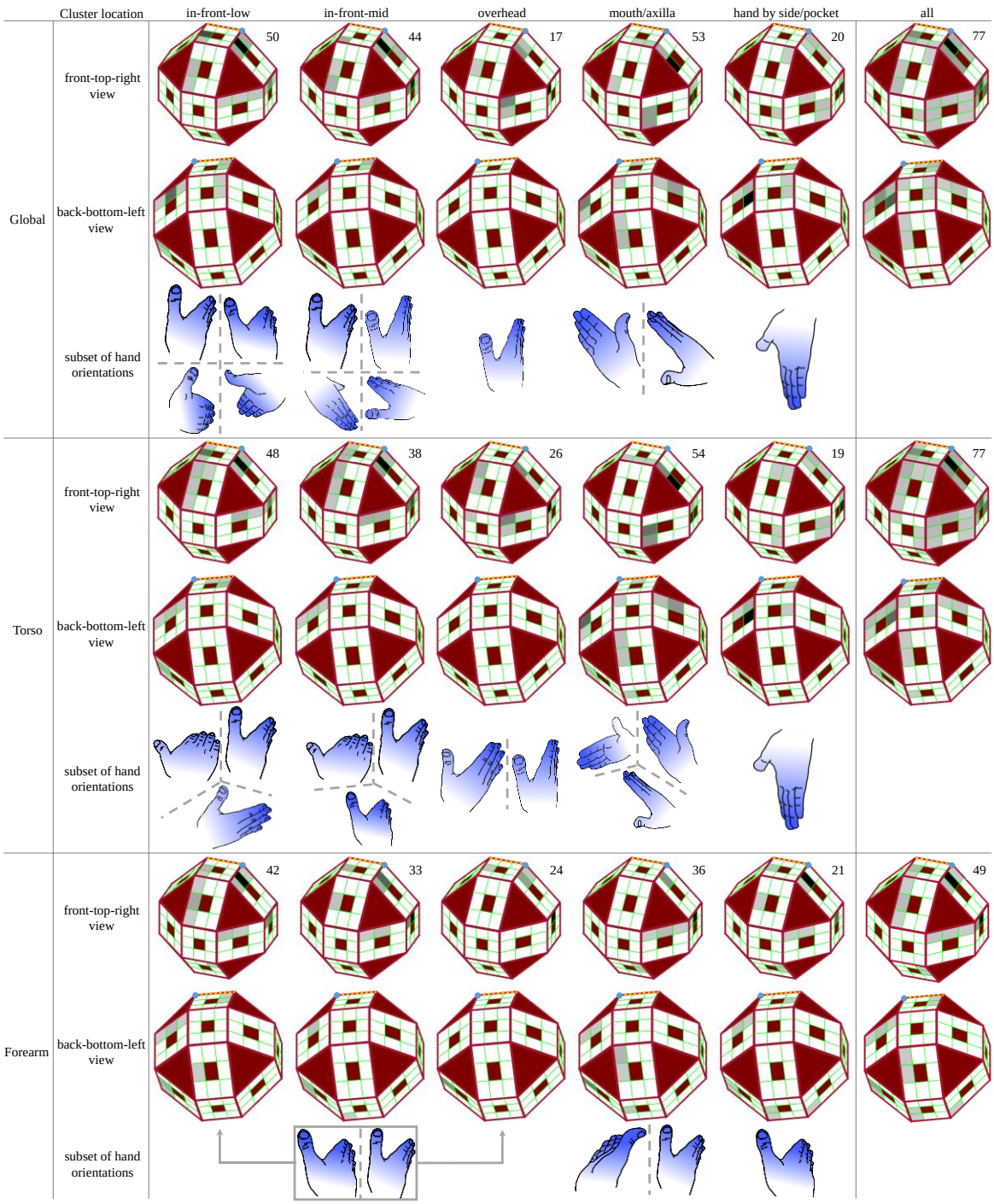

Fig 3.9 – Distributions of the hand orientations are shown in each of the three reference frames (right column), as well as within each end-point location cluster. Subsets of the distribution, found by re-clustering, are shown below each respective distribution. Some subsets are identical across distributions, as is seen for three of the clusters in the forearm reference frame. Dispersion values are displayed at the top right of each distribution.

A distance half matrix is shown in Fig. 3.10, highlighting the relative similarity between distributions. The range is normalized from 0, assigned to identical distributions, to 1, as identified by the most dissimilar pair of distributions. Note that the global and torso reference frames are more similar across than between clusters, indicated by the light diagonal.

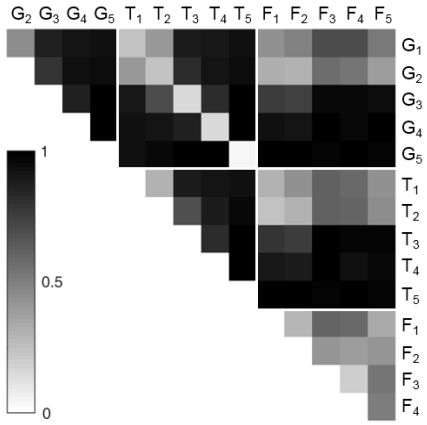

Fig 3.10 – Relative similarity between hand orientation distributions across clusters and reference frames. Reference frames are indicated by G, T, and F, for global, torso, and forearm respectively. Cluster indices 1-5 refer to clusters *in-front-low*, *in-front-mid*, *overhead*, *mouth/axilla*, and *hand-by-side and pocket*, respectively.

3.4 Discussion

End-point locations, path trajectories of the hand, and generated straight-line paths of the hand performing a set of ADL tasks were used to discretize the ADL workspace using data driven approaches. End-point representation identified the following discretization: *in-front-low*, *in-front-mid*, *overhead, mouth and axilla*, and *hand-by-side and pocket*. The original-path trajectory on the other hand identified the following discretization: *reach-to-pocket*, *reach-to-front*, *motions-in-front*, *drink-utensil-to-mouth*, and *reach-overhead*. Straight-line path clusters further differentiated some motions and merged others into the following groups: *reach-to-body*, *reach-to-front*, *reach-overhead*, *far-to-mouth*, *close-to-mouth*, *motions-in-front*, and *move-box*.

Differences between original-path and the straight-line path clusters includes a merging of *reach-to-pocket* with *reaching to axilla* motions, and differentiation of the *drink-utensil-to-mouth* cluster into motions that began closer to or further from the body. Unlike straight-line path clusters, original paths that pass by the mouth, such as transferring

the box from the bottom to the middle shelf and transferring the suitcase, clustered with drinking and eating motion segments. Original-path clusters also grouped *reach-overhead* with transferring a box task. These observations are largely impacted by a significant overlap that is not present when considering the straight-line path. This suggests that ADL tasks are not as distinguishable as they appear and that finer task segmentation could be more appropriate, for example, by splitting a transferring motion around the mid-point when the object is closest to the body.

Although many tasks included an object that was centered and placed in front of the subject, the end-point locations of the hand were primarily situated to one side of the body. This suggests that reaching motions were coordinated with the motion of the torso such that the arm did not move directly in front of the body; this was even the case for the door opening task when the hand was expected to come across the body when reaching for the door handle. An example of this can additionally be seen in Figure 3.5. Trajectory plots further verified this observation by demonstrating that the paths seldom traversed in front of the torso. Although it may seem trivial, many experiments and evaluations have consistently centered the testing platforms with respect to the center of the subjects' bodies. If we accept that in the body reference frame the arm indeed predominately appears to reach to one side, then results of those tests fail to account for the significance of body compensation due to the torso and potentially misevaluate upper-limb prosthesis or rehabilitation outcomes.

When evaluating the quality scores, we observe that end-point location clustering performs worse than path clustering for every number of clusters. This could be due to trajectories having more degrees of freedom than individual points in Cartesian space, and therefore contain sparser data. This is consistent with the original-path clustering also outperforming the generated straight-line paths at every number of clusters. Additionally, straight-line paths fail to capture characteristic hand motions and could therefore be the reason for its lower clustering quality. We also observe that path trajectories are more uniform between individuals and repetitions than end-point locations alone. Differences between methods are generally negligible for a few number of clusters, and selection of the representation is therefore highly application dependent. I proceeded with analyzing the hand orientations within the end-point location clusters as they generalize to either of the trajectory representations while enabling an intuitive control interface as is discussed below.

A semi-autonomous control application of this work would enable users to operate multiple DOF without the associated increase in cognitive burden. For example, a 7 DOF (shoulder-elbow-wrist) prosthetic device could be first controlled by selecting one of the 5 desired locations followed by a selection of hand orientations; automatically

selected when there is one associated orientation. Switching from one location to another or moving within the same location would then correspond to which trajectories are available; e.g. starting with hand-by-side, there are 3 possibilities, *reach-to-front*, *reach-overhead*, and *reach-pocket*. This particular implementation could take advantage of already existing myoelectric interfaces on the market and simultaneously operate multiple DOF rather than just one at a time. With capable location sensing, a prosthetic wrist device could likewise reorient itself from one 3 DOF hand orientation directly to another by providing users a succinct list of orientations to pick from. The user control process could be streamlined for locations that had an orientation dispersion value below 22.5°, such as hand by *side/pocket*, by coupling the location to a single hand orientation. Various other permutations of location and trajectory sequential control are possible.

Relative distances demonstrated that the distribution of hand orientations is more similar across global and torso frames than between clusters. While this may not be surprising, this reaffirms the potential interchangeability of the two reference frames; an important feature in modelling the world space in mobile robots and prosthetics. One application is the implementation of an IMU in a prosthetic device [79] to orient it either with respect to gravity or the torso, which may include other hardware considerations.

While similar, the global and torso reference frames still have certain noteworthy differences that do not make them completely interchangeable, so while a robotic arm is generally fixed to a base normal to the ground, a prosthetic arm could either be assumed to be on a moving base in some scenarios and not in others. Given that the global reference frame places no restrictions on hand orientation, I suspected that it would always have a more dispersed distribution than the torso or forearm reference frame, however, the opposite was the case for two clusters. This suggests that the distribution of hand orientations of some objects or locations is more consistent in the global reference frame. One way to exploit this is to use the more compact reference frame that includes the fewest representative hand orientations for different tasks.

The forearm reference frame orientation distribution is the most compact of the three, and would likely be the best control option for transradial amputees looking to use a prosthetic wrist device. Most bins are anatomically impossible to reach, and the vast majority of orientations appear to lie within a narrow range along the pronation-supination axis of rotation; this may explain why the first three location clusters have the same set of representative hand orientations. One implementation may include interpolating the current orientation and the desired final orientation, rotating as the hand traverses its trajectory. However, it might not be appropriate in prosthetic devices for

transhumeral and shoulder disarticulate amputees since positioning of the end effector would highly depend on device capability. Specifically, setting the position and orientation of the forearm would have to be a precursor to positioning of the hand, which is not a challenge for transradial devices. Additionally, since the global and torso reference frame distributions are generalizable, these are likely to be more useful for non-anthropomorphic robotic arms that may have an unconventional forearm or forearm control [80]. For example, while reaching for an object, it may be necessary for a robotic arm to position the forearm in extreme orientations in order to avoid an obstacle, or in the case of hyper-redundant manipulators that lack a well-defined forearm altogether.

In wheelchair-mounted robotic arm applications the cluster locations will most likely need to be dynamically adaptive to account for the variance, which could come in the form of a second input or computer vision. While the choice of references frames was based on the perspective of a prosthesis user, various other custom reference frame considerations [81] should be made depending on the application. The results are also dependent on the selected task list, which by no means is exhaustive, hence the framework could be extended to other applications by including relevant tasks.

4 EFFICACY OF VIRTUAL REALITY TESTING

In order to test the proposed prosthesis control methods, access to 3 DOF wrist, 4 DOF elbow-wrist, and 7 DOF shoulder-elbow-wrist prosthetic devices was needed. Due to the unavailability of commercial devices, virtual reality (VR) was used instead, avoiding the need to develop physical devices in-lab. In this chapter I discuss the VR platform set up and its efficacy through a series of pilot studies. Here, 3 DOF prototypical wrist motions identified in Chapter 2 are implemented to demonstrate the efficacy of both the control method as well the ability of the VR system and controller to accurately represent the outcomes of real device testing. I also aim to address the following questions regarding the feasibility of the use of the control method in prosthetic devices: do prototypical motions help reduce the time it takes to align the hand, do they mitigate body compensation, and do users have a preference.

4.1 Background

Myoelectric prostheses commonly use a standard 2-site surface electromyography (sEMG) control interface in which users drive the hand to open or close with their flexion or extension muscles [18]. Switching between grasp types occurs during co-contracting where both sEMG signals fire simultaneously. Co-contraction can also be programmed to switch between hand closure and wrist rotation in devices that include a wrist. I take advantage of this architecture and propose that instead of joints, users control whole motions that consist of multiple DOF.

The tested control method in this chapter takes advantage of prototypical motions of the wrist, namely *trajectory* control. In *sequential* control, users select controllable DOF and then rotate around it one at a time. In *trajectory* control, each prototypical motion is implemented as a controllable mode in a *sequential* control manner: users select a desired motion trajectories and then are able to move forward and back along the coordinated angle path, embedded in a single dimension. The primary difference between the two controls is that because prototypical motions are independent of one another and correspond to specific tasks, unlike in *sequential* control, they do not “stack”. This means that switching between modes resets the joint angles to a position on the next mode.

VR and has been embraced across wide range of applications [82], including within the prosthesis community, as a low-cost method to iterate and test new device designs and controls that extend to a real world setting [83], [84]. Given that complex prosthetic devices that we are testing are not are not presently on the market, implementing a protocol in VR avoids needing to build them. Other applications of VR include training to use a prosthesis [85], fitting [23], and rehabilitation [86], [87]. This suggests that observations regarding prosthesis use made in VR would likely reflect those made in the real world as well. Virtual reality environment (VRE) has also been demonstrated to be convincing enough to treat phantom limb pain [88], [89], further reassuring its use in testing our proposed controls.

4.2 Pilot Study with Trajectory Control

It is hypothesized that most of the range of motion a fully articulated prosthetic device goes unused and that prototypical motions that are embedded in a single dimension are primarily all that a user would need to complete tasks related to ADL. While it may seem that *trajectory* control is limited in that the motion modes do not stack like they do in *sequential* control, they were designed to span a large set of tasks. Here I describe the set up aimed at demonstrating that *trajectory* control is indeed capable of completing tasks, and potentially outperform *sequential* control on a number of metrics.

Two participants took part in this initial run of the study (Table 4.1) that lasted approximately 2 hours. These were right handed individuals without motion or visual impairments, and were comfortable being immersed in VR. Data collected from the experiment was exported and analyzed using MATLAB 2019a.

Table 4.1 – Participant characteristics

Participant	Sex	Age	Weight (lbs)	Height (inches)	Arm Length (inches)[1]
P1	M	27	135	67.5	27.5
P2	M	23	160	70	28

[1]Measured from the shoulder to the tip of the middle finger

4.2.1 Virtual Reality Set Up

The study was designed to provide participants a fully immersive VRE, where they can view a virtual arm in place of their own and complete ADL tasks as they would in real life (Figure 4.1). Unity software was used to create

the VRE as well as to interface with the inputs streaming from the users. Virtual objects were either designed within the Unity environment, created in Maya 3D modeling software, or obtained for free from the web. Object models were scaled to the task requirements, while the virtual prosthetic hand, forearm, and humerus models were scaled to the average human arm dimensions. Since the focus of testing wrist control is to correctly orient the hand, rather than grasping, kinematic and dynamic model interactions were turned off, and the need for the participants to grasp the objects was omitted.

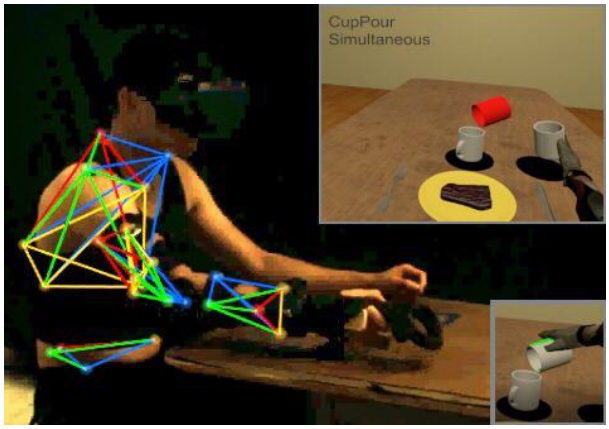

Fig 4.1 – Subject performing a cup pouring task, seen wearing the HMD and is using the controller to operate the virtual wrist. In the top right a semi-transparent red cup is visible indicating the desired cup orientation goal, which turns green (bottom right) once the cup reaches the target.

4.2.2 Control Inputs

Motion tracking has been shown to be an effective input to kinematically controlling a hand in VR [90]. This study used 12 Vicon Bonita cameras to track the subjects' hand and forearm, in the case when participants used their own hand, and forearm and humerus, for all other testing conditions. In addition to providing participants an immersive experience by displaying a virtual arm in place of their own, this also offered them a reference when operating the simulated prosthetic device. The respective reflective marker clusters are shown in Figure 4.2. Additional markers that were placed around the subject's humerus, torso, and pelvis were not streamed into Unity, but were included for body compensation analysis. The reflective marker locations include bony landmarks (seen in Figure 4.1) that were used to calculate the joint coordinate reference frames according to [42].

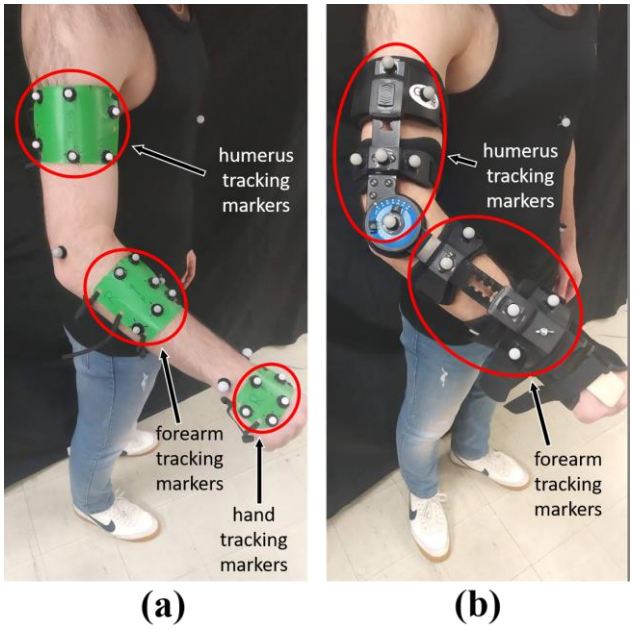

Fig 4.2 – (a) Marker arrangement for the positive control; participants' arms were unconstrained. Hand markers were used to control the location and orientation of the virtual hand while the rest of the markers were exported for further body motion analysis. (b) Braced condition used for the other four control modes. Forearm markers were used to control the virtual forearm, while the virtual hand was either fixed in place (negative control), or operated using the hand held Vive controller. Wooden piece was inserted into the brace to ensure a fixed flexion-extension position. The elbow brace hinge was given full range of motion.

Participants used a Vive controller, rather than an sEMG input, to operate their simulated prosthetic devices, providing the benefit of an intuitive interface that required virtually no training (Figure 4.3). This streamlined the training process for able bodied participants who might not be as familiar with an sEMG interface, thereby emulating experienced powered device users. Specifically, the standard contralateral two-site sEMG control is imitated by using two antagonistic buttons on the Vive controller, one near the index and one near the thumb. If *trajectory* control outperforms other types of control using the Vive controller, then I claim that this difference in control performance would appear when using sEMG as well. This claim is tested with a pilot and described in more detail in section 4.4. Head tracking was also performed through HTC's head mounted display (HMD). Calibration between the two systems, Unity and Vicon tracking, was performed by matching the Vive controller as it was tracked by the HTC cameras and Vicon.

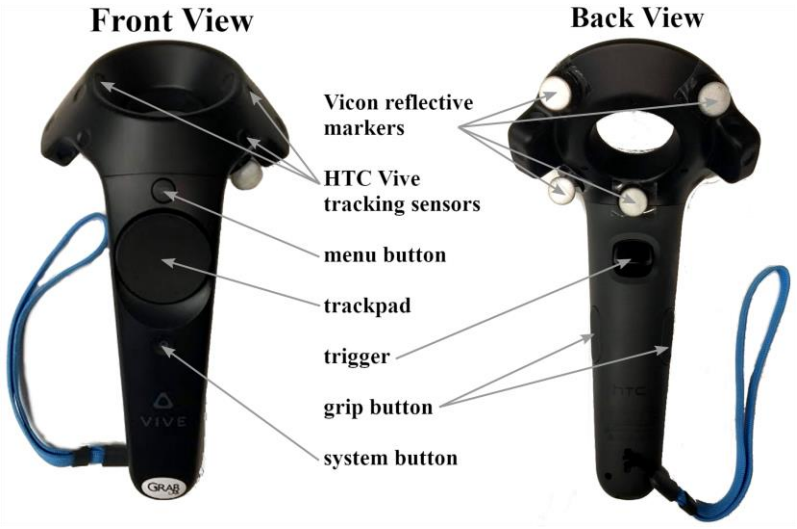

Fig 4.3 – Standard HTC Vive Controller. Vicon reflective markers were placed in a known arrangement around the controller's head and were used to calibrate the virtual space between Vicon and HTC.

4.2.3 Control Modes

Each participant began the experiment by first completing the tasks using a positive and a negative control. The *positive* control allowed users to use their own unencumbered hand to complete the tasks; this served as a performance benchmark that participants aspired to achieve when using the prostheses. With the aid of a marker cluster placed on the back of the hand, participants saw the virtual hand closely match the position and orientation of their real hand. I also refer to this mode as *natural* control.

For the other four modes, the wrist was fixed in place using a custom made wrist brace (Figure 4.2b), similar to the one used in [4]. The orthopedic wrist brace (DonJoy ComfrotFORM Wrist Support Brace – DJO Global, Vista CA, USA) was combined with an elbow brace (Orthomen ROM Elbow Brace) using Velcro straps and a bolt. The elbow brace was given full range of motion and served to limit the pronation-supination of the wrist without hindering elbow motion.

A negative control was included in the experiment, a condition in which the virtual prosthesis lacked wrist mobility, and was also referred to as the *no-wrist* control condition. For this mode, subjects had to complete tasks without the ability to rotate their wrist and had to compensate for it using their residual limb and torso. Although task

performance was closely monitored by the experimenters, subjects were additionally instructed to indicate if a task could not be completed.

Sequential control aimed to represent current myoelectric technologies on the market where users have access to only two control inputs. The Vive controller's (Figure 4.3) trigger and trackpad button took the place of the two-site contralateral sEMG that are often placed on amputees' forearm; in the case of powered prosthetic devices. On the controller, the trigger drove the wrist forward along a specified direction and the trackpad button drove it backward. A simultaneous press of both inputs switched the DOF along which the wrist rotated. When switching between DOF, the order of rotations cycled from pronation-supination, flexion-extension, to radial-ulnar deviation. This mode switching scheme is often used to switch between grasps in powered prostheses.

Simultaneous control granted individuals access to all control inputs at the same time by leveraging all the buttons that were available on the Vive controller. Similar to the positive control, this mode represented the state of the art and a theoretical condition where users have 6 control inputs available to them. The Vive controller's trackpad is a single button with location sensing in two dimensions, which I took advantage of by offering 2 DOF control of the wrist; pressing the trackpad while the thumb is at the top, bottom, left, and right of the trackpad drove the hand to extend, flex, radially deviate, and ulnarly deviate, respectively. Pressing the trackpad in the intermediate space, say top left corner, would simultaneously rotate the wrist in both directions, in this case simultaneously extend and radially deviate. The trigger and grip button were used to supinate and pronate, respectively, and could be operated concurrently with the other 2 DOF.

Finally, I wanted participants to test the proposed *trajectory* control. In this mode participants only had access to two inputs, trigger and trackpad, similar to *sequential* control. In total there were five wrist prototypical motions to pick from, directly implemented from Chapter 2; all rotate the hand along all 3 DOF simultaneously and had a predefined start and end point beyond which the wrist would not continue to rotate. Although all 3 DOF are used in each prototypical motion, they can be generally described as follows: supination/ulnar deviation, flexion/ulnar deviation, supination/flexion, supination/extension, and extension/ulnar deviation (Figure 4.4). The proposed version of *trajectory* control would cycle between these the motions when both buttons (trigger and trackpad) were pressed, however, since only one motion is needed for each task, mode switching did not occur. At the beginning of each task a prototypical motion was preselected, and participants would only have to drive the wrist along a single trajectory to achieve the desired goal using either the trigger or the trackpad, depending at which end of the trajectory the task

began. Each task had a single corresponding motion (Table 4.2) that would begin at either end of the trajectory, which was also predefined. These tasks can be found in Table 2.1 as subtasks. Whichever orientation the wrist began at in this mode, would also be the start orientation for the *sequential* and *simultaneous* control modes.

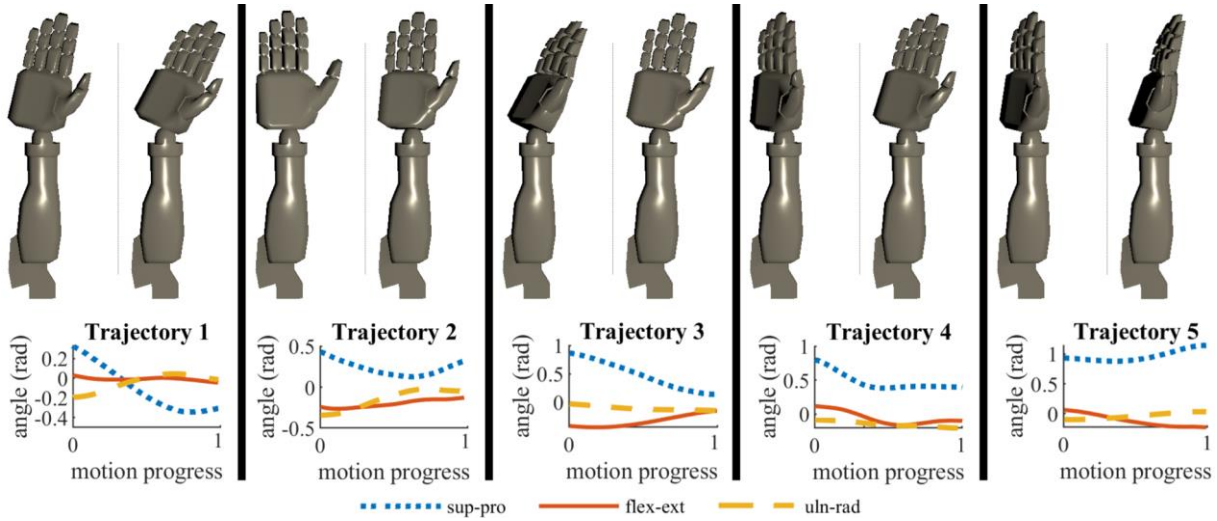

Fig 4.4 – Each of the five wrist trajectory modes are depicted. First row represents the beginning and end (left to right) of each wrist trajectory respectively. Second row displays the actual 3 DOF angle trajectory. The order of rotations is supination-pronation, flexion-extension, and ulnar-radial deviation. Positive values correspond to supination, flexion, and ulnar deviation. Motion progress is scaled from 0 to 1, or 100% of the motion.

Table 4.2 – Task description and corresponding prototypical motions

Task description	Prototypical motion used
Reach to cup	4: supination-extension
Drink from cup	2: flexion-ulnar deviation
Reach to suitcase	5: extension-ulnar deviation
Transfer suitcase	4: supination-extension
Reach overhead	4: supination-extension
Bring can down	2: flexion-ulnar deviation
Reach to fork	5: extension-ulnar deviation
Use fork	4: supination-extension
Eat from fork	1: supination-ulnar deviation
Pour from cup	3: supination-flexion

4.2.4 Study Procedure

The role of an upper limb prosthesis is primarily to restore independent living by enabling amputees perform ADL tasks. The protocol therefore included a set of tasks inspired by work done in evaluating upper-limb prosthesis performance [39]. The virtual set up of the environment and objects are created to scale and are set up according to the dimensions described in Figure 2.2. I selected a set of 10 ADL tasks that require the use of only the right hand, cover a variety of locations, and include both reaching motion and object manipulation: *i*) *reach to cup*, *ii*) *drink from cup*, *iii*) *reach to briefcase*, *iv*) *transfer briefcase*, *v*) *reach overhead*, *vi*) *bring down can*, *vii*) *reach to fork*, *viii*) *use fork*, *ix*) *eat from fork*, and *x*) *pour*. These were also selected in such a way as to span each of the wrist's prototypical motions, such that each motion was used at least once.

During reaching tasks participants were asked to begin with their hands relaxed by their side, and proceed with matching the orientation and location of the end effector, indicated with a semi-transparent red hand model (Figure 4.5). Each task included a goal and tolerance for both the location and orientation; generally within 2 centimeters and 10°, inspired by previous pilot studies that I conducted. As such, task goals were defined agnostic to the control methodology and did not specifically align with any of the prototypical motions, and therefore it was possible that a

given motion was insufficient and participants would need to use some amount of body compensation to ultimately reach the desired goal.

Fig 4.5 – Example of a reach to a cup task. (a) Semi-transparent hand indicates the desired goal position of the user-controller hand, which dims as the hand approaches it. A red arrow is included next to the hand to assist with visualizing the current hand orientation. (b) Task completion occurs when the hand is within the Euclidean tolerance and the corresponding orientation arrow is within the tolerance cone.

Therefore, after the reaching task, objects were automatically placed within the hand akin to how they would be grasped when using a natural hand. Participants were then asked to match the object location and orientation in a similar way, starting from where they "grasped" it. For sitting tasks, which included fork use and pouring tasks, participants were asked to place the hand in a relaxed position on the table prior to reaching, which was placed in front of them matching the virtual table's location and height. When using a control mode, the hand was reset to match the first frame of the trajectory control mode applicable to that task. Close attention was paid to how participants accomplished the task, such that the task was not deemed complete when participants unintentionally passed the hand through the goal, estimated based on how long the participant maintained the goal pose. Therefore participants were asked to repeat a task in which they could not maintain the goal pose for more than 1 second.

Tasks were performed in a semi-randomized order, with same-object reaching and manipulation occurring directly after one another. Each set of 10 tasks were performed in the following order: *natural*, *no-wrist*, *sequential*, *simultaneous*, and *trajectory* control.

In order to mitigate training effects when faced with an unfamiliar environment or control interface, participants were given time to practice controlling the wrist prior to each task. Training ended when participants felt comfortable and had a strategy as to how they were going to accomplish the task, such that they were not hesitating when recording started. For *trajectory* control, a mode was preselected during training and placed at either end of the trajectory, according to the task requirements. During recording users would simply need to move along it to achieve the desired orientation.

4.2.5 Data Analysis

Several metrics were considered in assessing whether there is a benefit to trajectory control. These include evaluating the range of motion (ROM) and Cartesian trajectory length of each joint as an indicator of natural movement, and were calculated for each control mode and task condition. Arm joints and torso coordinate systems were calculated according to [42]. Torso angles were calculated with respect to the pelvis and are described in the following order: torso flexion-extension (leaning forward or back), turning left-right (twisting), and leaning left-right, where extension, turning left, and leaning right are positive directions. Cartesian trajectory length, *L*, of each body segment was calculated as a sum of Euclidean distances between sampled points,

$$L = \sum_{i=1}^{j-1} \sqrt{(X_i - X_{i+1})^2 + (Y_i - Y_{i+1})^2 + (Z_i - Z_{i+1})^2} \tag{7}$$

where *X*, *Y*, and *Z* correspond to the three Cartesian components of a trajectory in space and *j* is the total number of sample points in that trial.

The start of the trial manually detected by the researchers when participants began to move, while the end was automatically determined by the software when the goal was reached. Time to accomplish the task was recorded for each task condition and would point to the simplicity of operating each control.

At the end of the experiment participants were asked to fill out a survey that included questions about their preferences and whether the control modes were easy to learn, intuitive, and appeared/felt natural. The latter is referred to as movement cosmesis.

4.3 Results

The time it took each participant to perform the set of tasks was recorded, and can be seen in Figure 4.6. An aggregate time was assessed by summing across tasks for each control mode. The positive (*natural*) control was consistently the shortest for both participants, while *sequential* control took the longest. Of the three wrist controls, *trajectory* control was the fastest for both participants.

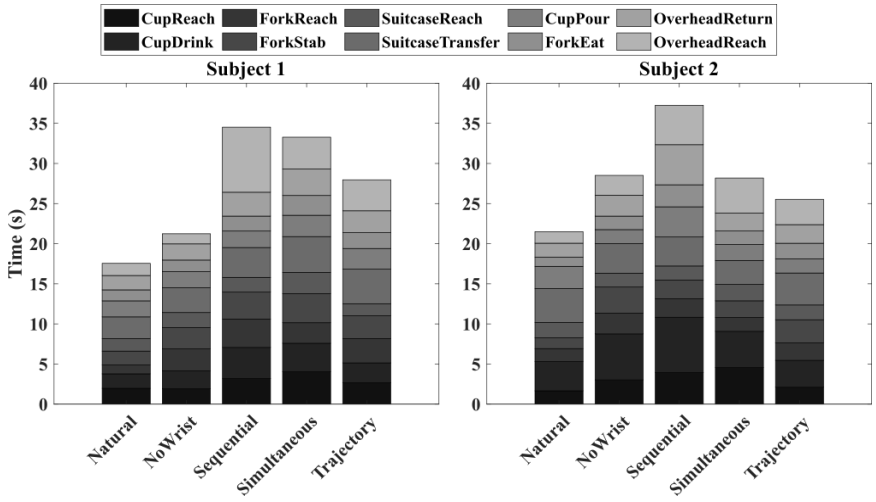

Fig 4.6 – Time each subject took to perform the tasks using the five control modes. Each column represents a control mode and is broken up by individual task.

Range of motion of each joint angle was assessed to evaluate body compensation under different conditions and control modes (refer to Figure 4.7 for the summary data, and Figure 4.8 for the individual results). The negative control (*no-wrist* condition) generally lead to larger torso and shoulder ranges of motion. While humeral elevation (Shoulder2 in the figures) was the lowest for trajectory control, other joints were higher. However, as a whole, results indicate very similar performance between *trajectory* control and the *sequential* and *simultaneous* controls. Additionally, negative control ("No Wrist" in the figures) had the highest range of motion for the torso angles and humeral elevation, consistent with expectation. Positive control ("Natural" in the figures) generally sustained the largest wrist angles range of motion, which likely contributed to the lowest torso and shoulder ranges.

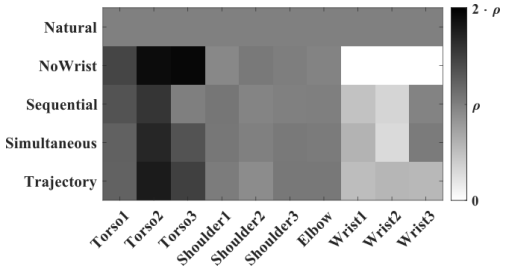

Fig 4.7 – Average range of motion (ROM) results, for each condition across both participants, is displayed as a heat map, normalized for each column by the positive control (natural condition). Variable ρ represents the range of motion of the positive control. Joint angles are on the horizontal axis while control conditions are on the vertical axis.

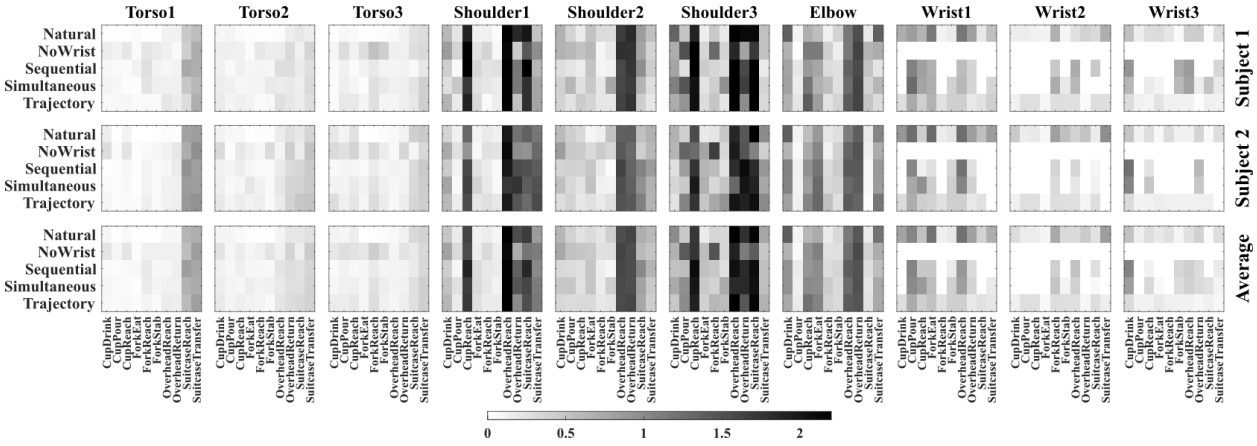

Fig 4.8 – Range of motion (ROM) for each joint angle for each control mode and task is displayed, displayed as a heat map scaled to the largest angle (in radians). The first row corresponds to data obtained from the first subject, the second row corresponds to the second subjects, and the third row represents the average. Note that the wrist angles under the negative control (no wrist) condition is consistently at zero, given that the wrist was fixed.

Cartesian trajectory length of each joint is summarized in Figure 4.9, averaged across both participants; displayed as a heat map. Each joint angle is normalized, from smallest to largest, to distinguish control mode performance. Total trajectory length is calculated by summing the lengths for each task while weighing them all equally; calculated as the sum of normalized lengths. Summing the unnormalized Cartesian lengths would result in a few tasks biasing the

control mode performance. Positive and negative control dominated the two ends of the spectrum, while it was difficult to distinguish between the performances of the other three wrist controls.

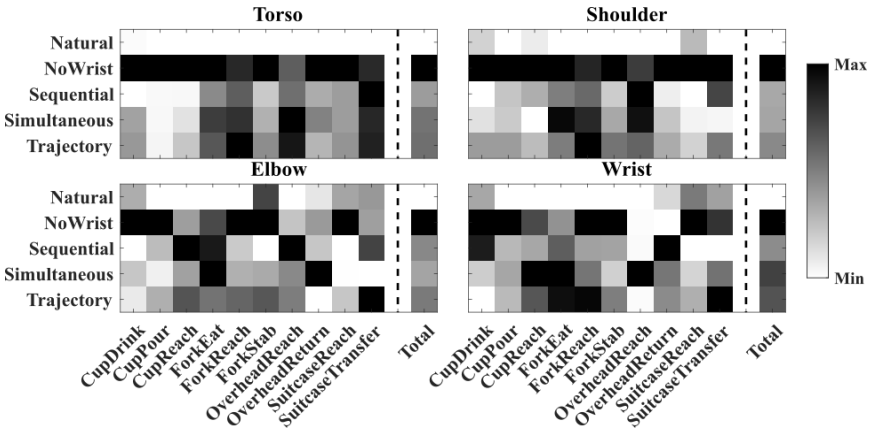

Fig 4.9 – Cartesian trajectory length for each joint across each task and control condition. Vertical columns on the right summarize the results for each control condition. Columns are scaled independently from the smallest value (generally the Natural condition, positive control), to the largest value (generally the No Wrist condition, negative control).

After each experiment session subjects had the opportunity to give feedback by ranking various control qualities on a scale from 1 to 5 (Table 4.3). Both subjects ranked the positive control highest for training, intuition, movement cosmesis, and overall preference (full score of 5). Negative control received lowest marks for looking natural, and overall preference (1 or 2), however participants disagreed on whether training was easy or intuitive; average score of 3. Out of the three controllable wrist strategies, sequential performed the worst, while the trajectory control slightly outperformed simultaneous.

Table 4.3 – Survey results: mean score

	Sequential	**Simultaneous**	**Trajectory**	**No Wrist**	**Natural**
Training was easy	4	4	4.5	3.5	5
Intuitive	1	4	4.5	3	5
Appeared natural	1.5	2.5	4	1.5	5
Overall preference	2	4*	4*	1	5

*One participant ranked one of the modes higher than the other; on average they received the same score.

4.4 Pilot Study with sEMG

To demonstrate that the results obtained using an HTC Vive controller are relevant in myoelectric devices, the above set up and controls were piloted using an sEMG interface as well. The virtual wrist device was controlled using a two-site surface sEMG and tested on two tasks with two prototypical motions. The results reaffirmed the previous observations; prototypical motions were more intuitive to use and appeared more natural without inducing further body compensation when compared to *sequential* control.

4.4.1 Control Input

To control the virtual hand, the participant's forearm was outfitted with two sEMG sensors (MyoWare™ Muscle Sensor AT-04-001), placed on the flexor and extensor muscle groups of the forearm under the elbow brace (see Figure 4.10), connected to an Arduino Uno. Sensor readings were translated to either on or off according to a calibrated threshold value. This corresponded to the trigger and thumb pad joystick inputs.

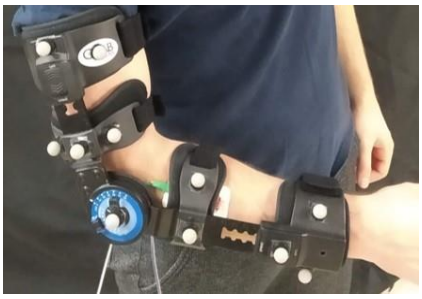

Fig 4.10 – The brace and marker set remained the same form the previous pilot and is based on Figure 4.2b. sEMG sensors were placed over the skin around the forearm can be seen underneath the elbow brace.

4.4.2 Procedure

In this pilot study, one healthy right-handed participant (male, age 28) performed two tasks related to ADL in VR by attempting to align the end effector with the desired goal. The subject did not have any visual or motion impairment and was comfortable using VR. Tasks included in this pilot study are described in more detail in Table 4.4. Because each prototypical motion corresponded to a specific task, they were included in the table for reference. Only two tasks were tested in this pilot, therefore only trajectories (4) and (3) (see Figure 2.7 for detail) were used, for *reaching to the cup* and *pouring with the cup*, respectively. Prior to each task, the participant was given ample time to practice and develop a strategy that they're comfortable with using during the task recording; the purpose was simulate the

performance likely achieved by an experienced user. For the *cup pouring* task, the cup object was automatically placed within the hand.

Table 4.4 – sEMG pilot tasks

Task	Task description	Corresponding wrist trajectory
Reach to cup	Standing, starting with the hand by the side, reach to the cup on the table	(4) supination/extension
Pour from cup	Sitting, transfer the cup from the table to the pouring location and orientation	(3) supination/flexion

4.4.3 Evaluation

In this brief pilot the participant's performance was assessed in two ways. Because the goal is to improve prosthesis use in the real world, the focus was placed on the time it takes to complete a task and movement cosmesis. The participant provided feedback and helped guide our interpretation of his performance. While cognitive effort to control the prosthesis was not directly measured, it may be inferred from the time measurements.

4.4.4 Results

Recorded wrist joint motion trajectories for each of the trials are displayed in Figure 4.11. Motions were segmented according to when the participant's hand began to move and when the target end effector position and orientation, was reached.

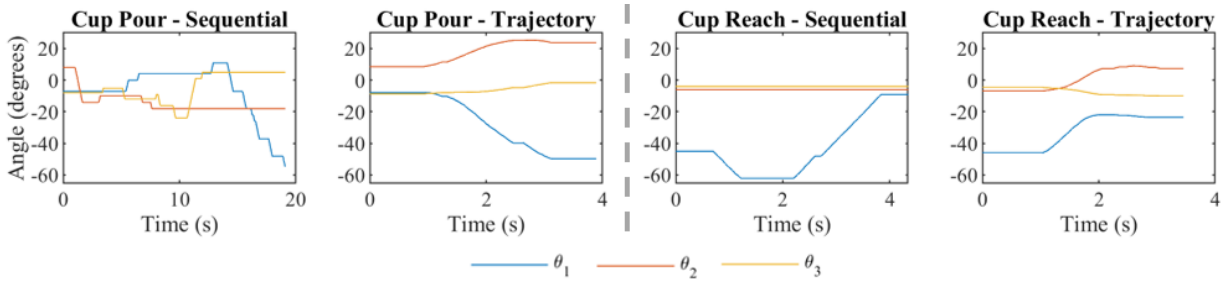

Fig 4.11 – The 3 DOF wrist joint angle trajectories are displayed for each trial. θ_1, θ_2, and θ_3 correspond to pronation, flexion, and ulnar deviation respectively. The left two plots correspond to the cup pouring task under the two different control strategies, sequential and trajectory control, while the right two images correspond to the cup reaching task. Wrist rotation did not necessarily begin when the hand started to move.

The participant was able to complete both tasks faster using *trajectory* control. *Sequential* control for the *cup pouring* task took significantly longer than when using *trajectory* control, while the times were much closer for the cup reaching task. This is likely because the task required switching between the different joint angles, which can be challenging, or even confusing, for the user. The *cup reaching* task did not require switching between the different DOF, and supination alone was sufficient.

Wrist motions appeared more natural under *trajectory* control. This is largely due to the lack of simultaneous access to all 3 DOF of the wrist during *sequential* control, as is evident in Figure 4.10. Without haptic feedback, the user appeared to be looking down at their simulated device. This was exacerbated when multiple mode switching was required, such as for the cup pouring task with sequential control. Trajectory control for both tasks did not require mode switching, since a single mode, corresponding to the respective task, was sufficient.

The results obtained in this pilot largely overlap with those found using the HTC Vive controller. This suggests that observations made with controller inputs other than sEMG can be insightful. In particular *trajectory* appeared to outperform *sequential* control on a number of criteria.

4.5 Discussion

The performance of a novel wrist prosthesis control methodology, namely *trajectory* control, was assessed by comparing to alternative methods. Assessments included evaluating body compensation and cognitive load that users inevitably experience when faced with complex orienting tasks. None of the participants reported an issue with

achieving the end effector goal location and orientation, and felt that the tolerances were fair, even when struggling to complete certain tasks using the *no-wrist* control condition.

Participants were expected, but not required, to make use of the wrist control modes to assist them in completing the tasks. However, the three participants consistently elected to use wrist functionality in every task with every DOF at some point being used throughout the experiment. On a preference level, this marks the importance of a wrist prosthesis.

During the sEMG pilot, when using *sequential* control, the participant generally relied on fewer DOF than were available. This was likely the easiest way to control the wrist without having to repetitively switch between DOF. This showcases the benefits of trajectory control whereby all 3-DOF of the wrist are at use while maintaining a simple and intuitive control strategy.

Participants did not use *simultaneous* control as expected, and largely operated the DOF sequentially. This is likely due to the difficulty associated with visualizing the interaction between different DOF and operating them simultaneously. However, because switching between modes was not required, task completion was nonetheless faster. This contributed to participants identifying this mode as easier to operate. This is consistent with previous findings [91]. Although possible, switching was not necessary for trajectory control, since a desired trajectory was preselected during training. This has the potential to bias results related to time. However, this was deliberately done so that I could demonstrate that orienting the hand using the novel control methodology is feasible, and perhaps superior to other control methods when orienting is analyzed in isolation. In order to fully assess *trajectory* control, a more comprehensive task protocol will be used that includes ADL tasks that require switching and grasping, and is presented in Chapter 5.

Trajectory modes were faster compared to alternative control approaches, requiring users to operate a single embedded DOF that automatically oriented the wrist close to the desired goal. Given that the five trajectories were created using a much larger set of motions, I did not expect the final hand orientation to be exact. However, body compensation, measured as ROM and Cartesian path length, was largely comparable to the other controls that had the capacity to orient the hand in any desired way. This suggests that the reduced cognitive burden is worth the reduction in direct orientation control. One interesting finding was that the *no-wrist* condition was overall faster for one of the subjects. I suspect it was due to the reduced cognitive burden and perhaps due to the simplicity of the orienting strategy. Despite that, it had the largest amount of body compensation, appeared unnatural, and was the least preferred by both

participants, suggesting that movement cosmesis, or perhaps a reduced amount of physical exertion, is likely more important than speed.

While training time was not quantified, I made a few observations. Training time for the *natural* and *no-wrist* conditions was unsurprisingly very short, and time was primarily spent trying to simply understand what hand positions satisfied the task conditions. Out of the three wrist control conditions, I observed that training time for the *trajectory* control was the fastest, as participants did not have to figure out a sequence of inputs. However, this is only the case if a mode is known in advance, as it was in our experiment. The next chapter investigates what happens when mode switching is required, as it will be in the real world where multiple trajectory sequences are used to complete a series of tasks, and I suspect that training time will increase and participants will have to focus on memorizing which modes are useful to which tasks.

Preliminary results demonstrate the ability of the trajectories to effectively carry out the tasks they are supposed to represent, by demonstrating that participants were able to complete all the tasks without major body compensation motions. This suggests that the prototypical motions could be practical in everyday use. To further validate their use, the test protocol would need to expand to tasks beyond the ones that the motions constitute. It might be the case that the trajectories do not fully generalize and additional modes or fine tuning of the hand orientation will be required. Grasping, commonly the sole mode in powered transradial prosthetic devices, was also omitted as the focus was primarily on positioning the hand, but will be included in our next experiment described in Chapter 5 to assess whether the additional cognitive burden dissuade users from engaging with wrist control.

4.6 Conclusion

In this chapter the benefits of a novel wrist control are highlighted, based on 3 DOF trajectories, in completing daily tasks in VR. Additionally, the pilot studies have successfully validated the use of VR and have informed improvements that are included in Chapter 5. A vast reduction in cognitive burden associated with operating a 3 DOF wrist device was observed while maintaining the benefits of a fully articulated wrist. Although participants did not have full control over the orientation of the hand, the much simplified *trajectory* control was nonetheless comparable with alternative approaches when evaluating time to complete the tasks and body compensation. Prototypical motions appeared to generalize well to the tasks, without requiring the user to excessively compensate with their residual limb

or torso. These preliminary findings motivate the recruitment of more subjects and a larger investigation into wrist trajectory control as well as the development of a physical 3 DOF wrist device.

Because rejection rates appear to be higher for more proximal levels of amputation [92], I believe that the application of this work will be even more valuable to elbow-wrist, and shoulder-elbow-wrist prosthetic devices [93]. I therefore expand the VR platform to address these in Chapter 5 using the additional prototypical motions identified in Chapter 2.

5 EXPERIMENT IN VIRTUAL REALITY

The next step in testing prototypical motions as a novel prosthesis control method is to implement a more comprehensive test. The pilot studies, described in detail in the previous chapter, indicated that *trajectory* control was superior to both *sequential* and *simultaneous* control on a number of criteria, however, testing was limited to a 3 DOF device, subtasks were not strung together, and grasping was not required. In this work I make use of VR and participants with unaffected limbs to test whether leveraging learned motions to control 3, 4, and 7 DOF devices outperforms alternative control approaches, while avoiding having to build and implement the physical device hardware. I address the following questions regarding *trajectory* control use in a prosthetic device: does it reduce the time it takes to position and orient the hand, does it mitigate body compensation, and do users have a preference. By exhibiting controls' efficacy in VR, I hope to provide a foundation for the development of physical complex prosthetic devices in the future. More specifically, I look to demonstrate *trajectory* control as a feasible control method to position and orient the end-effector of various prosthetic devices. For a full description of how the prototypical motions were obtained I direct the reader to Chapter 2.

5.1 Experiment Protocol

Several changes were made to the VR set up to account for the 4 DOF and 7 DOF devices as well as address the shortcomings of the previous iteration. Primary changes include the addition of virtual body segments for participants to use as a reference when operating different devices. This also required the implementation of a new control input since the HTC Vive controller was limited to 3 paired inputs, accounting for at most 3 DOF *simultaneous* control. Finally, changes to the protocol included a more comprehensive list of tasks that required grasping and the sequential completion of subtasks.

In this updated version of the VR protocol, twelve right-handed participants (ages 18-53) completed the study over one session, lasting from 6 to 8 hours. In addition to lunch, participants were encouraged to take as many breaks as they needed. Data processing and analysis was performed in MATLAB 2021a.

5.1.1 Virtual Reality Environment

Virtual objects related to the expanded task list were added as well as a virtual computer monitor was designed to help participants monitor their prosthesis use in VRE (Figure 5.1). This was done to mimic what a potential real-world use might look like, where prosthesis users may have a tablet on hand as an aid during training or general use. The virtual computer monitor displayed the mode and controls that the device was currently in and the control inputs coming from the user. It was always placed in front of the user on the virtual table. Additional visual feedback was included in the form of two posters, placed on the left and right walls of the virtual room listing the modes for the participants to reference (Figure 5.2).

Fig 5.1 – Four tasks are highlighted, starting at the top left going clockwise: kettle, screw, cook, and fork use. The kettle, screw, and cooking tasks were included in the protocol to test the ADL generalizability of *trajectory* controls. Poster listing the prototypical motions for trajectory control can be seen in the top left panel. Poster listing the order of joints can be seen in the bottom left panel.

All segments of the prosthesis (humerus, forearm, and hand) were scaled to the average human arm dimensions. Although included in this iteration of the experiment, given that grasping is nonetheless not the focus of this work, in-hand object kinematics and dynamics were not considered; successful initiation of a grasp (and likewise release)

resulted in the object to automatically connect to the palm of the end effector as if they had grasped it using a natural hand.

5.1.2 Control Input

To ensure that the prosthesis control inputs remained consistent across prosthetic devices and control conditions, a modular control board was implemented: MIDI audio interface, K-Mix (Keith McMillen Instruments, Berkeley CA, USA) (Figure 5.2). To imitate sEMG inputs found in myoelectric devices, slider intensity corresponded to a velocity input. For each slider, one inch in the middle of each slider was dedicated to a "dead zone", where velocity input remained at zero, and whose value gradually increased or decreased towards the ends. This was done so that participants could rest their finger on the slider without inducing motion; a particularly important feature for simultaneous control when multiple sliders were being used. A digital keyboard was selected over an analog due to the ability to program a "zeroing" of the sliders when a finger was no longer making contact. The keyboard is set on the torso pad worn by the participants and is meant to be controlled with the left hand for the 3 and 4 DOF device, freeing up the right arm to move around. For 7 DOF device, both hands are free to control the device since all the arm joints are controlled with the keyboard (Figure 5.3).

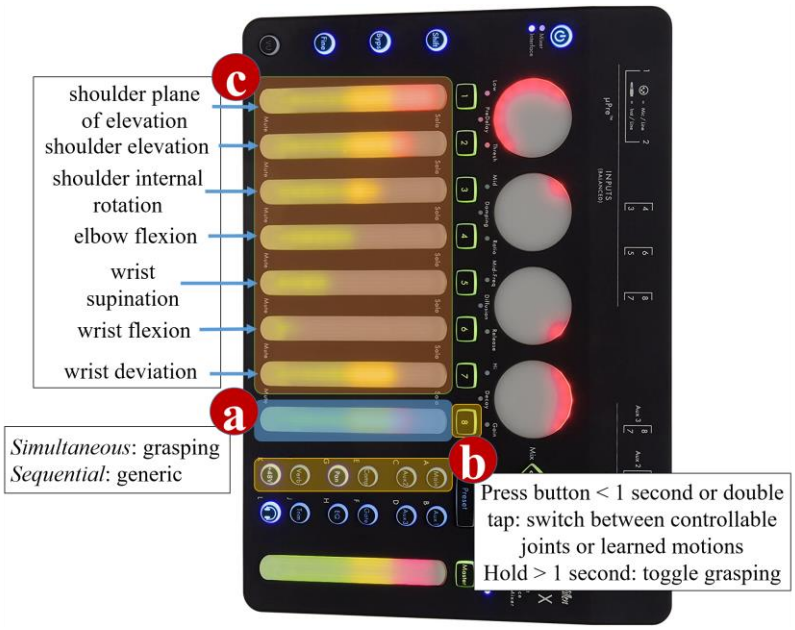

Fig 5.2 – K-Mix MIDI keyboard. This keyboard was converted to a prosthesis controller by programming the buttons and sliders. (a) This slider was used in conjunction with any one of the buttons highlighted in (b) for both *sequential* and *trajectory* control. The right side of the slider was the "forward" direction and the left was "backward", while buttons were used as toggles between grasping or for switching between joints or learned motions. (c) These sliders were dedicated for *sequential* control, with each corresponding to a different arm joint. For *sequential* control, slider (a) was used for grasping. All other buttons and sliders were not used.

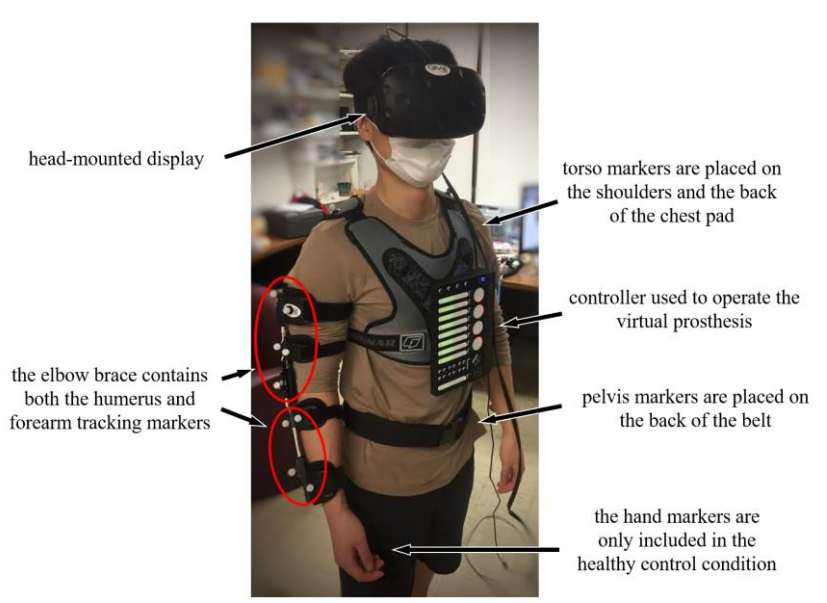

(a)

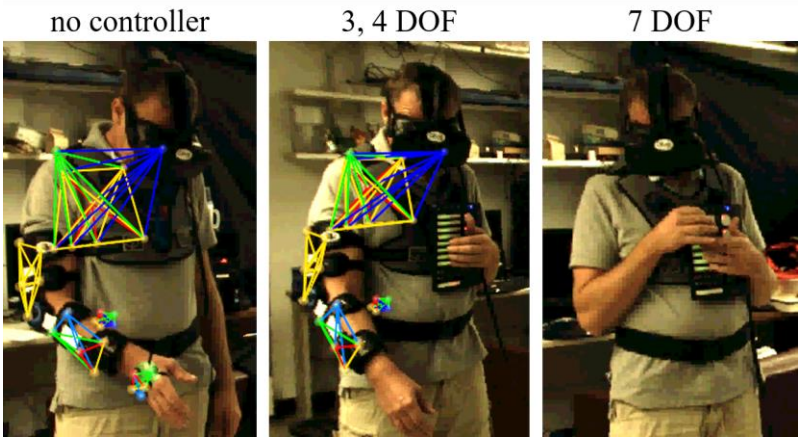

(b)

Fig 5.3 – (a) Each component of the input is described. (b) Left panel: highlighted marker clusters correspond to each body segment. Pelvis markers are seen as a small cluster near the forearm. Marker arrangement tracking the hand were used using the natural control condition, and ignored for the no-wrist control condition. The elbow brace was allowed full range of motion. Middle panel: the controller was operated using the left hand. Forearm markers were tracked for 3 DOF control but ignored for 4 DOF control where only the humerus markers was needed. The elbow brace could be allowed full range of motion in both cases, though all participants found it helpful to lock the brace into a single position for the 4 DOF controls. Right panel: since, the participant operated a 7 DOF virtual arm, tracking the humerus was no longer needed. Torso and pelvis markers are present but not highlighted in the image.

For easy donning, markers were placed on wearables. To track the hand markers were placed on a small pad with elastic straps. An orthopedic elbow brace (Orthomen ROM Elbow Brace, Foothill Ranch CA, USA) was used to track the forearm and humerus. A modified lacrosse pad (Gait Gunnar Lacrosse Shoulder Pads) was used to track the torso. Finally, a nylon tactical belt with a plastic buckle was used for pelvis tracking. Marker clusters for the torso and the pelvis were placed on the dorsal side to avoid optical occlusions (Figure 5.3).

Certain segments were left untracked when a virtual prosthetic device was being used, for example, the hand and forearm were not tracked when the participants operated the elbow-wrist prosthetic device; the input came directly from the controller.

5.1.3 Control Modes

The control modes used in Chapter 4 are included in the expanded version as well, and include several changes. For both the *natural* and *no-wrist* trials only, grasping was instantaneously initiated when the hand reached the target location and orientation. Negative controls in which the virtual prosthesis lacked an elbow or a shoulder control were not included due to the inability to perform the majority of tasks.

In *sequential* control, only one slider was in use, while switching was relegated to a button, mimicking the mode switching in myoelectric devices. While this set up seems distinct to the two-site sEMG input in myoelectric devices, functionally they are the same: each half of the slider rotates a joint either forward or backward. A single button press toggled the control mode down the joint list, a double tap toggled the mode up the list, and a prolonged 1 second press of the button toggled grasping (or releasing). Switching between controllable joints cycles in the following order: *i*) shoulder plane of elevation, *ii*) elevation, *iii*) shoulder internal rotation, *iv*) elbow flexion-extension, *v*) wrist pronation-supination, *vi*) flexion-extension, and *vii*) radial-ulnar deviation [42]. Only the relevant joints are included for the 3 and 4 DOF devices. This sequence was listed on a poster in the VRE that the participants could reference at any time (Figure 5.1).

One of the main reasons for moving away from the Vive controller was its limited number of inputs. To simultaneously control a virtual 7 DOF arm and grasping functionality, 2×8 inputs were needed, impractical with either the Vive controller or standard sEMG. Multiple sliders were made available on the MIDI keyboard and button functionality was no longer needed. Each slider corresponded to a single DOF, and participants could decide whether

they wanted to operate them using several fingers concurrently or one at a time. Much like each of the controllable joints, grasping and releasing was also performed using a dedicated slider.

In *trajectory* control participants had the same interface in *sequential* control: one slider was used to move forward and backward along a prototypical arm motion, and a button to toggle between the modes and initiate a grasp. Implementing the learned motions from Figure 2.10, 2.12, and 2.14, there were 5, 11, and 11 options for the 3, 4, and 7 DOF devices, respectively; examples of what these looked like VR are seen in Figure 5.4. Each motion was listed on a poster in the VRE accompanied by a list of tasks from which the motions were extracted from (Figure 5.1), and would likely be the best candidates to help users complete those tasks. Prior to each task, participants had the ability to try out the motion trajectories and decide with which mode they ultimately would like to begin.

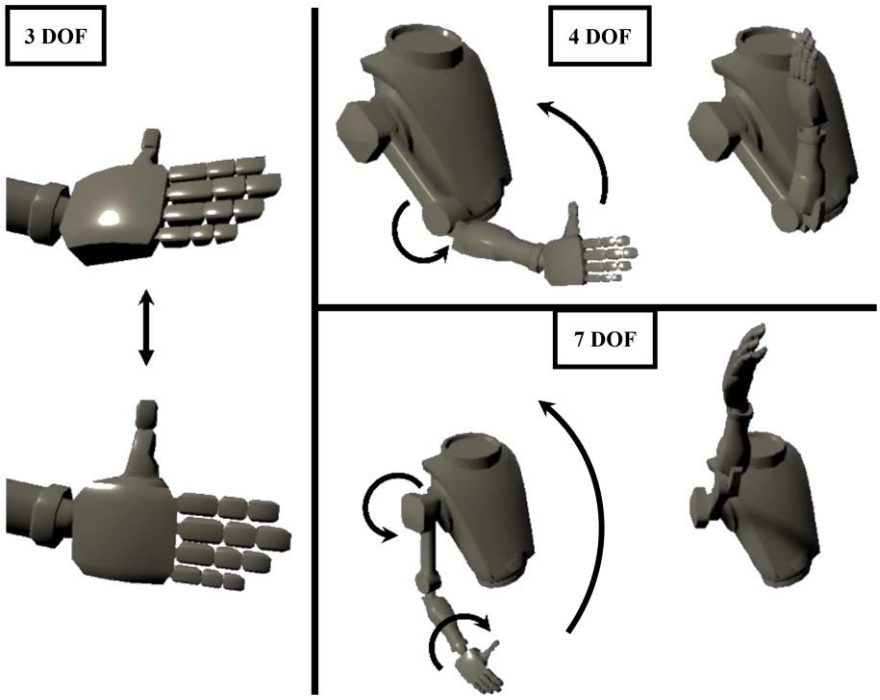

Fig 5.4 – An example of a prototypical motion is shown for each device. In the 4 DOF case, the humerus is stationary.

5.1.4 Study Procedure

In total, 12 ADL tasks were selected that required the use of only the right arm, covered a variety of locations, and included both reaching motion and object manipulation (Table 5.1); these were also chosen to span as many of the learned motion modes in *trajectory* control as possible. The VRE and objects were created to scale (Figure 5.1), and 9 of the 12 tasks were set up according to dimensions described in Figure 2.3; 3 tasks were added to the protocol

to test trajectories against tasks that were not included in generating them. Therefore, there is not necessarily a *trajectory* mode designed for every task or target condition. Tasks included different number of subtasks, totaling to 43 subtasks, composed of 30 reaches and transfers and 13 grasps and releases. Each set of 12 blocks was completed by each control mode in the order depicted in Figure 5.5.

Table 5.1 – Protocol tasks

standing tasks[a]

axilla	(1) reach axilla
briefcase	(1) reach briefcase (2) grab (3) transfer to table
cell phone	(1) bring cell phone to ear
cook	(1) reach pan handle (2) grab (3) transfer pan to stove (4) release (5) reach knob (6) grab (7) turn knob 90 degrees counterclockwise
cup drink	(1) reach cup (2) grab (3) bring cup to mouth (4) return cup to table
door knob	(1) reach door knob (2) grab (3) turn knob 90 degrees clockwise
kettle	(1) reach kettle handle (2) grab (3) pour into container
overhead	(1) reach can on top shelf (2) grab (3) bring to front of body (4) return can to middle shelf (5) release
suitcase	(1) reach suitcase (2) grab (3) transfer

sitting tasks[a]

cup pour	(1) reach cup (2) grab (3) pour into container (4) return to table
fork	(1) reach fork (2) grab (3) stab food (4) bring fork to mouth
spoon	(1) reach spoon (2) grab (3) transfer spoon to bowl (4) scoop (5) bring spoon to mouth

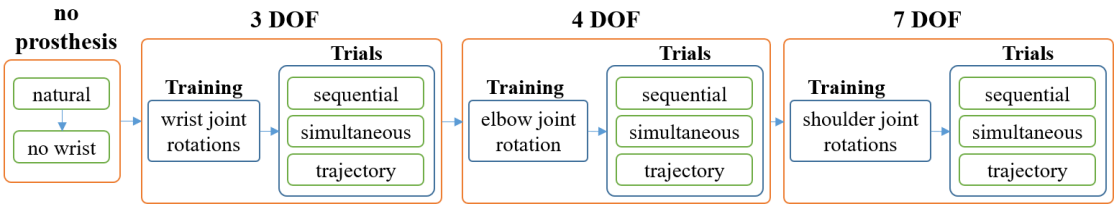

Fig 5.5 – The experiment protocol consisted of eleven blocks of testing, corresponding to each control mode and device combination (in green). Each block consisted of a randomized order of the twelve tasks. The first and second blocks corresponded to *natural* and *no-wrist* conditions, respectively, so that participants could familiarize themselves with the testing environment and target requirements before attempting to use the virtual prostheses. In sets of three blocks, 3, 4, and 7 DOF devices were used, in that order. Each set of three blocks corresponded to *sequential*, *simultaneous*, and *trajectory* controls, allocated randomly. Training periods were included to familiarize the participants with the body joints.

Prior to each tasks, participants were to begin with their hands relaxed by their side if standing or on their laps if sitting. Each task had to be completed all at once, without breaks between subtasks, and included matching the end effector to its target pose. A successful completion of a grasping subtask resulted in the object to automatically be attached to the hand, and is followed by a transferring subtask in which the object, rather than the end effector, is required to be placed in a new location and orientation starting from where they grasped it. For sequential and simultaneous control, the controllable joints were reset to zero prior to the start of a new task. To ensure that participants intentionally completed the tasks, the target pose had to be held for one second.

Several conditions were implemented to ensure that the virtual tasks were representative of a hypothetical real device. As in real life, if a cup was tilted beyond 180 degrees during a transferring phase, then the whole task failed; this condition is unique to the cup drinking and the cup pouring tasks. Screwing and turning a knob would likewise fail if the end effector did not maintain its position while rotating. Finally, tasks were flagged as incomplete if the participant was unable to complete a subtask within one minute.

5.1.5 Data Analysis

During the experiment the following were captured: position and orientation of the different body segments, inputs from the MIDI controller, and task success/failure status. Similar to the pilot study in Chapter 4, the start of the trial was manually detected when participants began to move, while the end was automatically determined by the

software when the target pose for the final subtask was reached and held for 1 second. A moving average of window size 5 was used to smooth the data after large discontinuities were manually removed.

Several processing steps were taken to ensure interpretable results. According to the shoulder angle definitions [35], a discontinuity appears when the humerus is perfectly vertical, aligning the plane of elevation and internal rotation axes. Therefore the plane of elevation and internal rotation data was ignored when calculating ROM or Cartesian path length when humeral elevation is below 15 degrees. Otherwise, refer to Chapter 4 for details regarding ROM and Cartesian path length calculation.

At the end of the experiment participants were asked to fill out a survey that included questions about their overall preference of control methods on a scale of 1 (did not like) to 5 (very much liked). Participants were also asked to indicated on a scale of 1 (disagree) to 5 (agree) to the following statements about each control-device combination: (a) easy to learn, (b) appeared natural (did the motion resemble a healthy arm), (c) mentally challenging (gauges the cognitive burden), and (d) physically challenging (gauges the amount of body compensation).

Before running statistical comparisons, missing data due to failed tasks was estimated using Multiple Imputation method with Monte Carlo Markov Chain (SPSS 2019). Tasks that were not completed by any participants with a given device and control condition cannot be imputed and were therefore omitted from the analysis for the other control conditions as well. Approximately 7.4% of the distributions being compared did not strictly meet the assumption of normality under the Shapiro-Wilk test. The data across all conditions did appear to come from a normal distribution, so the analyses proceed. Multivariate analysis of variance (MANOVA) was performed for each device to test if there was a significant difference between controls (excluding *natural* and *no wrist* conditions). The α-level was adjusted to 0.0031 using Bonferroni correction to account for repeated MANOVA calculations; 16 tests in total were made for each device. Follow up analysis of variance (ANOVA) tests were performed between pairs of controls. Repeated testing was adjusted with Bonferroni correction as well, accounting for tests within each dependent variable category (i.e. time, Cartesian path length, and ROM). Because the order of the 3, 4, and 7 DOF devices were not randomized in the experiment protocol, quantitative and qualitative assessment comparisons were not made between them but within each device category, i.e. the 4 DOF trajectory control was only compared to the other two 4 DOF controls.

5.2 Results

All participants completed the experiment to the best of their ability, though most were not able to complete every task with every control mode. Reasons for failing to complete a task included timing out, failing a transferring condition, or quitting. Some tasks under certain control conditions were not completed by any participant and included *reach to axilla* and the *eating with a spoon* tasks using the *no-wrist* control, *reach to axilla* task with the 3 DOF *trajectory* control, and *cooking* with the 7 DOF *sequential* control. A detailed list of which modes lead to the most failed tasks is shown in Figure 5.6.

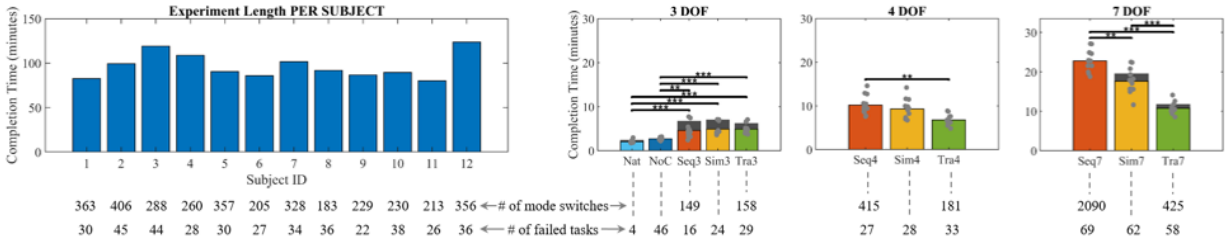

Fig 5.6 – Experiment completion times are displayed per subject and per control. Colored bars all contain the same data, while dark bars may contain tasks that other control modes do not include. Each participants' total time spent using each control mode and device is displayed as a dot. ANOVA results are displayed between pairs of controls for each device; significance levels were set at p-values of 0.05, 0.01, and 0.001 after adjusting for repeated testing. Numbers below the three bar charts on the right indicate the number of mode switching that occurred and the number of failed tasks, whether per subject or per control. Training periods were included to familiarize the participants with the body joints, but omitted in the time calculation above.

After accounting for the variability between subjects and tasks, time was found to be significantly different ($p < 0.001$, MANOVA) between prosthesis control conditions for both 4 and 7 DOF devices; it was not significant for 3 DOF devices, with p-value = 0.86. The time it took each participant to complete the entire experiment is displayed in Figure 5.6, along with the number of mode switching that occurred when using sequential and trajectory controls and the total number of failed tasks. A mean completion time for each test condition was calculated by summing the average task times across participants. Because some participants were not able to complete every task, the average time it took one participant to complete the tasks was on average shorter than the representative completion time.

After accounting for the variability between subjects and tasks, Cartesian path length was found to be significantly different in the wrist both the 4 DOF ($p = 0.002$) and 7 DOF ($p < 0.001$) devices. Representative Cartesian path length of each joint center is summarized in Figure 5.7. Similar to the representative completion times, these were calculated by summing the average lengths per task for each control condition. Distal joints on average travelled further than proximal ones. Thus, differences between control modes increase in the distal joints, an observation that can be seen to further increase the more DOF were controlled. For tasks that no participant was able to complete with a given condition, that task was removed from the colored bars, as well as the analysis, and included in the black bars in Figure 5.7. For the 7 DOF device, the black bars in sequential and trajectory controls are nonetheless shorter than the colored bar in sequential, pointing to the inefficiency of sequential control.

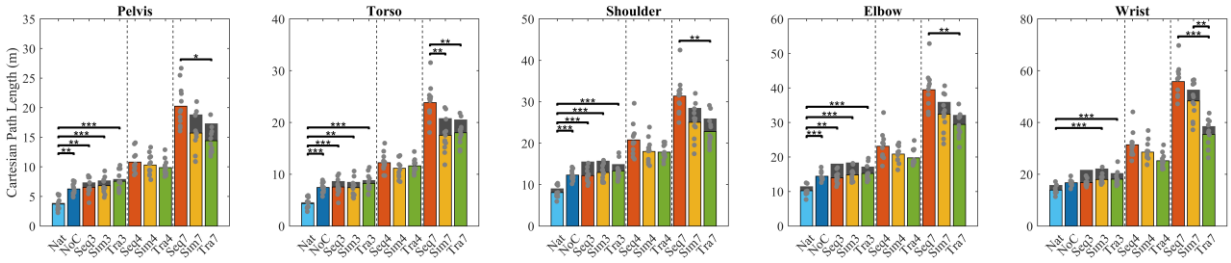

Fig 5.7 – Representative Cartesian path lengths are displayed as colored and dark bars. Colored bars all contain the same data, while dark bars may contain tasks that other control modes do not include. Each participants' total Cartesian path length for each control mode and device is displayed as a dot. ANOVA results are displayed between pairs of controls for each device; significance levels were set at p-values of 0.05, 0.01, and 0.001 after accounting for repeated testing.

Significant differences in ROM between control conditions are summarized in Table 5.2: using MANOVA, p-values are calculated to test the significance of the difference between control methods for each device and joint angle. ROM of each joint angle was assessed to evaluate body compensation under different conditions and control modes by calculating the average ROM across tasks and participants (Figure 5.8). For the 3 DOF condition results, the negative control (no-wrist condition) generally had the largest torso, shoulder, and elbow ROM, while the positive control (*natural*) had the highest wrist ROM and the lowest ROM in the other joints, satisfying the control expectations. Significance levels are included, though likely due to the conservative Bonferroni method, significant difference between two conditions related to a body joint, rather than a prosthesis joint, were not found. The torso,

shoulder, and elbow ROM were generally mixed between the three prosthesis control conditions. While ROM is primarily analyzed with respect to body compensation, it can also be used to evaluate device usage as it relates to power consumption and motion efficiency.

Table 5.2 – ROM MANOVA p-values

		Device		
		3 DOF	4 DOF	7 DOF
torso	flexion	0.34	0.35	0.03
	lean	0.71	0.22	0.02
	turn	0.30	0.63	0.34
shoulder	plane of elevation	0.02	<0.01*	0.01
	elevation	0.55	0.01	<0.01*
	internal rotation	0.34	0.01	0.30
elbow	flexion	0.38	<0.01*	0.45
wrist	supination	0.44	0.29	0.04
	flexion	0.17	0.42	0.19
	deviation	0.14	<0.01*	0.03

Adjusted α-level identified significance when p-values were below 0.0031, denoted with an *

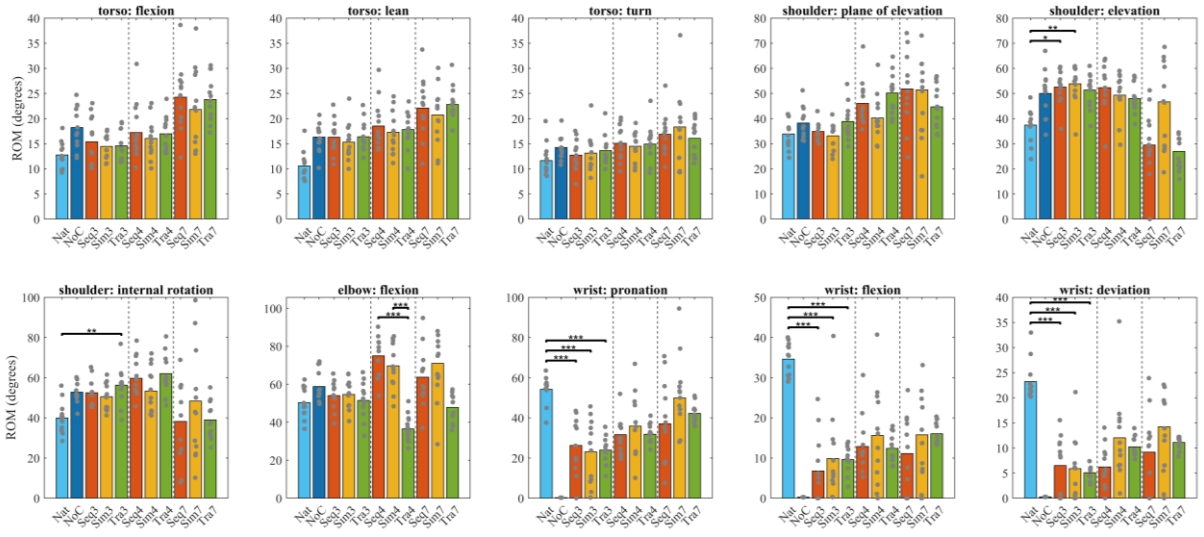

Fig 5.8 – Representative ROM values averaged across all tasks are displayed. Each participants' average ROM for each control mode and device is displayed as a dot. ANOVA results are displayed between pairs of controls for each device; significance levels were set at p-values of 0.05, 0.01, and 0.001 after accounting for repeated testing. Significance bars were omitted for the wrist joint angles in the *no wrist* conditions.

After each experiment session subjects had the opportunity to give verbal feedback as well as rank the controls on various qualities on a scale from 1 to 5 (Figure 5.9). Between the three prosthesis controls, there appear to be several trends that gradually change from 3 to 4 DOF and 4 to 7 DOF devices. For example the preference given to trajectory control appear to improve relative to the other modes the more DOF a device had. Note that the scores are a reflection of the participants' perceptions, so survey results may end up being inconsistent with the quantitative measures. For example while the trajectory control was perceived less physically challenging in the 7 DOF than the 4 DOF device, ROM results indicate otherwise.

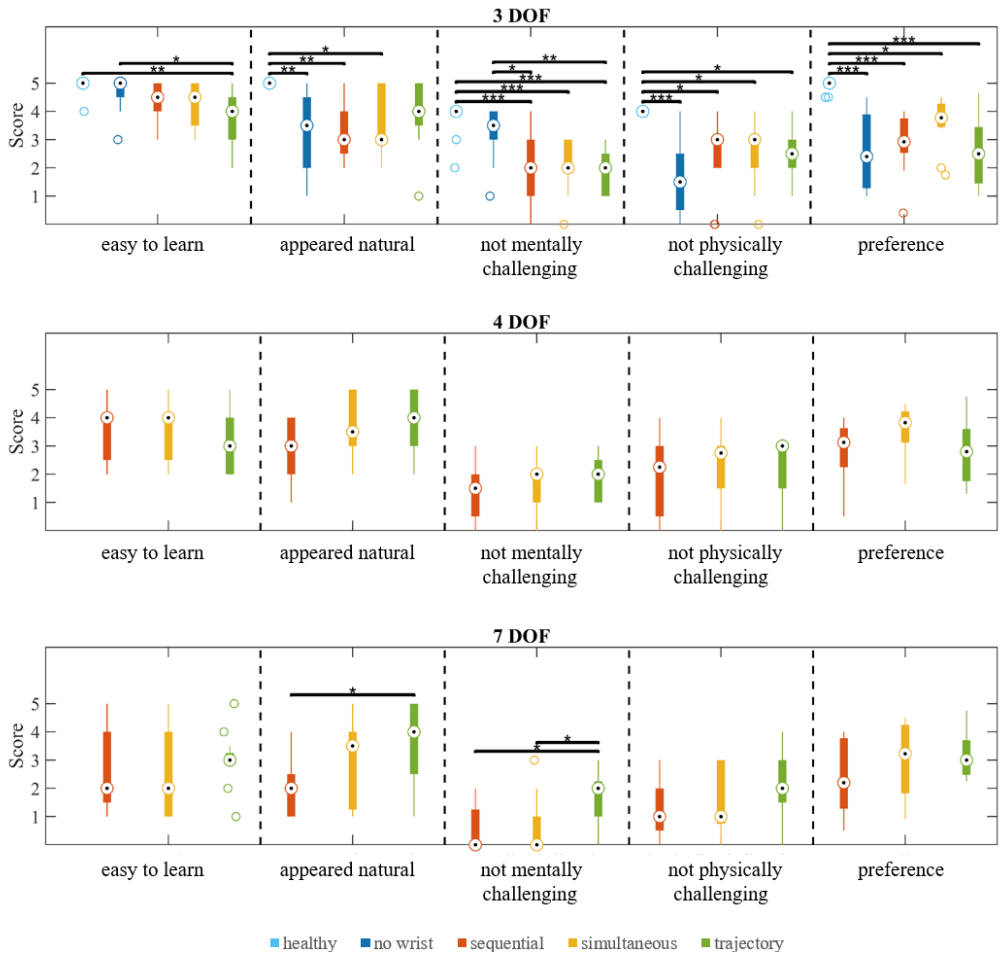

Fig 5.9 – Box plots indicate the median, 25th and 75th interquartile range, and outliers of survey results, separated by device type. Mentally challenging and physically challenging are displayed not mentally and physically challenging by flipping responses from 1-5 to 5-1, such that a higher value was indicative of predilection across all fields. ANOVA results are displayed between pairs of controls for each device; significance levels were set at p-values of 0.05, 0.01, and 0.001 after accounting for repeated testing.

5.3 Discussion

Many of the observations that were made in the pilot study are reaffirmed on here and expanded through an analysis of 4 and 7 DOF devices. While the overall message remains the same, new insights were discovered and are discussed below.

In this protocol I tabulated the number of times participants switched between modes. The effect of switching may have contributed to a shorter completion time when using *simultaneous* compared to *sequential* control [91] for the 4 and 7 DOF. This likely contributed to participants to consistently identify *simultaneous* control as easier to operate, and generally preferred over *sequential*, despite a lack of distinction in the time it took to complete the tasks with the 3 DOF device. I noticed that despite *trajectory* control requiring users to use mode switching as well, the time to complete the tasks was shorter still in the 4 and 7 DOF devices. This demonstrates that positioning and orienting the hand using learned prototypical motions is not only feasible, but potentially superior under certain conditions to the other control methods.

When it comes to completing the tasks in a natural way with low extraneous movements and at a timely manner, there appears to be a tradeoff. One interesting finding was that the *no-wrist* control was significantly faster than the other 3 DOF controls. I suspect it was due to the reduced cognitive burden and likely due to the simplicity of the orienting strategy; participants had a clear expectation of what was possible, and thus vastly simplified their control plan. However, it also had the largest amount of body compensation, appeared unnatural, and was the least preferred by all participants, suggesting that movement cosmesis and reduced body compensation are likely more important than speed alone. This is reaffirmed by the observation that participants engaged with all the controllable joints in each of the devices, even at the cost of longer completion times. Ensuring that participants were not feeling pressured to use the device, they reassured that it was entirely because they wanted to mitigate body compensation.

As participants moved from the 3 to the 4 DOF device the training time was shorter for the *sequential* and *simultaneous* controls gotten longer for *trajectory* control. When controlling the joints independently, the addition of an elbow did not impose much more complexity and largely overlapped with the 3 DOF controls, whereas the participants had to relearn a brand new and larger set of motions for *trajectory* control. The opposite was observed for the 7 DOF device. Relearning a new set of motions for *trajectory* control was not only similar, but participants noted that they were more intuitive than the 4 DOF motions given the more straightforward association between whole arm motions and tasks. The same was not true for controlling the joints independently, and the addition of three new controllable DOF (i.e. shoulder), was significantly more difficult to intuitively grasp than the previous joints. However, when using *sequential* and *simultaneous* control, participants seldom referenced the virtual posters. The opposite was true when using *trajectory* control, where participants referenced the poster almost every time they

looked to switch modes. Training time appeared to have been relegated to the poster, so a more in depth investigation in the future should address learning and memorization of the learned motions in *trajectory* control.

Participant feedback confirmed several notable observations. Those that had an easier time controlling the devices at a joint level, normally preferred the *sequential* and *simultaneous* controls, though most participants preferred trajectory the more DOF were being controlled. For the 7 DOF device, *sequential* control was preferred by some over *simultaneous*, noting that *simultaneous* control had too many inputs to keep track of, but on the other hand, the excessive mode switching that was necessitated in *sequential* was cumbersome. Most participants preferred *trajectory* control in the 7 DOF device, as it combined the simplicity of controlling one DOF at a time and simultaneous joint movement. Therefore, it is very likely that *trajectory* control will have the most impact in the 4 and 7 DOF devices, especially since transhumeral and shoulder disarticulate patients have higher rates of prosthesis rejection [92].

Trajectory control mode was successful in completing three ADL tasks beyond the motions that it was design after, and thus highlighting its versatility. On the other hand, participants failed to complete the *axilla* task for the 3 DOF device, suggesting that there are still certain limitations and perhaps the addition of a second input, such as one based on fPCA, could push this method further. I suspect that the concept of using learned motions could be extended to other devices and sets of tasks, such as the JACO wheelchair-mounted robotic arm [17].

I reaffirm previous findings in the pilot studies that there is not a significant or consistent distinction in body compensation, whether Cartesian path length or ROM, between the different prosthesis controls. *Sequential* control generally appeared to have the most body compensation, particularly in the Cartesian path lengths of the arm joints. This suggests that despite switching and a limitation to specific motions, the benefits of *trajectory* control, namely completion time, human-like appearance, and control intuition, are worth exploring further.

6 CONCLUSION

The aim of this thesis was to propose novel control methods, develop them using data driven approaches, and validate them through a series of human subject testing. Findings provide strong motivation for the development of complex prosthetic devices as well as offer insight into the biomechanics of our arms and categorizations of real world tasks.

6.1 Summary

In Chapter 2, categories of arm motion were identified as well as their respective averages and variation. This chapter in particular emphasized the exploration of unsupervised learning methods. It is generally accepted to report the performance of several, if not many, common algorithms. In the present case, the selection of the primary algorithm was largely heuristically driven, though comparisons to other algorithms were also made. Given that the application of this work was to be implemented in a device operated by humans, efforts were made to ensure that results were useful and intuitive. One major observation was the number of groupings that emerged for each arm model (3, 4, or 7 DOF), as these not only provide a lower dimensional representation of the upper-limb biomechanics, but is also useful for prosthesis implementation. The prototypical motions of each group could on one hand be implemented in hardware, as has been suggest with DTM [94], though in software all motions would be accessible.

This was taken as step further in Chapter 3 by reducing the dimensionality of the 6 DOF hand alone. A prosthesis implementation is proposed whereby users would select from a list of task locations followed by a selection of hand orientation. It was found that certain locations were coupled with orientation, further reducing the dimensionality of the workspace. As with choosing an analysis pipeline, there were multiple ways to obtain features from the data. By analyzing different approaches, namely hand trajectories, straight-line trajectories, and task-locations, additional biomechanical observations were made possible. For example, what constitutes a subtask or a submotion has commonly been heuristically identified and used as a ground truth to test data driven approaches, yet our intuition may have overlooked a submovement during certain reaching and transferring tasks that passed by the body.

In Chapter 4, a series of pilot tests were presented measuring both the efficacy and potential use of prototypical motions as well as the ability of the VR testing platform to provide accurate measurement of prosthesis use performance. The performance of users operating the 3 DOF wrist with the proposed control method outperformed the state of the art, motivating a comprehensive test protocol. Observations were consistent across different control interfaces as well. However, several simplifications were made, such as analyzing each subtask independently of one another rather than strung together as part of a single task.

Expansions to both the protocol and controls were made in Chapter 5. Quantitative and qualitative evaluations were made to assess the proposed *trajectory* control against the state of the art for 3, 4, and 7 DOF devices. The changes in the protocol have shed further insight into some of the preliminary findings in the pilot studies. For example, the time it took participants to complete tasks with the 3 DOF device was not necessarily faster with *trajectory* control after all, likely due to the necessity to switch between modes, which entailed referencing the virtual poster. On the other hand, the completion time relative to the other control methods did get shorter with added device complexity. The same was observed for Cartesian path length of the body segments, while ROM was largely very similar between control methods. The primary takeaway was that body compensation was not exacerbated despite taking away the ability to rotate the joints in any desired way, while reaping the benefits based on completion time and user feedback.

6.2 Tabulation of Heuristics and Considerations

The field of research regarding dimensionality reduction of upper-limb use has yet to be fully explored, and there are few, if any, established methods of developing upper-limb prosthesis controls. Therefore, many data analysis tools in this thesis were chosen heuristically. In this section I provide a clear outline of all such decisions, listed in chronological order as they appear in the main text.

ADL tasks – the protocol tasks that were selected were identified based on several factors, such as whether they appeared in rehabilitation evaluation or surveys. However, a major concern was whether prosthesis users would ever opt to use their prosthetic device when completing certain tasks. For example, during feeding, no matter how capable a future prosthesis might be, cutting a piece of food would almost certainly be performed with the sound hand with the prosthetic hand holding the fork in place. Likewise for brushing teeth, combing

hair, using scissors, and writing. When given certain task choices, I expect a prosthesis user to simply use their sound limb. Therefore, tasks that users would likely opt to use the device for, or tasks that simply necessitated prosthesis use (such as bimanual manipulation or reaching to the contralateral axilla), were ultimately selected. We often must carry or manipulate objects in our sound limb, so simple tasks that could be feasibly completed by a prosthetic device were likely candidates, and include basic reaching and transferring motions.

Arm model – the decision to use arm joint angles over Cartesian coordinates of the segments or the other considerations cited in the main text ultimately came down to dimensionality and interpretability of the representation. Only 7 joint angles are needed to represent the full arm, while 27 dimensions are needed if using Cartesian coordinates. Additionally, joint angles lend themselves to a forward kinematic implementation of the virtual device. If using Cartesian coordinates, then cluster results and ROM would nonetheless need to be converted to joint angle representation for interpretability.

Similarity measure – Similarity between time-series data can be performed in many ways. One common method is to find the Euclidean distance between feature vectors of the motions. Reducing the dimensionality of motion of an entire trajectory includes sampling points of interest and modeling the data and using the coefficients. These methods attempt to capture certain characteristics of motion, but ultimately result in loss of data that we believed was meaningful for a motion to appear natural. This could be abated if a highly dimensional function was fit to the data, but provided that some of the motions were 7 DOF, this would've resulted in the curse of dimensionality, i.e. the data would have been too sparse for meaningful clusters. Alternatively, calculating the frame-by-frame distance between motions would be possible with resampling. Linear resampling was not a good candidate since nearly identical arm motions would likely appear further from one another due phase shifts (the peaks would unlikely match). Ultimately, DTW was selected due to its ability to resample the time-series data while matching epochs.

Averaging time-series – The rationale behind the decision to use DBA overlaps with the decision to use DTW: a method that does not result in loss of data through modeling and is capable of matching characteristic epochs of motion.

Clustering time-series – The choice of a clustering algorithm was limited by the desire to obtain "spherically" distinct clusters. Algorithms such as spectral clustering [95] and DBScan [96] are excellent at identifying clusters

that could be arbitrarily shaped, and were therefore not considered. For example, the average of a U-shaped cluster would fall outside its own boundary and would likely be unlike any of the cluster members, potentially resulting in a "useless" prototypical motion. There are several ways to perform hierarchical clustering, with different linkage distance criterion resulting in vastly different clusters. Ultimately Ward's distance was selected as it accounted for both the between and within variance. However, other methods distances could be considered, such as furthest distance.

Cluster method evaluation – The presence of task repetitions lent itself to validation of the clustering approach. Without repetitions, there is no ground truth. I therefore suspect that whenever possible, repetitions should be collected and used for validation.

Motion variation – Motion variation was found using fPCA, however the way by which this is done is application dependent. Here, fPCA requires the motions to be modelled, and one common approach is with B-splines. However, the type of B-splines and number of knots can be application specific. Our decision was to use 4 knots, corresponding to 3 phases of each motion (i.e. start, middle, and end), and using cubic splines. Complexity of motion was the large determinant of the number of knots, and given that we have already segment full tasks into submovements, our conservative 4 knots were appropriate. We were cognizant of both prior literature and the ability of cubic Bezier curves to accurately compress motion data [56] and the sparsity associated with additional splines or increasing power. Only the kinematics of motion were considered, and therefore the selected method was appropriate. In applications were velocity or higher order features are considered, higher dimensional B-splines should be used instead. When motion is cyclical, cyclical representations should be used, such as wavelets or Fourier series.

Orientation distribution - I believe this is the first documented attempt at using the rhombicuboctahedron as a tool to visualize the distributions of 3D orientations. Initial attempt at using a cube resulted in crude classification, while geometric shapes with a greater number of facets would lose their intuition. The selected hedron geometry, an intermediate, appeared to be the most intuitive, though this could be further established.

Clustering orientations – Because hand orientations are in SO(3), it did not make sense to cluster them using traditional approaches; clustering will be affect by how the sphere is unwrapped. Here, I also attempted to minimize number of representative hand orientations while affirming that the prototypical hand orientations are "useful" for task completion. To that end, a dispersion was used that aimed to cap the divisive clustering

algorithm when the average distance between orientations reached 22.5°. This limit corresponded to the limit of the classification of the rhombicuboctahedron (halfway between two facets), and should therefore result in orientations that are likewise intuitive as the hedron classes themselves. Other approaches that characterize hand orientations, such as the principal geodesic analysis [97], could be explored in the future.

Virtual reality – The capabilities of a virtual environment to provide results related directly to the real-world is something that has been supported, but not directly established. Therefore, we conscientiously rely on the results as a step towards testing the device in the real world. Drawbacks to using any virtual reality system include the following limitations: field of view, video quality, screen-door effect, wires, sound, weight of the headset, and other sensors that may be placed on the body that otherwise would not be needed in the real world.

Virtual prostheses – The focus of the experiment protocol was to demonstrate that using a series of preplanned prototypical motions is a feasible approach to assisting participants to complete a series of ADL tasks. Therefore, several simplifications and assumptions were made. These included ignoring the following: dynamic considerations, such as inertial forces, physical constraints, power consumption, interaction effects between the end-effector and object, and gravity. The device was simply controlled in velocity control that could be operated with maximum fidelity; it would stop the moment the user ceased using the controller without any motor backlash. Finally, the results are based on hypothetical prosthetic devices that do not currently exist. Although a shoulder and elbow prosthetic joints can be found in the commercial Luke/DEKA arm, much like other devices, it lacks a 3 DOF wrist.

Controller – One major decision that was iterated on in the thesis was the decision of a controller. The initial joystick controller maintained all prosthesis controls to the affect limb, while the keyboard relegated the controls almost entirely to the sound limb. A modular controller that could accommodate up to 8 simultaneous dual-site inputs was selected to be as agnostic to input as possible. A complex placement of sEMG on various parts of the body or a controller in the hand would be susceptible to bias of some inputs and not others. A modular controller, on the other hand, places all inputs in the same plane and the same effort is required to use any one of them.

Participant selection and training – How much naïve participants should be trained prior to testing prosthesis is something we had to consider when designing the experiment protocol. A decision was made not to convert

the participants to experts through extensive training, since I hoped to evaluate the intuition of the control methods. At the same time, I ensured participants understood the control methods and provided the opportunity for them to practice.

6.3 Lessons Learned and Future Work

Some improvements to the experimental design can be made. Both time and survey responses attempted to indirectly capture the cognitive burden associated with each of the control modes. However, pupillometry has been shown to measure it directly [98], and has been used across various fields, including prosthesis use [99] as well as driving [100]. Dynamics too play a role in prosthesis use that are not currently captured in our set up. For full immersion, and to simulate real world prosthesis use, future efforts may consider expanding our platform and task conditions to require object interaction dynamics, akin to [83]. However, using state of the art motion tracking, HMD, and control input, I believe this is the closest a simulation can get to testing prostheses without using the actual prosthetic device. Nonetheless, there is always room for improvement, and certain changes in the future could fully bridge the gap between simulation and reality. These include adding haptic feedback, inertia, wider field of view and resolution in the HMD, and improving the realism of the virtual environment design.

Bimanual tasks were deliberately avoided in our experiment due to the lack of haptic feedback and the complexity associated with coordinating control with the healthy hand. It is the reason why amputees rarely perform bimanual interactions and why the research community is biased towards assessing unilateral tasks [101]. Given that the learned motions encompass bimanual interactions, namely *transferring a box*, future efforts ought to evaluate if *trajectory* control can assist with bimanual tasks as well. I suspect this will be intractable without adding sensing complexity. Since *trajectory* control includes a pre-specified set of prototypical motions, participants inevitably failed certain tasks. It is suggested that the variation in motion that was identified in Chapter 2 could be used to dynamically adjust the end point. However, this would require added sensing, though, depending on the level of amputation, this could be manageable. For, example, for transhumeral amputees, the residual translational motion in the shoulder could be used to adjust the end-effector.

As a proxy to sEMG control inputs, the keyboard was used to assess prosthesis control. While for *sequential* and *trajectory* control the input is a single slider, *simultaneous* control involved up to eight sliders. This particular interface involved some level of finger dexterity that will unlikely be present in a marketable device. As an imperfect imitation

of sEMG, it introduces error. While I hope the comparison stands, further improvements to the cognitive burden and robustness of operating several DOF simultaneously [16], [102], [103] could ultimately outweigh the simplicity of *trajectory* control. Finally, it is likely that endpoint control is what humans use to program reaching and grasping movements [104], so the idea of using a predefined set of locations and orientations, rather than joint motions, could be a possible future direction. In the meantime, trajectory control highlights the benefits of using learned motions and suggests that a complex, yet practical, solution will likely be a semi-autonomous one and where additional trajectories can be added by end-users.

The initial 3 DOF prosthesis control investigation demonstrated that under certain assumptions prototypical motions have the capacity to outperform the state of the art in prosthesis controls. The assumptions, however, are not trivial, and deserve their own in-depth study. The assumptions were removed for the more comprehensive investigation, and it was evident that for the proposed control method to match the performance of a healthy arm, mode selection and mode switching will need to be addressed. Mode selection could potentially be solved through a semi-autonomous interface that predicts intent and shuffles the order of the modes such that participants only need to switch once. Another solution is to improve mode switching such that it can be performed very quickly, accurately, and intuitively; though this method will nonetheless require users to either memorize the order of the modes or carry a reference list.

It seems to me that in its present form, *trajectory* control is not nearly intuitive enough to outperform other control methods for the 3 DOF device. Initially, 3 DOF motion categories were labeled according to the major joint rotations as can be seen in Chapter 2. When implementing in the VR, the posters listing the motions instead referred to the tasks that those motions are able to complete. However, this is not a generalizable approach, and a better labeling system is much needed. It is here that I believe that the decoupled orientation analysis will likely be most useful. Perhaps the wrist orientation would be most intuitive along major axes, such as those on the surface of the rhombicuboctahedron. Users would simply select a hand orientation from a succinct list of available hand orientations, rather than whole trajectories. Additionally, most participants did not consider the trajectory path that the prototypical motions performed, and primarily concerned themselves with the target location and orientation. This again reaffirms the potential use case of decoupling the location and orientation control

Alternative arm features have been proposed in the literature, such as the arm triangle [105], or defining a new angle eliminating one of the discontinuities [106], either of which could be used in future iterations. However, they

carry a tradeoff that would make the results less interpretable and clinically relevant. On the other hand, if simply programed into *trajectory* control, then these could have resulted in more robust motion categories. With so many considerations to make when designing a prosthesis control and an experiment protocol, it is genuinely hard to say that my approach was ultimately was the right one. Is *trajectory* control the future? What about decoupled selection of hand location and orientation? If brute force is not an option, we are left to use our heuristics and creativity until we identify a method that ultimately grants us a seamless control. One thing is for certain, rehabilitation and prosthetics continue to be rich fields for research and innovation.

In our findings, there were significant differences in performance between certain participants, and evaluation was largely contingent on their learning. This raises the question of the purpose of prosthesis control evaluation. When evaluating a new prosthetic device or a control method, should we be considering a novice user or an expert? In practice, users develop expertise over a prolonged period of time, something that cannot be captured in a single laboratory visit. What does it mean for a prosthesis control to be "good"? It cannot simply be the feasibility of a prosthesis to complete the task or any other single metric. User experience must be taken into account, and is likely the main factor that leads to prosthesis acceptance [107]. Therefore, in addition to quantitative measures, insight can often be found in surveys evaluating each participant's personal perspective and through conversation. Despite these efforts, the proposed control method would still need to be evaluated in the real world where users would likely need to memorize the control methods and make voluntary control decisions. There is a risk, of course, that much like has been observed with current devices [108], that the prosthesis controls will not be used in the intended way simply because of the user experience. Although ultimately, nothing provides insight as much as the experience of trying out the device yourself, whether in virtual reality or in the real world.

BIBLIOGRAPHY

[1] C. J. van Andel, N. Wolterbeek, C. A. M. Doorenbosch, D. J. (H E. J.). Veeger, and J. Harlaar, "Complete 3D kinematics of upper extremity functional tasks," *Gait Posture*, vol. 27, no. 1, pp. 120–127, 2008.

[2] A. M. Oosterwijk, M. K. Nieuwenhuis, C. P. van der Schans, and L. J. Mouton, "Shoulder and elbow range of motion for the performance of activities of daily living: A systematic review," *Physiother. Theory Pract.*, vol. 34, no. 7, pp. 505–528, 2018.

[3] F. Montagnani, M. Controzzi, and C. Cipriani, "Is it Finger or Wrist Dexterity That is Missing in Current Hand Prostheses?," *IEEE Trans. Neural Syst. Rehabil. Eng.*, vol. 23, no. 4, pp. 600–609, 2015.

[4] A. J. Spiers, Y. Gloumakov, and A. M. Dollar, "Examining the Impact of Wrist Mobility on Reaching Motion Compensation Across a Discretely Sampled Workspace," *Int. Conf. Biomed. Robot. Biomechatronics*, vol. 2018-Augus, pp. 819–826, 2018.

[5] C. R. Gambrell, "Overuse syndrome and the unilateral upper limb amputee: Consequences and prevention," *J. Prosthetics Orthot.*, vol. 20, no. 3, pp. 126–132, 2008.

[6] E. Biddiss and T. Chau, "Upper limb prosthesis use and abandonment: A survey of the last 25 years," *Prosthetics and Orthotics International*, vol. 31, no. 3. pp. 236–257, 2007.

[7] W. Schweitzer, M. J. Thali, and D. Egger, "Case-study of a user-driven prosthetic arm design: Bionic hand versus customized body-powered technology in a highly demanding work environment," *J. Neuroeng. Rehabil.*, vol. 15, no. 1, pp. 1–27, 2018.

[8] S. D. Iftime, L. L. Egsgaard, and M. B. Popovic, "Automatic Determination of Synergies by Radial Basis Function Artificial Neural Networks for the Control of a Neural Prosthesis," *IEEE Trans. Neural Syst. Rehabil. Eng.*, vol. 13, no. 4, pp. 482–489, 2005.

[9] D. Blana, T. Kyriacou, J. M. Lambrecht, and E. K. Chadwick, "Feasibility of using combined EMG and kinematic signals for prosthesis control: A simulation study using a virtual reality environment," *J. Electromyogr. Kinesiol.*, vol. 29, pp. 21–27, 2016.

[10] R. R. Kaliki, R. Davoodi, and G. E. Loeb, "Prediction of Distal Arm Posture in 3-D Space From Shoulder Movements for Control of Upper Limb Prostheses," *Proc. IEEE*, vol. 96, no. 7, pp. 1217–1225, 2008.

[11] P. K. Artemiadis and K. J. Kyriakopoulos, "EMG-Based Control of a Robot Arm Using Low-Dimensional Embeddings," *Trans. Robot.*, vol. 26, no. 2, pp. 393–398, 2010.

[12] R. Garcia-Rosas, Y. Tan, D. Oetomo, and C. Manzie, “On-line Synergy Identification for Personalized Active Arm Prosthesis: A Feasibility Study,” *Proc. Am. Control Conf.*, vol. 2018-June, pp. 514–519, 2018.

[13] D. A. Bennett and M. Goldfarb, “IMU-Based Wrist Rotation Control of a Transradial Myoelectric Prosthesis,” *Trans. Neural Syst. Rehabil. Eng.*, no. 99, 2016.

[14] R. Garcia-Rosas, D. Oetomo, C. Manzie, Y. Tan, and P. Choong, “Task-Space Synergies for Reaching Using Upper-Limb Prostheses,” *IEEE Trans. Neural Syst. Rehabil. Eng.*, vol. 28, no. 12, pp. 2966–2977, 2020.

[15] R. Volkmar, S. Dosen, J. Gonzalez-Vargas, M. Baum, and M. Markovic, “Improving bimanual interaction with a prosthesis using semi-autonomous control,” *J. Neuroeng. Rehabil.*, vol. 16, no. 1, pp. 1–13, 2019.

[16] S. L. Phillips, L. Resnik, C. Fantini, and G. Latlief, “Endpoint control for a powered shoulder prosthesis,” *J. Prosthetics Orthot.*, vol. 25, no. 4, pp. 193–200, 2013.

[17] A. Campeau-Lecours *et al.*, “JACO Assistive Robotic Device: Empowering People With Disabilities Through Innovative Algorithms,” in *Rehabilitation Engineering and Assistive Technology Society of North America*, 2016.

[18] A. Fougner, Ø. Stavdahl, P. J. Kyberd, Y. G. Losier, and P. A. Parker, “Control of Upper Limb Prostheses : Terminology and Proportional Myoelectric Control — A Review,” *IEEE Trans. Neural Syst. Rehabil. Eng.*, vol. 20, no. 5, pp. 663–677, 2012.

[19] E. Biddiss, D. Beaton, and T. Chau, “Consumer design priorities for upper limb prosthetics,” *Disabil. Rehabil. Assist. Technol.*, vol. 2, no. 6, pp. 346–357, 2007.

[20] M. J. Gielniak, C. K. Liu, and A. L. Thomaz, “Generating human-like motion for robots,” *Int. J. Rob. Res.*, vol. 32, no. 11, pp. 1275–1301, 2013.

[21] M. J. Gielniak and A. L. Thomaz, “Spatiotemporal correspondence as a metric for human-like robot motion,” *HRI 2011 - Proc. 6th ACM/IEEE Int. Conf. Human-Robot Interact.*, pp. 77–84, 2011.

[22] R. Rasch, S. Wachsmuth, and M. König, “A joint motion model for human-like robot-human handover,” in *IEEE-RAS International Conference on Humanoid Robots*, 2018.

[23] M. Hauschild, R. Davoodi, and G. E. Loeb, “A Virtual Reality Environment for Designing and Fitting Neural Prosthetic Limbs,” in *IEEE Transactions on Neural Systems and Rehabilitation Engineering*, 2007, vol. 15, no. 1, pp. 9–15.

[24] T. Kang, J. He, and S. I. H. Tillery, “Determining natural arm configuration along a reaching trajectory.,” *Exp.*

brain Res., vol. 167, no. 3, pp. 352–361, 2005.

[25] A. Spiers, S. G. Khan, and G. Herrmann, *Biologically Inspired Control of Humanoid Robot Arms: Robust and Adaptive Approaches*, 1st ed. Springer International Publishing AG Switzerland, 2016.

[26] N. Hogan and D. Sternad, "Dynamic primitives of motor behavior," *Biol. Cybern.*, vol. 106, no. 11–12, pp. 727–739, 2012.

[27] T. Flash and N. Hogan, "The coordination of arm movements: an experimentally confirmed mathematical model," *J. Neurosci.*, vol. 5, no. 7, pp. 1688–1703, 1985.

[28] M. Merad, A. Roby-Brami, and N. Jarrasse, "Towards the implementation of natural prosthetic elbow motion using upper limb joint coordination," in *International Conference on Biomedical Robotics and Biomechatronics*, 2016, pp. 821–826.

[29] C. Wang *et al.*, "Kinematic Redundancy Analysis during Goal-Directed Motion for Trajectory Planning of an Upper-Limb Exoskeleton Robot," in *Proceedings of the Annual International Conference of the IEEE Engineering in Medicine and Biology Society*, 2019, pp. 5251–5255.

[30] D. Farina *et al.*, "The Extraction of Neural Information from the Surface EMG for the Control of Upper-Limb Prostheses : Emerging Avenues and Challenges," *Trans. Neural Syst. Rehabil. Eng.*, vol. 22, no. 4, pp. 797–809, 2014.

[31] L. Bi, A. Feleke, and C. Guan, "A review on EMG-based motor intention prediction of continuous human upper limb motion for human-robot collaboration," *Biomed. Signal Process. Control*, vol. 51, pp. 113–127, 2019.

[32] C. L. Pulliam, J. M. Lambrecht, and R. F. Kirsch, "EMG-Based Neural Network Control of Transhumeral Prostheses," *J. Rehabil. Res. Dev.*, vol. 48, no. 6, pp. 739–754, 2013.

[33] G. Averta, C. Della Santina, E. Battaglia, F. Felici, M. Bianchi, and A. Bicchi, "Unvealing the Principal Modes of Human Upper Limb Movements," *Front. Robot. AI*, vol. 4, no. 37, pp. 1–12, 2017.

[34] S. Sheikholeslami, G. Lee, J. W. Hart, S. Srinivasa, and E. A. Croft, "A Study of Reaching Motions for Collaborative Human-Robot Interaction," in *International Symposium on Experimental Robotics*, 2018, pp. 584–594.

[35] T. M. Tuan, P. Souères, M. Taïx, M. N. Sreenivasa, and C. Halgand, "Humanoid human-like reaching control based on movement primitives," in *Proceedings - IEEE International Workshop on Robot and Human*

Interactive Communication, 2010, pp. 546–551.

[36] D. Kulić, W. Takano, and Y. Nakamura, "Online segmentation and clustering from continuous observation of whole body motions," *IEEE Trans. Robot.*, vol. 25, no. 5, pp. 1158–1166, 2009.

[37] D. H. Gates, L. S. Walters, J. Cowley, J. M. Wilken, and L. Resnik, "Range of Motion Requirements for Upper-Limb Activities of Daily Living," *Am. J. Occup. Ther.*, vol. 70, no. 1, 2016.

[38] D. J. Magermans, E. K. J. Chadwick, H. E. J. Veeger, and F. C. T. van der Helm, "Requirements for upper extremity motions during activities of daily living," *Clin. Biomech.*, vol. 20, no. 6, pp. 591–599, 2005.

[39] L. Resnik *et al.*, "Development and Evaluation of the Activities Measure for Upper Limb Amputees," *Arch. Phys. Med. Rehabil.*, vol. 94, no. 3, pp. 488–494, 2013.

[40] C. S. Chung, H. Wang, and R. A. Cooper, "Functional assessment and performance evaluation for assistive robotic manipulators: Literature review," *J. Spinal Cord Med.*, vol. 36, no. 4, pp. 273–289, 2013.

[41] F. Cordella *et al.*, "Literature review on needs of upper limb prosthesis users," *Front. Neurosci.*, vol. 10, pp. 1–14, 2016.

[42] G. Wu *et al.*, "ISB recommendation on definitions of joint coordinate systems of various joints for the reporting of human joint motion — Part II : shoulder, elbow, wrist and hand," *J. Biomech.*, vol. 38, no. 5, pp. 981–992, 2005.

[43] C. A. M. Doorenbosch, J. Harlaar, and D. Veeger, "The globe system: An unambiguous description of shoulder positions in daily life movements," *J. Rehabil. Res. Dev.*, vol. 40, no. 2, p. 147, 2003.

[44] J. Barbic, A. Safonova, J.-Y. Pan, C. Faloutsos, J. K. Hodgins, and N. S. Pollard, "Segmenting Motion Capture Data into Distinct Behaviors," in *Proceedings of Graphics Interface*, 2004, pp. 185–194.

[45] D. Kulić, C. Ott, D. Lee, J. Ishikawa, and Y. Nakamura, "Incremental learning of full body motion primitives and their sequencing through human motion observation," *Int. J. Rob. Res.*, vol. 31, no. 3, pp. 330–345, 2011.

[46] G. Xia, H. Sun, L. Feng, G. Zhang, and Y. Liu, "Human Motion Segmentation via Robust Kernel Sparse Subspace Clustering," *Trans. Image Process.*, vol. 27, no. 1, pp. 135–150, 2018.

[47] X. Zan, W. Liu, and W. Xing, "A framework for human motion segmentation based on multiple information of motion data," *Trans. Internet Inf. Syst.*, vol. 13, no. 9, pp. 4624–4644, 2019.

[48] T. Bhattacharjee, G. Lee, H. Song, and S. S. Srinivasa, "Towards Robotic Feeding: Role of Haptics in Fork-Based Food Manipulation," *IEEE Robot. Autom. Lett.*, vol. 4, no. 2, pp. 1485–1492, 2019.

[49] H. Sakoe and S. Chiba, “Dynamic Programming Algorithm Optimization for Spoken Word Recognition,” *IEEE Trans. Acoust.*, vol. 26, no. 1, pp. 43–49, 1978.

[50] M. Linardi, Y. Zhu, T. Palpanas, and E. Keogh, “Matrix profile X: VALMOD-scalable discovery of variable-length motifs in data series,” *Proc. ACM SIGMOD Int. Conf. Manag. Data*, pp. 1053–1066, 2018.

[51] F. Petitjean, A. Ketterlin, and P. Gancarksi, “A global averaging method for dynamic time warping, with applications to clustering,” *Pattern Recognit.*, vol. 44, no. 3, pp. 678–693, 2011.

[52] M. Cuturi and M. Blondel, “Soft-DTW: a Differentiable Loss Function for Time-Series,” in *Proceedings of the 34th International Conference on Machine Learning*, 2017.

[53] B. S. Everitt, S. Landau, M. Leese, and D. Stahl, *Cluster Analysis*, 5th ed. West Sussex, U.K.: John Wiley & Sons, 2011.

[54] A. Saxena *et al.*, “A review of clustering techniques and developments,” *Neurocomputing*, vol. 267, pp. 664–681, 2017.

[55] S. Salvador and P. Chan, “Determining the Number of Clusters/Segments in Hierarchical Clustering/Segmentation Algorithms,” in *International Conference on Tools with Artificial Intelligence*, 2004.

[56] O. Arikan, “Compression of Motion Capture Databases,” *ACM Trans. Graph.*, vol. 25, no. 3, pp. 890–897, 2006.

[57] J. J. Faraway, M. P. Reed, and J. Wang, “Modelling three-dimensional trajectories by using Bezier curves with application to hand motion,” *J. R. Stat. Soc. Ser. C Appl. Stat.*, vol. 56, no. 5, pp. 571–585, 2007.

[58] J. Ramsay and B. W. Silverman, *Functional Data Analysis*, 2nd ed. Springer-Verlag New York, 2005.

[59] A. Kassidas, J. F. MacGregor, and P. A. Taylor, “Synchronization of Batch Trajectories Using Dynamic Time Warping,” *Am. Inst. Chem. Eng.*, vol. 44, no. 4, pp. 864–875, 1998.

[60] C. de Boor, *A Practical Guide to Splines.*, 1st ed. Springer-Verlag New York, 1978.

[61] P. Morasso, “Spatial Control of Arm Movements,” *Exp. Brain Res.*, vol. 42, pp. 223–227, 1981.

[62] F. Montagnani, M. Controzzi, and C. Cipriani, “Exploiting arm posture synergies in activities of daily living to control the wrist rotation in upper limb prostheses: A feasibility study,” in *Proceedings of the 2015 International Conference of the IEEE Engineering in Medicine and Biology Society*, 2015, pp. 2462–2465.

[63] H. Moritomo, E. P. Apergis, G. Herzberg, F. W. Werner, S. W. Wolfe, and M. Garcia-Elias, “2007 IFSSH Committee Report of Wrist Biomechanics Committee: Biomechanics of the So-Called Dart-Throwing Motion

of the Wrist," *J. Hand Surg. Am.*, vol. 32, no. 9, pp. 1447–1453, 2007.

[64] S. Aghabozorgi, A. Seyed, and T. Y. Wah, "Time-series clustering – A decade review," *Inf. Syst.*, vol. 53, pp. 16–38, 2015.

[65] B. S. Row and P. R. Cavanagh, "Reaching upward is more challenging to dynamic balance than reaching forward," *Clin. Biomech.*, vol. 22, no. 2, pp. 155–164, 2007.

[66] K. J. Wisneski and M. J. Johnson, "Quantifying kinematics of purposeful movements to real, imagined, or absent functional objects: Implications for modelling trajectories for robot-assisted ADL tasks," *J. Neuroeng. Rehabil.*, vol. 4, no. 7, pp. 1–14, 2007.

[67] S. Li, P. N. Pathirana, M. P. Galea, G. Ottmann, and F. Khan, "Quantitative Assessment of ADL: A Pilot Study of Upper Extremity Reaching Tasks," *J. Sensors*, 2015.

[68] D. B. Chaffin, "On simulating human reach motions for ergonomics analyses," *Hum. Factors Ergon. Manuf.*, vol. 12, no. 3, pp. 235–247, 2002.

[69] F. Lacquaniti and J. F. Soechting, "Coordination of arm and wrist motion during a reaching task.," *J. Neurosci.*, vol. 2, no. 4, pp. 399–408, 1982.

[70] A. Roby-Brami, N. Bennis, M. Mokhtari, and P. Baraduc, "Hand orientation for grasping depends on the direction of the reaching movement," *Brain Res.*, vol. 869, no. 1–2, pp. 121–129, 2000.

[71] T. A. Lenssen, L. Cappello, D. H. Plettenburg, C. Cipriani, and M. Controzzi, "Principal orientations of the wrist during ADLs: Towards the design of a synergetic wrist prosthesis," in *International Conference on NeuroRehabilitation*, 2018, vol. 21, pp. 339–343.

[72] L. Paninski, S. Shoham, M. R. Fellows, N. G. Hatsopoulos, and J. P. Donoghue, "Superlinear Population Encoding of Dynamic Hand Trajectory in Primary Motor Cortex," *J. Neurosci.*, vol. 24, no. 39, pp. 8551–8561, 2004.

[73] N. Hogan *et al.*, "Motions or muscles? Some behavioral factors underlying robotic assistance of motor recovery," *J. Rehabil. Res. Dev.*, vol. 43, no. 5, pp. 605–618, 2006.

[74] Y. Mao and S. K. Agrawal, "Design of a cable-driven arm exoskeleton (CAREX) for neural rehabilitation," *Robot. IEEE Trans.*, pp. 1–10, 2012.

[75] V. Maheu, J. Frappier, P. S. Archambault, and F. Routhier, "Evaluation of the JACO robotic arm: Clinico-economic study for powered wheelchair users with upper-extremity disabilities," in *IEEE International*

Conference on Rehabilitation Robotics, 2011.

[76] A. Borboni, G. Carbone, and N. Pellegrini, *Reference Frame Identification and Distributed Control Strategies in Human-Robot Collaboration*, vol. 84. Springer International Publishing, 2020.

[77] F. L. Markley, Y. Cheng, J. L. Crassidis, and Y. Oshman, "Averaging Quaternions," *J. Guid. Control. Dyn.*, vol. 30, no. 4, pp. 1675–1682, 2007.

[78] Y. Cao and L. Petzold, "Accuracy limitations and the measurement of errors in the stochastic simulation of chemically reacting systems," *J. Comput. Phys.*, vol. 212, no. 1, pp. 6–24, 2006.

[79] N. A. Alshammary, D. A. Bennett, and M. Goldfarb, "Synergistic Elbow Control for a Myoelectric Transhumeral Prosthesis," *IEEE Trans. Neural Syst. Rehabil. Eng.*, vol. 26, no. 2, pp. 468–476, 2018.

[80] H. Su, C. Yang, G. Ferrigno, and E. De Momi, "Improved human-robot collaborative control of redundant robot for teleoperated minimally invasive surgery," *IEEE Robot. Autom. Lett.*, vol. 4, no. 2, pp. 1447–1453, 2019.

[81] H. Nguyen, M. Ciocarlie, K. Hsiao, and C. C. Kemp, "ROS commander (ROSCo): Behavior creation for home robots," *Proc. - IEEE Int. Conf. Robot. Autom.*, pp. 467–474, 2013.

[82] S. Greengard, *Virtual Reality*, 1st ed. Cambridge, MA: The MIT Press, 2019.

[83] J. M. Lambrecht, C. L. Pulliam, and R. F. Kirsch, "Virtual reality environment for simulating tasks with a myoelectric prosthesis: An assessment and training tool," *J. Prosthetics Orthot.*, vol. 23, no. 2, pp. 89–94, 2011.

[84] B. N. Perry *et al.*, "Virtual Integration Environment as an Advanced Prosthetic Limb Training Platform," *Front. Neurol.*, vol. 9, 2018.

[85] L. Resnik, K. Etter, S. L. Klinger, and C. Kambe, "Using virtual reality environment to facilitate training with advanced upper-limb prosthesis," *J. Rehabil. Res. Dev.*, vol. 48, no. 6, pp. 707–718, 2011.

[86] D. E. Levac, M. E. Huber, and D. Sternad, "Learning and transfer of complex motor skills in virtual reality: A perspective review," *J. Neuroeng. Rehabil.*, vol. 16, no. 1, pp. 1–15, 2019.

[87] M. Kuttuva *et al.*, "The Rutgers Arm, a Rehabilitation System in Virtual Reality: A Pilot Study," *Cyberpsychology Behav.*, vol. 9, no. 2, pp. 148–151, 2006.

[88] B. N. Perry, C. Mercier, S. R. Pettifer, J. Cole, and J. W. Tsao, "Virtual reality therapies for phantom limb pain," *Eur. J. Pain*, vol. 18, no. 7, pp. 897–899, 2014.

[89] A. L. Alphonso *et al.*, “Use of a virtual integrated environment in prosthetic limb development and phantom limb pain,” *Stud. Health Technol. Inform.*, vol. 181, pp. 305–309, 2012.

[90] D. Putrino, Y. T. Wong, A. Weiss, and B. Pesaran, “A Training Platform for Many-Dimensional Prosthetic Devices Using a Virtual Reality Environment,” *J. Neurosci. Methods*, vol. 244, pp. 68–77, 2015.

[91] W. Zhang *et al.*, “Cognitive workload in conventional direct control vs. pattern recognition control of an upper-limb prosthesis,” *Int. Conf. Syst. Man, Cybern.*, pp. 2335–2340, 2017.

[92] L. V. McFarland, S. L. Hubbard Winkler, A. W. Heinemann, M. Jones, and A. Esquenazi, “Unilateral upper-limb loss: Satisfaction and prosthetic-device use in veterans and servicemembers from Vietnam and OIF/OEF conflicts,” *J. Rehabil. Res. Dev.*, vol. 47, no. 4, pp. 299–316, 2010.

[93] L. Resnik, S. L. Klinger, and K. Etter, “The DEKA Arm: Its features, functionality, and evolution during the veterans affairs study to optimize the DEKA Arm,” *Prosthet. Orthot. Int.*, vol. 38, no. 6, pp. 492–504, 2014.

[94] M. Davidson, C. Bodine, and R. F. f. Weir, “User surveys support designing a prosthetic wrist that incorporates the Dart Thrower’s Motion,” *Disabil. Rehabil. Assist. Technol.*, vol. 14, no. 3, pp. 312–315, 2019.

[95] F. Zhou, S. Member, F. De Torre, and J. K. Hodgins, “Hierarchical Aligned Cluster Analysis for Temporal Clustering of Human Motion,” *Trans. Pattern Anal. Mach. Intell.*, vol. 35, no. 3, pp. 582–596, 2013.

[96] M. Ester, H.-P. Kriegel, J. Sander, and X. Xu, “A Density-Based Algorithm for Discovering Clusters,” *Proc. KDD*, pp. 226–231, 1996.

[97] S. Said, N. Courty, N. Le Bihan, and S. J. Sangwine, “Exact principal geodesic analysis for data on SO(3),” *Eur. Signal Process. Conf.*, no. Eusipco, pp. 1701–1705, 2007.

[98] J. Beatty, “Task-Evoked Pupillary Responses, Processing Load, and the Structure of Processing Resources,” *Psychol. Bull.*, vol. 91, no. 2, pp. 276–292, 1982.

[99] M. M. D. Sobuh *et al.*, “Visuomotor behaviours when using a myoelectric prosthesis,” *J. Neuroeng. Rehabil.*, vol. 11, no. 1, pp. 1–11, 2014.

[100] O. Palinko, A. L. Kun, A. Shyrokov, and P. Heeman, “Estimating cognitive load using remote eye tracking in a driving simulator,” *Eye Track. Res. Appl. Symp.*, pp. 141–144, 2010.

[101] A. Chadwell *et al.*, “Upper limb activity in myoelectric prosthesis users is biased towards the intact limb and appears unrelated to goal-directed task performance,” *Sci. Rep.*, vol. 8, no. 1, pp. 1–12, 2018.

[102] T. A. Kuiken *et al.*, “Targeted muscle reinnervation for real-time myoelectric control of multifunction artificial

arms," *JAMA - J. Am. Med. Assoc.*, vol. 301, no. 6, pp. 619–628, 2009.

[103] J. Doubler and D. Childress, "An analysis of extended physiological proprioception as a prosthesis-control technique," *J. Rehabil. Res. Dev.*, vol. 21, no. 1, pp. 5–18, 1984.

[104] R. F. Keulen, J. J. Adam, and M. H. Fischer, "Selective Reaching : Evidence for Multiple Frames of Reference," *J. Exp. Psychol. Hum. Percept. Perform.*, vol. 28, no. 3, pp. 515–526, 2002.

[105] C. Fang and X. Ding, "A Set of Basic Movement Primitives for Anthropomorphic Arms," in *IEEE International Conference on Mechatronics and Automation*, 2013, pp. 639–644.

[106] T. Masuda, A. Ishida, L. Cao, and S. Morita, "A proposal for a new definition of the axial rotation angle of the shoulder joint," *J. Electromyogr. Kinesiol.*, vol. 18, no. 1, pp. 154–159, 2008.

[107] L. J. Resnik, F. Acluche, and S. L. Klinger, *User experience of controlling the DEKA Arm with EMG pattern recognition*, vol. 13, no. 9. 2018.

[108] J. C. Cochran, A. J. Spiers, and A. M. Dollar, "Analyzing Exfordance Use by Unilateral Upper-Limb Amputees," *Proc. IEEE RAS EMBS Int. Conf. Biomed. Robot. Biomechatronics*, vol. 2018-Augus, pp. 86–93, 2018.